

① Ford
② Bralbury

LBL-23987
UC-70



Lawrence Berkeley Laboratory

UNIVERSITY OF CALIFORNIA

EARTH SCIENCES DIVISION

Transport of Radioactive Decay Chains in Finite and Semi-Infinite Porous Media

H.-C. Lung, P.L. Chambré, T.H. Pigford, and W.W.-L. Lee

September 1987



HYDROLOGY DOCUMENT NUMBER 228

DISCLAIMER

This document was prepared as an account of work sponsored by the United States Government. Neither the United States Government nor any agency thereof, nor The Regents of the University of California, nor any of their employees, makes any warranty, express or implied, or assumes any legal liability or responsibility for the accuracy, completeness, or usefulness of any information, apparatus, product, or process disclosed, or represents that its use would not infringe privately owned rights. Reference herein to any specific commercial products process, or service by its trade name, trademark, manufacturer, or otherwise, does not necessarily constitute or imply its endorsement, recommendation, or favoring by the United States Government or any agency thereof, or The Regents of the University of California. The views and opinions of authors expressed herein do not necessarily state or reflect those of the United States Government or any agency thereof or The Regents of the University of California and shall not be used for advertising or product endorsement purposes.

Printed in the United States of America
Available from
National Technical Information Service
U.S. Department of Commerce
5285 Port Royal Road
Springfield, VA 22161
Price Code: A06

Lawrence Berkeley Laboratory is an equal opportunity employer.

LBL-23987
UCB-NE-4112
UC-70

TRANSPORT OF RADIOACTIVE DECAY CHAINS IN FINITE AND SEMI-INFINITE POROUS MEDIA

H.-C. Lung, P. L. Chambré, T. H. Pigford and W. W-L. Lee

Earth Sciences Division, Lawrence Berkeley Laboratory

and

Department of Nuclear Engineering

University of California

Berkeley, CA 94720

September 1987

Work supported in part by U. S. Department of Energy contract DE-AC03-76SF00098

The authors invite comments and would appreciate
being notified of any errors in the report.

T. H. Pigford
Department of Nuclear Engineering
University of California
Berkeley, CA 94720

Table of Contents

1. Introduction	1
2. Mass Transport through a Finite Medium	3
2.1 Theoretical Analysis	3
2.2 Numerical Evaluations	15
2.2.1 Case 1: Constant Concentration at Boundaries	16
2.2.2 Case 2: Bateman-type boundary condition	35
3. Mass Transport through a Semi-infinite Medium	53
3.1 Theoretical Analysis	53
3.2 Numerical Evaluations	55
3.2.1 Case 1: Constant Concentration at Boundaries	55
3.2.2 Case 2: Bateman-type boundary condition	63
4. Conclusions	76
References	79
Appendix A	A-1
Appendix B	B-1

List of Figures

- Fig. 1. Normalized concentration profiles for $^{234}\text{U} \rightarrow ^{230}\text{Th} \rightarrow ^{226}\text{Ra}$ in backfill as functions of distance at 10 years; concentration-limited boundary condition. 22
- Fig. 2. Normalized concentration profiles for $^{234}\text{U} \rightarrow ^{230}\text{Th} \rightarrow ^{226}\text{Ra}$ in backfill as functions of distance at 10^3 years; concentration-limited boundary condition. 24
- Fig. 3. Normalized concentration profiles for $^{234}\text{U} \rightarrow ^{230}\text{Th} \rightarrow ^{226}\text{Ra}$ at backfill/rock interface as functions of time; concentration-limited boundary condition. 25
- Fig. 4. Normalized mass fluxes for $^{234}\text{U} \rightarrow ^{230}\text{Th} \rightarrow ^{226}\text{Ra}$ at both ends of the backfill layer as functions of time; concentration-limited boundary condition. 26
- Fig. 5. Normalized concentration profiles for $^{234}\text{U} \rightarrow ^{230}\text{Th} \rightarrow ^{226}\text{Ra}$ in backfill as functions of distance at 10^3 years; $h = 10^4$ m/yr; concentration-limited boundary condition. 28
- Fig. 6. Normalized concentration profiles for $^{234}\text{U} \rightarrow ^{230}\text{Th} \rightarrow ^{226}\text{Ra}$ at backfill/rock interface as functions of time; concentration-limited boundary condition. 29
- Fig. 7. Normalized mass fluxes for $^{234}\text{U} \rightarrow ^{230}\text{Th} \rightarrow ^{226}\text{Ra}$ at both ends of the backfill layer as functions of time; $h = 10^4$ m/yr; concentration-limited boundary condition. 30
- Fig. 8. Normalized concentration profiles for $^{245}\text{Cm} \rightarrow ^{241}\text{Am} \rightarrow ^{237}\text{Np} \rightarrow ^{233}\text{U} \rightarrow ^{229}\text{Th}$ in backfill as functions of distance at 10 years; concentration-limited boundary condition. 32
- Fig. 9. Normalized concentration profiles for $^{245}\text{Cm} \rightarrow ^{241}\text{Am} \rightarrow ^{237}\text{Np} \rightarrow ^{233}\text{U} \rightarrow ^{229}\text{Th}$ in backfill as functions of distance at 10^3 years; concentration-limited boundary condition. 33
- Fig. 10. Normalized concentration profiles for $^{245}\text{Cm} \rightarrow ^{241}\text{Am} \rightarrow ^{237}\text{Np} \rightarrow ^{233}\text{U} \rightarrow ^{229}\text{Th}$ in backfill as functions of distance at 10^3 years; $h = 10^4$ m/yr; concentration-limited boundary condition. 34
- Fig. 11. Normalized concentration profiles for $^{234}\text{U} \rightarrow ^{230}\text{Th} \rightarrow ^{226}\text{Ra}$ in backfill as functions of distance at 10 years; Bateman-type boundary condition. 38
- Fig. 12. Normalized concentration profiles for $^{234}\text{U} \rightarrow ^{230}\text{Th} \rightarrow ^{226}\text{Ra}$ in backfill as functions of distance at 10^3 years; Bateman-type boundary condition. 39
- Fig. 13. Normalized concentration profiles for $^{234}\text{U} \rightarrow ^{230}\text{Th} \rightarrow ^{226}\text{Ra}$ in backfill as functions of distance at 10^5 years; Bateman-type boundary condition. 41
- Fig. 14. Normalized concentration profiles for $^{234}\text{U} \rightarrow ^{230}\text{Th} \rightarrow ^{226}\text{Ra}$ at both ends of the backfill layer as functions of time; Bateman-type boundary condition. 42
- Fig. 15. Normalized mass fluxes for $^{234}\text{U} \rightarrow ^{230}\text{Th} \rightarrow ^{226}\text{Ra}$ at both ends of the backfill layer as functions of time; Bateman-type boundary condition. 43
- Fig. 16. Normalized concentration profiles for $^{234}\text{U} \rightarrow ^{230}\text{Th} \rightarrow ^{226}\text{Ra}$ in backfill as functions of distance at 10^3 years; Bateman-type boundary condition. 45
- Fig. 17. Normalized concentration profiles for $^{234}\text{U} \rightarrow ^{230}\text{Th} \rightarrow ^{226}\text{Ra}$ in backfill as functions of distance at 10^5 years; Bateman-type boundary condition. 46

- Fig. 18. Normalized concentration profiles for $^{234}\text{U} \rightarrow ^{230}\text{Th} \rightarrow ^{226}\text{Ra}$ at both ends of the backfill layer as functions of time; Bateman-type boundary condition. 47
- Fig. 19. Normalized concentration profiles for $^{245}\text{Cm} \rightarrow ^{241}\text{Am} \rightarrow ^{237}\text{Np} \rightarrow ^{233}\text{U} \rightarrow ^{229}\text{Th}$ in backfill as functions of distance at 10 years; Bateman-type boundary condition. 49
- Fig. 20. Normalized concentration profiles for $^{245}\text{Cm} \rightarrow ^{241}\text{Am} \rightarrow ^{237}\text{Np} \rightarrow ^{233}\text{U} \rightarrow ^{229}\text{Th}$ in backfill as functions of distance at 10^5 years; Bateman-type boundary condition. 50
- Fig. 21. Normalized concentration profiles for $^{245}\text{Cm} \rightarrow ^{241}\text{Am} \rightarrow ^{237}\text{Np} \rightarrow ^{233}\text{U} \rightarrow ^{229}\text{Th}$ in backfill as functions of distance at 10^5 years; $h = 10^4$ m/yr; Bateman-type boundary condition. 51
- Fig. 22. Normalized concentration profiles for $^{245}\text{Cm} \rightarrow ^{241}\text{Am} \rightarrow ^{237}\text{Np} \rightarrow ^{233}\text{U} \rightarrow ^{229}\text{Th}$ in porous rock as functions of distance at 10 years; concentration-limited boundary condition. 58
- Fig. 23. Normalized concentration profiles for $^{234}\text{U} \rightarrow ^{230}\text{Th} \rightarrow ^{226}\text{Ra}$ in porous rock as functions of distance at 10^3 years; concentration-limited boundary condition. 59
- Fig. 24. Normalized concentration profiles for $^{245}\text{Cm} \rightarrow ^{241}\text{Am} \rightarrow ^{237}\text{Np} \rightarrow ^{233}\text{U} \rightarrow ^{229}\text{Th}$ in porous rock as functions of distance at 10^5 years; Bateman-type boundary condition. 60
- Fig. 25. Normalized concentration profiles for $^{245}\text{Cm} \rightarrow ^{241}\text{Am} \rightarrow ^{237}\text{Np} \rightarrow ^{233}\text{U} \rightarrow ^{229}\text{Th}$ in porous rock as functions of time at 10^3 m; concentration-limited boundary condition. 62
- Fig. 26. Normalized concentration profiles for $^{245}\text{Cm} \rightarrow ^{241}\text{Am} \rightarrow ^{237}\text{Np} \rightarrow ^{233}\text{U} \rightarrow ^{229}\text{Th}$ in porous rock as functions of distance at 10^5 years; concentration-limited boundary condition. 64
- Fig. 27. Normalized concentration profiles for $^{245}\text{Cm} \rightarrow ^{241}\text{Am} \rightarrow ^{237}\text{Np} \rightarrow ^{233}\text{U} \rightarrow ^{229}\text{Th}$ in porous rock as functions of time at 10^3 m; concentration-limited boundary condition. 65
- Fig. 28. Normalized concentration profiles for $^{234}\text{U} \rightarrow ^{230}\text{Th} \rightarrow ^{226}\text{Ra}$ in porous rock as functions of distance at 10 years; Bateman-type boundary condition. 68
- Fig. 29. Normalized concentration profiles for $^{234}\text{U} \rightarrow ^{230}\text{Th} \rightarrow ^{226}\text{Ra}$ in porous rock as functions of distance at 10^3 years; Bateman-type boundary condition. 69
- Fig. 30. Normalized concentration profiles for $^{234}\text{U} \rightarrow ^{230}\text{Th} \rightarrow ^{226}\text{Ra}$ in porous rock as functions of distance at 10^5 years; Bateman-type boundary condition. 70
- Fig. 31. Normalized concentration profiles for $^{234}\text{U} \rightarrow ^{230}\text{Th} \rightarrow ^{226}\text{Ra}$ in porous rock as functions of time at 10^3 m; Bateman-type boundary condition. 72
- Fig. 32. Normalized concentration profiles for $^{245}\text{Cm} \rightarrow ^{241}\text{Am} \rightarrow ^{237}\text{Np} \rightarrow ^{233}\text{U} \rightarrow ^{229}\text{Th}$ in porous rock as functions of distance at 10^5 years; Bateman-type boundary condition. 73
- Fig. 33. Normalized concentration profiles for $^{245}\text{Cm} \rightarrow ^{241}\text{Am} \rightarrow ^{237}\text{Np} \rightarrow ^{233}\text{U} \rightarrow ^{229}\text{Th}$ in porous rock as functions of time at 10^3 m; Bateman-type boundary condition. 74

EXECUTIVE SUMMARY

This report presents analytic solutions, numerical implementation and numerical illustrations for the transport of radioactive decay chains of arbitrary length in porous media of limited and unlimited extent.

The transport of long radioactive decay chains is especially important in the safety assessment of geologic repositories of spent nuclear fuel in which there are several long chains of the actinides. Failure to account for nuclides generated during transport may result in the underestimation of releases prescribed by regulations. Hitherto no analytic solution nor computer codes have been able to handle long chains. The solutions presented here are exact and general.

It is important to derive solutions for the problem of chain transport in porous media of limited extent for practical reasons. For example, the backfill layer in a nuclear waste package or the damaged rock zone in a repository is a porous medium of finite extent. A different solution is necessary because there may be different fluid flow conditions inside the backfill and outside the backfill in the rock.

The analytic solutions for the problem of chains transport in finite and semi-infinite media are complicated. Sophisticated numerical methods were required in order to implement the solutions as computer programs. These steps are detailed in the report.

The main part of this report are illustrations of the solutions with problems in nuclear waste disposal. We show the transport of two chains, $^{234}\text{U} \rightarrow ^{230}\text{Th} \rightarrow ^{226}\text{Ra}$ and $^{245}\text{Cm} \rightarrow ^{241}\text{Am} \rightarrow ^{237}\text{Np} \rightarrow ^{233}\text{U} \rightarrow ^{229}\text{Th}$, from concentration-limited boundary condition and Bateman-type boundary condition, in a porous region of limited extent such as a backfill and in a semi-infinite field. These illustrations are examples of the capabilities and usefulness of these solutions.

TRANSPORT OF RADIOACTIVE DECAY CHAINS IN FINITE AND SEMI-INFINITE POROUS MEDIA

1. Introduction

In the prediction of radionuclide migration to determine compliance with regulatory standards[1], it may be necessary to consider radioactive decay chains explicitly. Actinide isotopes in spent fuel are mostly members of radioactive decay chains. Failure to account for the generation of daughter nuclides during the migration of the chains may lead to under-estimating cumulative releases or release rates[2] prescribed by regulatory agencies. Available analytic solutions and computer codes such as UCBNE10.2 and UCBNE25[3] have limitations. The UCBNE10.2 code can only compute up to three members with dispersion, and although UCBNE25 gives a non-recursive general solution for a chain of arbitrary length, it can only solve the problem without dispersion. Recently Chambré has generalized the above two solutions[4] and made it possible to obtain non-recursive solutions for chain transport in porous media of both finite and infinite spatial extent.

Transport in a finite domain is of interest for several reasons. In a practical sense such a solution is needed in nuclear waste disposal to evaluate ground-water flow in the region near waste packages, such as within the backfill or damaged rock zone. It is also of general interest. Most systems of equations for ground-water contaminant transport invoke a concentration or flux boundary condition at some location, most often at infinity. In this work we used a mixed boundary condition, allowing the specification of concentration and flux at a specified location rather than at

infinity. We are not aware of other solutions of this type.

The following analyses deal with the migration of radioactive chains of arbitrary length in geologic media. The governing equations are sufficiently general to model species transport by advection and dispersion in a water-saturated porous medium. They can also be applied to diffusional transport of radioactive chains where advection is negligible.

The objectives of this study are: To obtain analytic solutions in closed form of the transport of radioactive decay chains of arbitrary length in porous media of finite and semi-infinite extent; to implement the solutions in computer codes which are practical to use; and use the computer codes for numerical illustrations to show the usefulness of the analytic solutions in the U. S. nuclear waste repository program.

The formulation of the equation system and its solution form are given in Sections 2 and 3 for finite and semi-infinite media, respectively. The solutions give nuclide concentrations in exact closed form (non-recursive) in finite and semi-infinite media. Numerical illustrations of the solutions follow in the respective sections.

Here h is the mass transfer coefficient describing the mass transport at $z=L$, into a medium $z>L$, in which the i^{th} species concentration is a prescribed function $N_i^l(t)$. The boundary position $z=L$ can, for example, be interpreted to represent the biosphere boundary or the backfill-rock interface. As h varies from 0 to ∞ , the flux through the boundary at $z=L$ varies from zero to some maximum value causing the species concentration to decrease there. The left hand side of both (2.3) and (2.4) represent the total fluxes of species i through the boundaries $z=0$ and $z=L$, respectively, while the right hand side represents the rate of supply of the same species in terms of the prescribed integrable function $N_i^p\phi_i(t)$ and $N_i^l(t)$ at $z=0$ and $z=L$, respectively. These functions describe the time release of the chain members from a waste form surface located at $z=0$ and from the biosphere or backfill-rock interface located at $z=L$. In case of no advection the terms involving v are dropped from (2.1) and replaced by other parameters in (2.3) and (2.4) as will be discussed later.

The general form of the equation system (2.1) is

$$\frac{K_i}{D_i} \frac{\partial N_i}{\partial t} + \frac{v}{D_i} \frac{\partial N_i}{\partial z} + \nu_i N_i = \frac{\partial^2 N_i}{\partial z^2} + \nu_{i-1} N_{i-1}, \quad i=1,2,\dots \quad (2.1a)$$

where

$$\nu_0=0, \quad \nu_i=\frac{K_i\lambda_i}{D_i}, \quad \nu_{i-1}=\frac{K_{i-1}\lambda_{i-1}}{D_i} \quad (2.1b)$$

The aim is to obtain the general (non-recursive) analytical solution for $N_i(z,t)$. On account of the linearity of (2.1), the solution for the individual chain member N_i can be represented as a sum of functions, which satisfy (2.1), and selected boundary conditions (2.3) and (2.4). We specify

$$N_1(z,t) = N_1^{(1)}(z,t)$$

$$N_2(z,t) = N_2^{(1)}(z,t) + N_2^{(2)}(z,t)$$

$$N_3(z,t) = N_3^{(1)}(z,t) + N_3^{(2)}(z,t) + N_3^{(3)}(z,t)$$

and for an arbitrary i^{th} member

$$N_i(z,t) = N_i^{(i)}(z,t) + \sum_{j=1}^{i-1} N_i^{(j)}(z,t) \quad (2.5)$$

Thus, in order to obtain the concentration of the i^{th} member, every function $N_i^{(j)}(z,t)$ must be known. We begin with the construction of $N_1^{(1)}(z,t)$. It is chosen to be a solution of (2.1a) (with $\nu_0 = 0$) which satisfies both the initial condition (2.2) and the boundary condition (2.3). This determines $N_1(z,t)$. To determine $N_2(z,t)$ we require two solutions of (2.1a). $N_2^{(1)}(z,t)$ is chosen so that it obeys the initial condition (2.2) and the homogeneous boundary condition (2.3) with $N_2^0 = 0$. This function yields the contribution to $N_2(z,t)$ which is due to the radioactive decay of its precursor $N_1(z,t)$.

$N_2^{(2)}(z,t)$ on the other hand is chosen to satisfy the inhomogeneous boundary condition (2.3), as well as of course (2.2). Since the precursor contribution to $N_2(z,t)$ is already accounted for, the inhomogeneous term $\nu_1 N_1$ is not included in (2.1a) when one solves for $N_2^{(2)}(z,t)$. One proceeds comparably in the construction of $N_3(z,t)$. $N_3^{(1)}(z,t)$ and $N_3^{(2)}(z,t)$ are precursor contributions stemming from chain members $N_1(z,t)$ and $N_2(z,t)$, respectively. Their solutions of (2.1a) satisfy homogeneous boundary conditions, with $N_3^0 = 0$, while $N_3^{(3)}(z,t)$ yields the contribution to $N_3(z,t)$ due to the inhomogeneous boundary condition (2.3), with $N_3^0 \neq 0$. However, for the determination of $N_3^{(3)}(z,t)$ the inhomogeneous term $\nu_2 N_2$ is dropped from (2.1a).

According to this decomposition of the problem, the functions $N_{\ell}^{(j)}(z, t)$ must satisfy the following equation system for $z \in D_{\ell}$, $t > 0$

$$\frac{K_{\ell}}{D_{\ell}} \frac{\partial N_{\ell}^{(j)}}{\partial t} + \frac{v}{D_{\ell}} \frac{\partial N_{\ell}^{(j)}}{\partial z} + \nu_{\ell} N_{\ell}^{(j)} = \frac{\partial^2 N_{\ell}^{(j)}}{\partial z^2} + \nu_{\ell-1} N_{\ell-1}^{(j)},$$

$$\nu_0 = 0, \quad \ell = 1, 2, \dots, i, \quad j \leq \ell. \quad (2.6)$$

The functions are subject to

$$N_{\ell}^{(j)}(z, 0) = 0 \quad (2.7)$$

$$-D_{\ell} \epsilon \frac{\partial N_{\ell}^{(j)}(0, t)}{\partial z} + v \epsilon N_{\ell}^{(j)}(0, t) = \delta_{\ell j} N_{\ell}^0 v \epsilon \phi_j(t), \quad j \leq \ell \quad (2.8)$$

$$-D_{\ell} \epsilon \frac{\partial N_{\ell}^{(j)}(L, t)}{\partial z} + v \epsilon N_{\ell}^{(j)}(L, t) = h \left[N_{\ell}^{(j)}(L, t) - \delta_{\ell j} N_{\ell}^1(t) \right], \quad j \leq \ell, \quad t > 0 \quad (2.9)$$

where $\delta_{\ell j}$ is the Kronecker delta which vanishes for $\ell \neq j$ and is unity for $\ell = j$. Furthermore

$$N_{\ell-1}^{(j)}(z, t) \equiv 0, \quad \text{for } \ell \leq j \quad (2.10)$$

which assures that for $\ell \leq j$ the inhomogeneous (source) term $\nu_{\ell-1} N_{\ell-1}$ vanishes. At this point one can verify that the solution to (2.6) through (2.8) when substituted into (2.5) will satisfy the original equation system (2.1) to (2.4) due to the linearity of this system.

We now take the Laplace transform of (2.6) with respect to the time variable and define

$$\bar{N}_{\ell}^{(j)}(z, s) \equiv \int_0^{\infty} e^{-st} N_{\ell}^{(j)}(z, t) dt; \quad \bar{\phi}_j(s) \equiv \int_0^{\infty} e^{-st} \phi_j(t) dt$$

The transform of (2.6), on utilizing the initial condition (2.8), yields

$$\frac{d^2 \bar{N}_\ell^{(j)}}{dz^2} - \frac{v}{D_\ell} \frac{d \bar{N}_\ell^{(j)}}{dz} - \left(\frac{K_\ell}{D_\ell} s + \nu_\ell \right) \bar{N}_\ell^{(j)} = -\nu_{\ell-1} \bar{N}_{\ell-1}^{(j)} \quad (2.11)$$

for $\bar{N}_\ell^{(j)} = \bar{N}_\ell^{(j)}(z, s)$. It is convenient to remove the first-order derivative term by setting

$$\bar{N}_\ell^{(j)}(z, s) = e^{\frac{v}{2D_\ell} z} n_\ell^{(j)}(z, s) \quad (2.12)$$

Then

$$\frac{d^2 n_\ell^{(j)}}{dz^2} - \left[\frac{K_\ell}{D_\ell} s + \nu_\ell + \left(\frac{v}{2D_\ell} \right)^2 \right] n_\ell^{(j)} = -\nu_{\ell-1} n_{\ell-1}^{(j)} e^{-\frac{vz}{2} \left(\frac{1}{D_\ell} - \frac{1}{D_{\ell-1}} \right)} \quad (2.13)$$

With

$$\mu_\ell \equiv \left[\frac{K_\ell}{D_\ell} s + q_\ell^2 \right], \quad q_\ell^2 \equiv \left[\nu_\ell + \left(\frac{v}{2D_\ell} \right)^2 \right], \quad \gamma_\ell \equiv \frac{v}{2} \left(\frac{1}{D_\ell} - \frac{1}{D_{\ell-1}} \right) \quad (2.13a)$$

(2.13) reduces to the compact form

$$\frac{d^2 n_\ell^{(j)}(z, s)}{dz^2} - \mu_\ell n_\ell^{(j)}(z, s) = -\nu_{\ell-1} n_{\ell-1}^{(j)}(z, s) e^{-\gamma_\ell z}, \quad j \leq \ell$$

This differential-difference equation system with variable coefficients is the governing equation of our problems. Also, (2.10) transforms to

$$n_{\ell-1}^{(j)}(z, s) \equiv 0, \quad \ell \leq j \quad (2.14)$$

The general solution to these equations is a matter of some complexity. Here we consider two special cases of (2.13) which describe a number of physically important models.

Equal Dispersion Coefficients

We assume the dispersion coefficients of the radioactive species in the medium are equal, i.e., $D_\ell = D$ for all ℓ . Then γ_ℓ vanishes, removing the complicating

exponential term from (2.13), resulting

$$\frac{d^2 n^{(j)}(z,s)}{dz^2} - \mu_\ell n^{(j)}(z,s) = -\nu_{\ell-1} n^{(j)}(z,s), \quad j \leq \ell \quad (2.15)$$

The boundary conditions transform to

$$-D\epsilon \frac{\partial n^{(j)}(0,s)}{\partial z} + h_1 n^{(j)}(0,s) = \delta_{\ell,j} N \gamma_\ell v \epsilon \phi_\ell(s), \quad j \leq \ell \quad (2.16)$$

$$D\epsilon \frac{\partial n^{(j)}(L,s)}{\partial z} + h_2 n^{(j)}(L,s) = \delta_{\ell,j} h \epsilon^{-\frac{vL}{2D}} N \gamma_\ell(s), \quad j \leq \ell \quad (2.17)$$

with $h_1 = \frac{\epsilon v}{2}$, $h_2 = h - \frac{\epsilon v}{2}$. The corresponding equation system (2.1) together with (2.2) to (2.4) describes the migration problem in the presence of advection and dispersion.

For a type-III boundary condition of the form (2.8) and (2.9), the general (non-recursive) analytical solution for radioactive chains of arbitrary length has so far not been available to us. As mentioned earlier, the most extensive model to date has been the recursive three-member chain in a semi-infinite domain D_∞ on which the computer code UCBNE10.2 is based. The other non-recursive solution/computer code, UCBNE25, applies only for the case $D=0$ in a semi-infinite domain. In this section we shall solve the problem in D_f , while in the next section a solution in D_∞ will be derived.

Negligible Ground-water Velocity

Consider again the governing equation (2.13) but now without advection, i.e., $v=0$. By (2.13a) γ_ℓ vanishes, thus removing the variable coefficient term from the differential-difference equation system. For this case, the species diffusion coefficient D_ℓ need not be identical in order to obtain an analytical solution. The advection-free

formulation is applicable to the rock fracture problem where one wishes to account for the diffusion of radioactive species into rock from water-filled fissures. Another possible application can be found in the analysis of the diffusive migration of radionuclide chains with small half-lives in a water-saturated backfill region which surrounds a waste form. Densely-packed backfill materials, such as bentonite, have very low permeability to water flow so that the principal mechanism of transport through the layer may occur by diffusion. In case of the rock fracture problem the domain can be either D_f or D_∞ while in the backfill problem it is D_f .

At the present time there appear to be insufficient data to apply the formulation to the diffusion of species with anisotropic diffusion coefficients. For this reason we conduct the analysis, assuming the radionuclides satisfy equation (2.15). The solution given below can however be readily generalized to include unequal D'_s if desired.

Since the boundary conditions remain the same mathematical form as in (2.16) and (2.17) it is seen that the advection-free problem is merely a special case of the equal-dispersion problem obtained by setting $v=0$ in the governing equation (2.13) and replacing the dispersion coefficient with the diffusion coefficient. The two quantities h_1 and h_2 defined in (2.16) and (2.17) as well as their right hand side functions also need to be specially assigned accordingly. In the following we shall concentrate on the solution of the equal-dispersion/diffusion case, and the solution procedures used there can also be applied to the problem in D_∞ .

The Solution of the Problem in D_f

The solution of the system of equations (2.15) in D_f is constructed with help of a finite Fourier transform with respect to the variable z . We define

$$n\{^j\}(\beta_m, s) = \int_0^L K(\beta_m, z) n\{^j\}(z, s) dz \quad (2.18)$$

The Fourier kernel $K(\beta_m, z)$ satisfies the Sturm-Liouville system

$$\frac{d^2 K(\beta_m, z)}{dz^2} + \beta_m^2 K(\beta_m, z) = 0 \quad (2.19)$$

$$-D\epsilon \frac{dK(\beta_m, 0)}{dz} + h_1 K(\beta_m, 0) = 0 \quad (2.20a)$$

$$D\epsilon \frac{dK(\beta_m, L)}{dz} + h_2 K(\beta_m, L) = 0 \quad (2.20b)$$

The β'_m 's are the positive eigenvalues of this system. The kernel has the form*

$$K(\beta_m, z) = \sqrt{2} \frac{\beta_m \cos(\beta_m z) + \alpha_1 \sin(\beta_m z)}{\left[(\beta_m^2 + \alpha_1^2) \left(L + \frac{\alpha_2}{\beta_m^2 + \alpha_2^2} \right) + \alpha_1 \right]^{1/2}} \quad (2.21)$$

where $\alpha_1 = \frac{h_1}{D\epsilon}$, $\alpha_2 = \frac{h_2}{D\epsilon}$. The eigenvalues form a discrete, countable spectrum which is given by the solutions of the transcendental equation

$$\tan(\beta_m L) = \frac{\beta_m (\alpha_1 + \alpha_2)}{\beta_m^2 - \alpha_1 \alpha_2}, \quad m=1, 2, \dots$$

If one applies the kernel to every term of (2.15) and integrates with respect to z over the interval $(0, L)$ there results in view of (2.18), since $\gamma=0$,

$$\int_0^L \frac{d^2 n\{^j\}(z, s)}{dz^2} K(\beta_m, z) dz - \mu_t n\{^j\}(\beta_m, s) = -\nu_{t-1} n\{^j\}_1(\beta_m, s) \quad (2.22)$$

The integral term J yields, with integration by parts,

$$J \equiv \int_0^L \frac{d^2 n\{^j\}(z, s)}{dz^2} K(\beta_m, z) dz = \left[K(\beta_m, z) \frac{dn\{^j\}(z, s)}{dz} - \right.$$

*P. L. Chambré, class notes taught in U. C. Berkeley.

$$-n^{(j)}(z,s) \frac{dK(\beta_m,z)}{dz} \Bigg|_{z=0}^{z=L} - \beta_m^2 n^{(j)}(\beta_m,s) \quad (2.23)$$

By (2.20) and (2.21)

$$\frac{dK(\beta_m,0)}{dz} = \alpha_1 K(\beta_m,0); \quad \frac{dK(\beta_m,L)}{dz} = -\alpha_2 K(\beta_m,L) \quad (2.24)$$

so that

$$\begin{aligned} J = & K(\beta_m,L) \left[\frac{dn^{(j)}(L,s)}{dz} + \alpha_2 n^{(j)}(L,s) \right] - \\ & - K(\beta_m,0) \left[\frac{dn^{(j)}(0,s)}{dz} - \alpha_1 n^{(j)}(0,s) \right] - \beta_m^2 n^{(j)}(\beta_m,s) \end{aligned} \quad (2.25)$$

On applying equations (2.16) and (2.17) together with (2.21) results in

$$J = K(\beta_m,L) \delta_{\ell j} \frac{h}{D\epsilon} e^{-\frac{vL}{2D}} N_1(s) + K(\beta_m,0) \delta_{\ell j} N_2^0 \frac{v}{D\epsilon} \phi_d(s) - \beta_m^2 n^{(j)}(\beta_m,s) \quad (2.26)$$

When this is substituted into (2.22), one obtains the difference equation

$$n^{(j)}(\beta_m,s) = \frac{[\nu_{\ell-1} n^{(j)}_1(\beta_m,s) + \delta_{\ell j} g_d(\beta_m,s)]}{\beta_m^2 + \mu_\ell}, \quad j \leq \ell \quad (2.27)$$

where

$$g_d(\beta_m,s) \equiv \frac{K(\beta_m,L)}{D\epsilon} h \epsilon^{-\frac{vL}{2D}} N_1(s) + \frac{K(\beta_m,0)}{D\epsilon} N_2^0 v \epsilon \phi_d(s) \quad (2.28)$$

and h is the mass transfer coefficient defined in (2.4). Equation (2.14) transforms to

$$n^{(j)}_1(\beta_m,s) = 0, \quad \ell \leq j \quad (2.14a)$$

Equation (2.27) is solved in a recursive manner by setting $j=1$ and letting ℓ run from $\ell=1$ to $\ell=i$. This process is repeated for $j=2,3,\dots,i$ in order to obtain the solution for the i members of the chain.

Starting with $j=1$, and letting ℓ run through the values $1, 2, \dots, i$, one takes from (2.14a) $n_\ell^{(j)}(\beta_m, s) = 0$, so that (2.27) yields

$$\begin{aligned} n_1^{(1)}(\beta_m, s) &= \frac{g_1(\beta_m, s)}{\beta_m^2 + \mu_1} \\ n_2^{(1)}(\beta_m, s) &= \frac{\nu_1 n_1^{(1)}(\beta_m, s)}{\beta_m^2 + \mu_2} = \frac{\nu_1 g_1(\beta_m, s)}{(\beta_m^2 + \mu_1)(\beta_m^2 + \mu_2)} \\ &\dots \dots \dots \\ n_i^{(1)}(\beta_m, s) &= \frac{\nu_1 \nu_2 \cdots \nu_{i-1} g_1(\beta_m, s)}{(\beta_m^2 + \mu_1)(\beta_m^2 + \mu_2) \cdots (\beta_m^2 + \mu_i)} \end{aligned}$$

Next one takes $j=2$ and lets ℓ run through the values $1, 2, \dots, i$. From (2.14a) one has $n_\ell^{(2)}(\beta_m, s) = 0$. Hence (2.27) yields

$$\begin{aligned} n_2^{(2)}(\beta_m, s) &= \frac{g_2(\beta_m, s)}{\beta_m^2 + \mu_2} \\ n_3^{(2)}(\beta_m, s) &= \frac{\nu_2 n_2^{(2)}(\beta_m, s)}{\beta_m^2 + \mu_3} = \frac{\nu_2 g_2(\beta_m, s)}{(\beta_m^2 + \mu_2)(\beta_m^2 + \mu_3)} \\ &\dots \dots \dots \\ n_i^{(2)}(\beta_m, s) &= \frac{\nu_2 \nu_3 \cdots \nu_{i-1} g_2(\beta_m, s)}{(\beta_m^2 + \mu_2)(\beta_m^2 + \mu_3) \cdots (\beta_m^2 + \mu_i)} \end{aligned}$$

Continuing in this manner one shows that in general,

$$n_i^{(j)}(\beta_m, s) = \frac{A_i^{(j)} g_j(\beta_m, s)}{\prod_{n=j}^i (\beta_m^2 + \mu_n)}, \quad i > j \quad (2.29)$$

where

$$A_i^{(j)} = \prod_{r=j}^{i-1} \nu_r, \quad (2.30)$$

while for $j=i$ one has

$$n_i^{(i)}(\beta_m, s) = \frac{g_i(\beta_m, s)}{\beta_m^2 + \mu_i} \quad (2.31)$$

Equations (2.29)-(2.31) represent the solution of the difference equations (2.27) and (2.28).

We turn next to the Laplace inversion process with respect to the t variable. By (2.13a), with $D_n = D$, one has $\beta_m^2 + \mu_n = \frac{K_n}{D}(s + \delta_n)$, where

$$\delta_n = \frac{D}{K_n}(\beta_m^2 + q_n^2). \quad (2.32)$$

Hence (2.29) becomes

$$n_i^{(j)}(\beta_m, s) = \frac{D}{K_i} C_i^{(j)} \frac{g_j(\beta_m, s)}{\prod_{n=j}^i (s + \delta_n)}, \quad (2.33)$$

with

$$C_i^{(j)} = \frac{A_i^{(j)}}{\prod_{n=j}^{i-1} \frac{K_n}{D}} = \prod_{n=j}^{i-1} \lambda_n \quad (2.34)$$

Now the inversion of $\prod_{n=j}^i (s + \delta_n)^{-1}$ is

$$\mathbf{L}^{-1} \left\{ \frac{1}{\prod_{n=j}^i (s + \delta_n)} \right\} = \sum_{n=j}^i \frac{e^{-\delta_n t}}{\prod_{\substack{r=j \\ r \neq n}}^i (\delta_r - \delta_n)} \quad (2.36)$$

If one applies the convolution theorem to $g_j(\beta_m, t)$ and $e^{-\delta_n t}$, with the $*$ denoting the convolution integral defined by

$$a(t) * b(t) \equiv \int_0^t a(\tau) b(t - \tau) d\tau,$$

equations (2.29) and (2.30) yield,

$$n_i^{(j)}(\beta_m, t) = \frac{D}{K_i} C_i^{(j)} \sum_{n=j}^i \frac{g_j(\beta_m, t) * e^{-\delta_n t}}{\prod_{\substack{r=j \\ r \neq n}}^i (\delta_r - \delta_n)}, \quad i > j \quad (2.37)$$

$$n_i^{(i)}(\beta_m, t) = \frac{D}{K_i} g_i(\beta_m, t) * e^{-\delta_i t} \quad (2.38)$$

This is followed by the Fourier inversion with respect to the z variable. The inverse transform of (2.18) is given by (with ℓ now replaced by i in $n_i^{(j)}$)

$$n_i^{(j)}(z, t) = \sum_{m=1}^{\infty} K(\beta_m, z) n_i^{(j)}(\beta_m, t), \quad i > j \quad (2.39)$$

$$n_i^{(i)}(z, t) = \sum_{m=1}^{\infty} K(\beta_m, z) n_i^{(i)}(\beta_m, t), \quad i = j \quad (2.40)$$

The $n_i^{(j)}(\beta_m, t)$ in the summation are taken from equations (2.37) and (2.38). The inversion can be shown to be valid if $n_i^{(j)}(z, t)$ is continuous and satisfies Dirichlet conditions on $0 \leq z \leq L$ with $t > 0$. From (2.32) one separates the β_m^2 dependence as follows

$$\delta_n - \delta_r = \Gamma_{rn} \beta_m^2 + \gamma_{rn} \quad (2.41)$$

where

$$\Gamma_{rn} = D \left(\frac{1}{K_n} - \frac{1}{K_r} \right), \quad \gamma_{rn} = \left[(\lambda_n - \lambda_r) + \left(\frac{v}{2D} \right)^2 \Gamma_{rn} \right] \quad (2.42)$$

There results with (2.37), (2.39), and (2.41), on substitution into (2.39) and (2.40), the inverse function

$$n_i^{(j)}(z, t) = \frac{D}{K_i} C_i^{(j)} \sum_{n=j}^i \sum_{m=1}^{\infty} \frac{K(\beta_m, z) g_j(\beta_m, t) * e^{-\delta_n t}}{\prod_{\substack{r=j \\ r \neq n}}^i (\Gamma_{nr} \beta_m^2 + \gamma_{nr})}, \quad i > j$$

$$n_i^{(i)}(z, t) = \frac{D}{K_i} \sum_{m=1}^{\infty} K(\beta_m, z) g_i(\beta_m, t) * e^{-\delta_i t}$$

On re-introducing the exponential multiplier of (2.12) into the last two equations one

obtains all component parts of the solution for the chain member i . The substitution into (2.5) yields the general, non-recursive solution in D_t ,

$$N_i(z,t) = e^{\frac{vz}{2D}} \frac{D}{K_i} \left[\sum_{m=1}^{\infty} K(\beta_m, z) g_i(\beta_m, t) * e^{-\delta_i t} + \sum_{j=1}^{i-1} C_i^{(j)} \sum_{n=j}^i \sum_{m=1}^{\infty} \frac{K(\beta_m, z) g_j(\beta_m, t) * e^{-\delta_n t}}{\prod_{\substack{r=j \\ r \neq n}}^i (\Gamma_{nr} \beta_m^2 + \gamma_{nr})} \right], \quad i=1, 2, \dots, z > 0, t > 0 \quad (2.43)$$

It is readily verified that the dimensional terms in these equations have the following units (cgs):

$$K(\beta_m, z) = [\sqrt{1/cm}], \quad g_j(\beta_m, t) = [gm/(cm)^{-9/2}], \quad * = [sec], \quad \delta_n = [sec^{-1}], \\ C_i^{(j)} = [sec^{j-i}], \quad \Gamma_{nr} = [cm^2/sec], \quad \beta_m^2 = [cm^{-2}], \quad \gamma_{nr} = [sec^{-1}], \quad D = [cm^2/sec]$$

It follows from this that $N_i(z,t) = [gm/cm^3]$, as required. The form of the solution (2.43) does not explicitly exhibit the steady state form of the solution $N_i(z, \infty)$. This limiting form is contained in the convolution time integrals and it results on letting $t \rightarrow \infty$. Alternately if one sets $s=0$ in (2.33) (for $i \geq j$) and proceeds with the Fourier inversion with respect to z , following the indicated steps, one is led to $N_i(z, \infty)$. The resulting series can in some instances be summed in terms of elementary functions.

2.2. Numerical Evaluations

We illustrate the theory with an application of the solution in the finite span $D_t: 0 < z < L$. It is assumed that the chains originate at the repository boundary $z=0$, i.e., there is no other source in the span. The boundary condition at $z=0$ will be of type I, which is a special case of the one specified in (2.3). The other boundary

condition at $z=L$ will be retained in its generality. Both type I and type III boundary conditions will be applied to $z=L$ while two kinds of initial conditions for $N_i(0,t)$, $i=1,2, \dots$ will be used.

2.2.1. Case 1: Constant Concentration at Boundaries

In the first example we use the backfill in a nuclear waste package as the porous medium of finite extent. At $z=0$ is the waste form-backfill interface and at $z=L$ is the outer edge of the backfill, or the backfill-rock interface. We use the following boundary conditions:

$$N_i(0,t)=N_i^0, \quad t>0, \quad i=1,2, \dots \quad (2.44)$$

$$N_i(L,t)=0, \quad t>0, \quad i=1,2, \dots \quad (2.45)$$

(2.44) means that the waste package holds intact long enough that all members in the specified decay chain have reached either their solubility limits or the secular equilibrium before they start leaching out. (2.45) implies that a sink (e.g., a strong water flow) exists outside the backfill. Later, this type I boundary condition at $z=L$ will be replaced by the general form of (2.4). As mentioned before, these boundary conditions are the special forms of (2.3) and (2.4) for which the original problem was solved. By specializing the parameters in the previous section, the solution to the present problem is obtained by a limiting procedure.

First the kernel function $K(\beta_m, z)$ is constructed from the equation system (2.19) and (2.20) with homogeneous boundary conditions of type I. The comparison shows that in the present case $D \rightarrow 0$ in (2.20a) and (2.20b), so that $\alpha_1 \rightarrow \infty$, $\alpha_2 \rightarrow \infty$. With this (2.21) yields in the limit the kernel function

$$K(\beta_m, z) = \sqrt{\frac{2}{L}} \sin(\beta_m z) \quad (2.46)$$

The eigenvalues β_m are determined from

$$\sin \beta_m L = 0$$

with the positive solutions

$$\beta_m = \frac{m\pi}{L}, \quad m=1, 2, \dots \quad (2.47)$$

Now the theory developed above, and specifically the set of equations (2.23) to (2.27), assumes that the boundary conditions for $K(\beta_m, z)$ at $z=0$ and $z=L$ are of type III, i.e., of the forms of (2.20a) and (2.20b). Since in the present case the boundary conditions are of type I and thus do not involve the derivative term one must formally make the following limiting replacements in (2.28):

$$\frac{K(\beta_m, L)}{D\epsilon} = -\frac{1}{h_2} \frac{\partial K(\beta_m, L)}{\partial z}; \quad \frac{K(\beta_m, 0)}{D\epsilon} = \frac{1}{h_1} \frac{\partial K(\beta_m, 0)}{\partial z} \quad (2.48)$$

where in this case $h_1 = \epsilon v$, $h_2 = h - \epsilon v$. Further, a comparison of (2.45) with (2.4) shows that $N_i^1(t) = 0$ so that $N_i^1(s) = 0$. This leaves only the second term in (2.28) which reduces in time domain with the above to

$$g_i(\beta_m, t) = \frac{\partial K(\beta_m, 0)}{\partial z} N_i^2 = \sqrt{\frac{2}{L}} \beta_m N_i^2 \quad (2.49)$$

With $K(\beta_m, z)$ and $g_i(\beta_m, t)$ determined the solution of the problem is given by (2.43)

which reduces to

$$N_i(z, t) = e^{-\frac{vz}{2D}} \frac{2}{L} \frac{D}{K_i} \left\{ N_i^2 \sum_{m=1}^{\infty} \frac{\beta_m \sin \beta_m z}{\delta_i} (1 - e^{-\delta_i t}) + \right.$$

$$+ \left. \sum_{j=1}^{i-1} C_i^{(j)} N_j^0 \sum_{n=j}^i \sum_{\substack{m=1 \\ r=j \\ r \neq n}}^{\infty} \frac{\beta_m \sin \beta_m z}{\prod_{r=j}^i (\Gamma_{nr} \beta_m^2 + \gamma_{nr}) \delta_n} (1 - e^{-\delta_n t}) \right\} z > 0, t > 0, i = 1, 2, \dots \quad (2.50)$$

Next we will show that Equation (2.50) is a special (limiting) case of the more general solution of type III boundary condition at $z=L$. Here we use the general form of (2.4), with $N_i^l=0$, instead of (2.45) at $z=L$, i.e.,

$$-D\epsilon \frac{\partial N_i(L,t)}{\partial z} + v\epsilon N_i(L,t) = hN_i(L,t), t > 0 \quad (2.51)$$

which means the material is transported into a medium with zero average concentration outside the domain D_f . This is true if the finite domain is surrounded by an infinite medium, e.g., a backfill layer surrounded by rock. Since in this case $D=0$ only in (2.20a), we have

$$\alpha_1 = \infty, \quad \alpha_2 = \frac{h_2}{D\epsilon} = \frac{h - \frac{v\epsilon}{2}}{D\epsilon}$$

and the kernel becomes

$$K(\beta_m, z) = \sqrt{\frac{2}{L + \ell_m}} \sin(\beta_m z), \quad (2.52)$$

where

$$\ell_m = \frac{\alpha_2}{\beta_m^2 + \alpha_2^2} \quad (2.53)$$

The eigenvalues β_m are now determined from

$$\tan \beta_m L = -\frac{\beta_m}{\alpha_2} \quad (2.54)$$

which is to be solved numerically. With the help of (2.48) now evaluated at $z=0$, one has

$$g_d(\beta_m, t) = \sqrt{\frac{2}{L + \ell_m}} \beta_m N_i^0 \quad (2.55)$$

The final result from (2.50) and (2.55) is

$$N_i(z, t) = e^{\frac{vz}{2D}} \frac{D}{K_i} \left\{ N_i^0 \sum_{m=1}^{\infty} \left(\frac{2}{L + \ell_m} \right) \frac{\beta_m \sin \beta_m z}{\delta_i} (1 - e^{-\delta_i t}) + \sum_{j=1}^{i-1} C_i^{(j)} N_j^0 \sum_{n=j}^i \sum_{m=1}^{\infty} \left(\frac{2}{L + \ell_m} \right) \frac{\beta_m \sin \beta_m z}{\prod_{\substack{r=j \\ r \neq n}}^i (\Gamma_{nr} \beta_m^2 + \gamma_{nr}) \delta_n} (1 - e^{-\delta_n t}) \right\}, \quad z > 0, t > 0, i = 1, 2, \dots \quad (2.56)$$

When h , the mass transfer coefficient, becomes very large, i.e., $h \rightarrow \infty$, which is simulated by a very strong water flow outside the domain D_f and results in a large mass transfer rate into the outside region, one finds from the definition of α_2 , that $\alpha_2 \rightarrow \infty$. From (2.53) one has $\ell_m \rightarrow 0$ and hence from (2.52) and (2.55)

$$K(\beta_m, z) = \sqrt{\frac{2}{L}} \sin(\beta_m z); \quad g_d(\beta_m, t) = \sqrt{\frac{2}{L}} \beta_m N_i^0$$

which are identical to (2.46) and (2.49), respectively, and the transcendental equation (2.54) returns to $\sin \beta_m L = 0$ with the positive solutions specified in (2.47). Therefore, the final solution (2.56) reduces to (2.50). This demonstrates that the boundary condition (2.45) and hence the solution (2.50) is a limiting case of the more general form (2.51) and (2.56) by letting $h \rightarrow \infty$.

Two computer codes were developed for the above two cases. UCBNE50 is used for equation (2.50) for infinite h and UCBNE51 is used for equation (2.56) for finite h . The following results are calculated using these programs.

Numerical Examples

The decay chains considered in this report are $^{245}\text{Cm} \rightarrow ^{241}\text{Am} \rightarrow ^{237}\text{Np} \rightarrow ^{233}\text{U} \rightarrow ^{229}\text{Th}$ and $^{234}\text{U} \rightarrow ^{230}\text{Th} \rightarrow ^{226}\text{Ra}$. The first one is chosen to show that our solution and algorithm are capable of computing the transport of a chain of more than three members, while the second one is an important chain as far as nuclear waste disposal and the human environment are concerned. The domain we consider in this and the next section is the backfill layer in a nuclear waste package. Because nuclear waste repositories are likely to be located in regions of low ground water flow, we will assume a zero pore water velocity ($v=0$) in the calculations though the solution and the computer code are not limited by this assumption.

The mass transfer coefficient, h , needs more consideration. Because we are not aware of any experimental data available for this parameter, two previous analyses are used to estimate a value [2]. Both analyses give the same result ($\sim 10^{-4}$ m/yr) which will be used as the basis for comparisons. For parametric studies another value of h used in the calculations is 10^4 m/yr, which simulates a very strong water flow outside the backfill.

The values for other parameters are for a potential wet-rock repository in basalt[5]. The values are: backfill thickness $L=30$ cm, diffusion coefficient $D=10^{-5}$ $\text{cm}^2/\text{sec} = 3.15 \times 10^{-2}$ m^2/yr , and porosity of the backfill $\epsilon=0.3$. Other parameters used

in these calculations are listed in the following tables and in the figures.

Figure 1 shows the concentration of the $^{234}\text{U} \rightarrow ^{230}\text{Th} \rightarrow ^{226}\text{Ra}$ chain, normalized to N_i^0 , as a function of distance at 10 years. ^{234}U travels faster than the other two nuclides due to the smaller retardation coefficient. At 10 years none of the nuclides have reached the outer boundary of the backfill, even for the fastest moving ^{234}U . At this time the boundary condition (2.51) has no effect at all. In fact, this figure is valid for all values of h at this time. This suggests that the semi-infinite medium solution to be discussed later can be used to evaluate nuclide concentrations during the early time period.

In (2.50) and (2.56), the solutions include multiple summations and one of which is an infinite series. Since we cannot in reality compute an infinite series, some error bound must be imposed to stop the calculations. Here we use 10^{-8} as our criterion. Thus when the sum of twenty (20) consecutive terms is less than 10^{-8} times the total sum, the computation of the infinite series is stopped. Since the number of terms

Parameters for Calculations

Nuclides	^{234}U	^{230}Th	^{226}Ra
K_i	120	1500	300
$T_{1/2}$ (yrs)	2.47×10^5	8×10^4	1600
N_i^0	1	1	10

Nuclides	^{245}Cm	^{241}Am	^{237}Np	^{233}U	^{229}Th
K_i	150	1020	60	120	1500
$T_{1/2}$ (yrs)	8500	430	2.14×10^6	1.59×10^5	7430
N_i^0	1	0.1	1	1	1

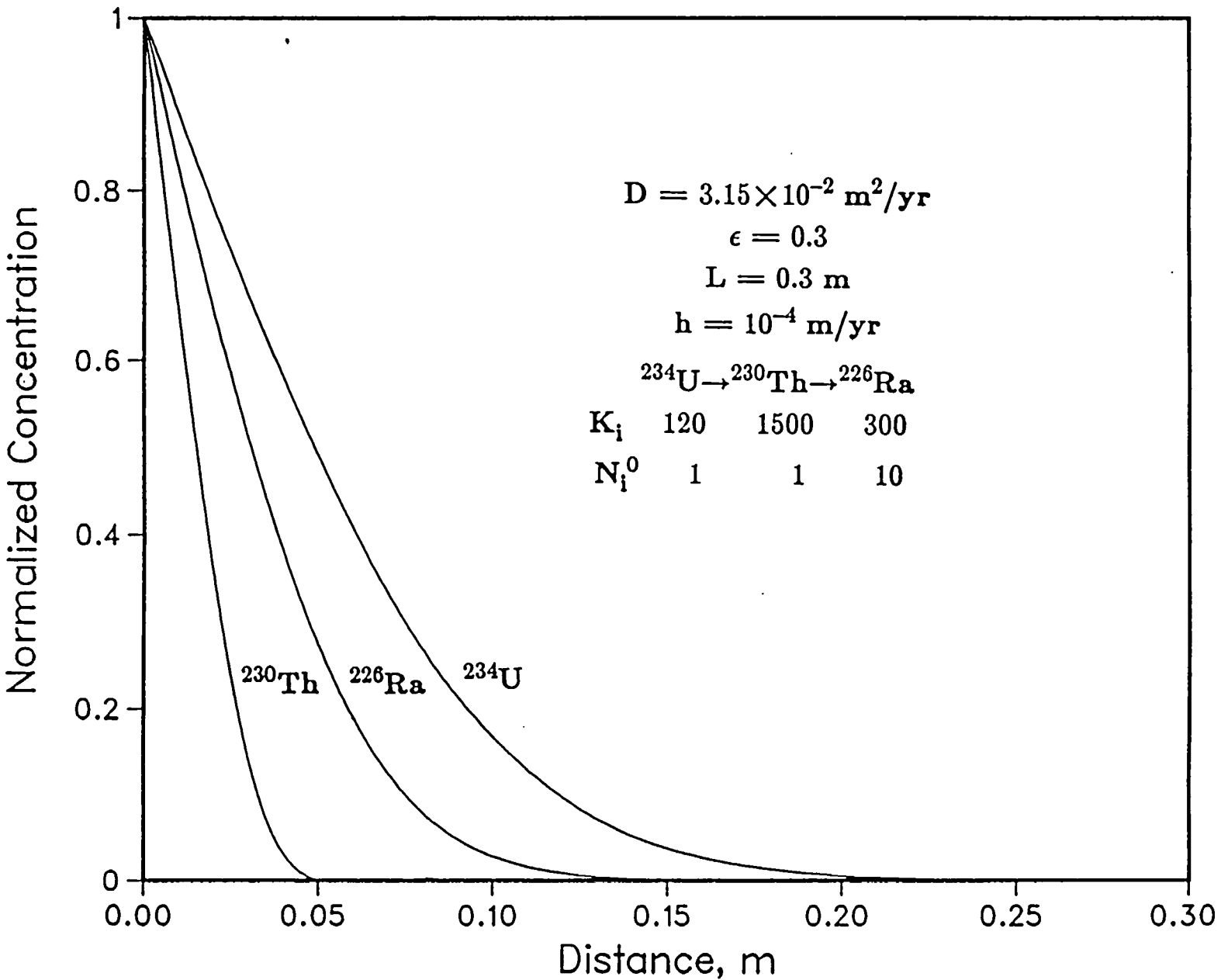


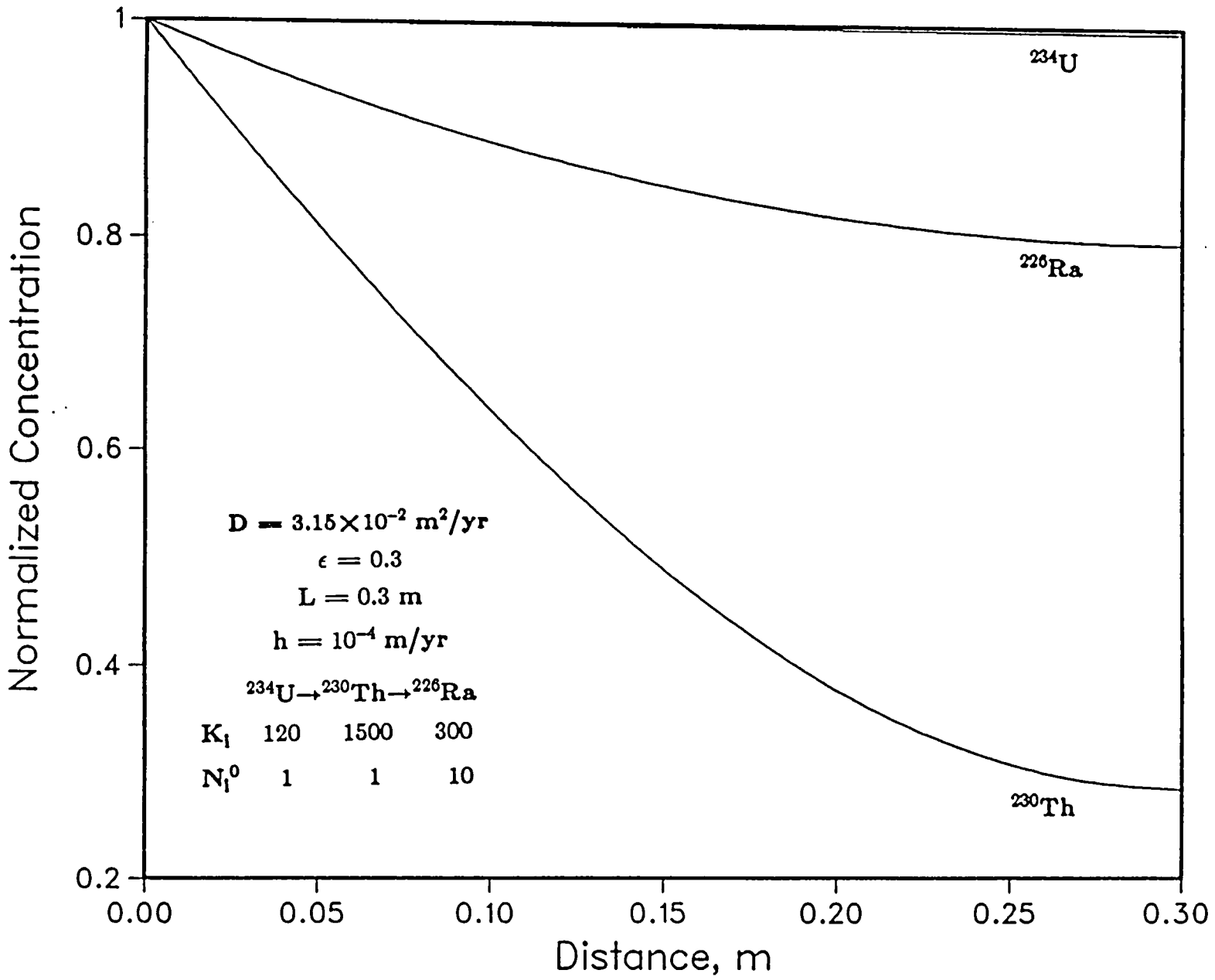
Fig. 1. Normalized concentration profiles for $^{234}\text{U} \rightarrow ^{230}\text{Th} \rightarrow ^{226}\text{Ra}$ in backfill as functions of distance at 10 years; concentration-limited boundary condition.

required is dependent upon the parameters used, it is difficult to predict the exact value of this number. However, one can see from the form of the solution that the sine series would converge very slowly at small t , since it behaves as $\sin(nz)/n$ for large n , as in (2.32) and (2.47). This means a large number of terms is needed to make such calculations. To avoid this difficulty use the semi-infinite medium solution for early time calculations. The semi-infinite solution will be derived in the next section and is much more convenient to use. It contains no infinite series and is more economic in computations. We will discuss this further in Section 3.

Figure 2 shows the concentration field at 1000 years. At this time ^{234}U has reached steady state and the backfill is no longer retarding its migration. Since the decay of ^{234}U is slow ($T_{1/2}=2.47\times 10^5$ years) its concentration is practically constant over the whole backfill. On the other hand, although ^{226}Ra is also in its equilibrium state (to be shown in Figure 4) the decay effect is readily observable from the concentration drop through the backfill ($\sim 20\%$). ^{230}Th , however, is not in its equilibrium state due to the high retardation coefficient ($K=1500$). The concentration profile of ^{230}Th is still rising at this time and will reach its steady state at about 10^4 years, as will be seen in next two figures. Another important fact is that for $h=10^{-4}$ m/yr the outer edge of the backfill acts as an insulated surface since the concentration gradient at $z=L$ is nearly zero, as shown in Fig. 2.

Figure 3 shows the normalized concentration as a function of time at the outer edge of backfill. Figure 4 shows the flux, normalized to N_0^0 , of each member at both ends of backfill as a function of time. The solid curves represent the mass fluxes at inner surface while the dashed curves the mass fluxes at outer surface. Both figures

Fig. 2. Normalized concentration profiles for $^{234}\text{U} \rightarrow ^{230}\text{Th} \rightarrow ^{226}\text{Ra}$ in backfill as functions of distance at 10^3 years; concentration-limited boundary condition.



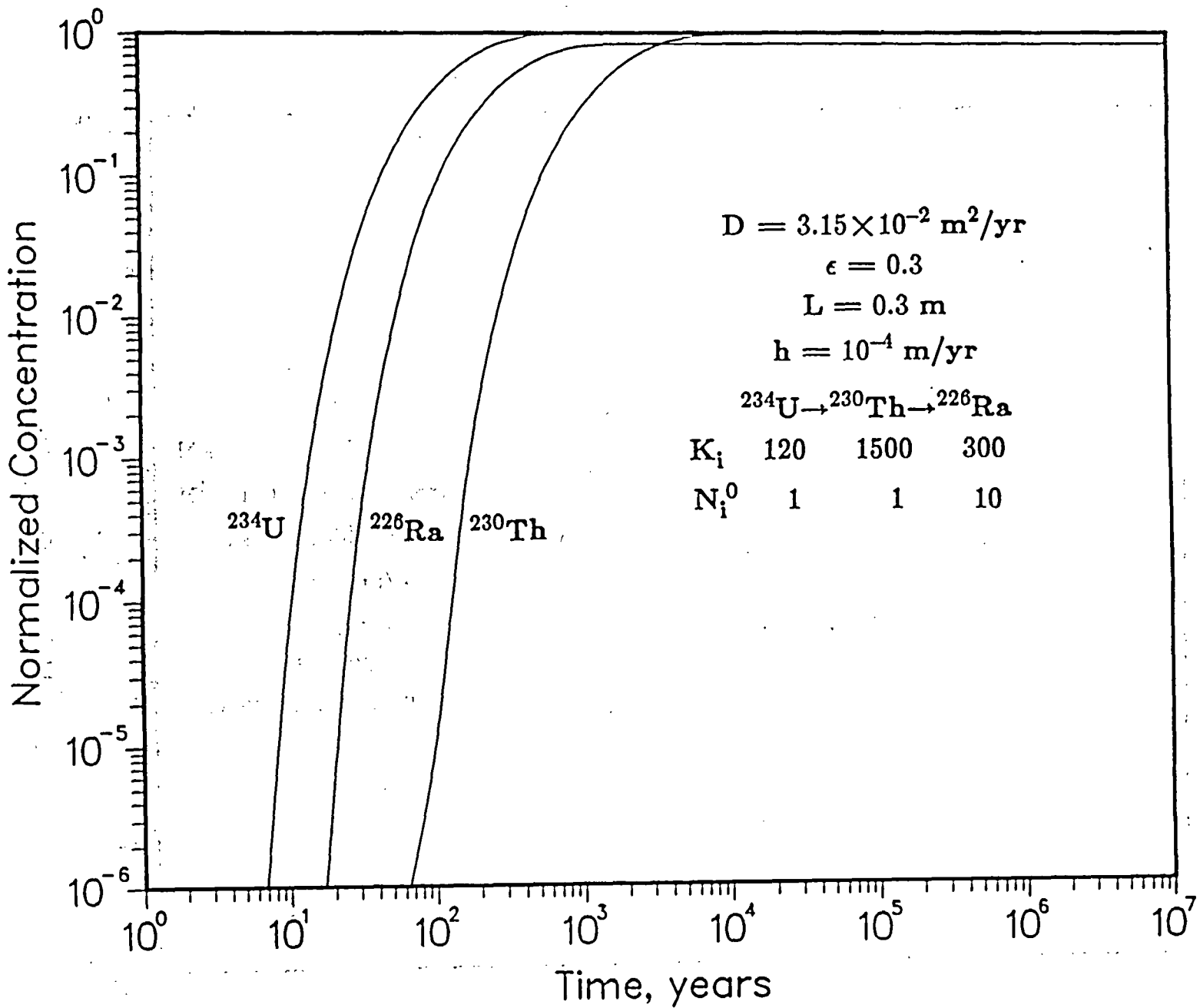
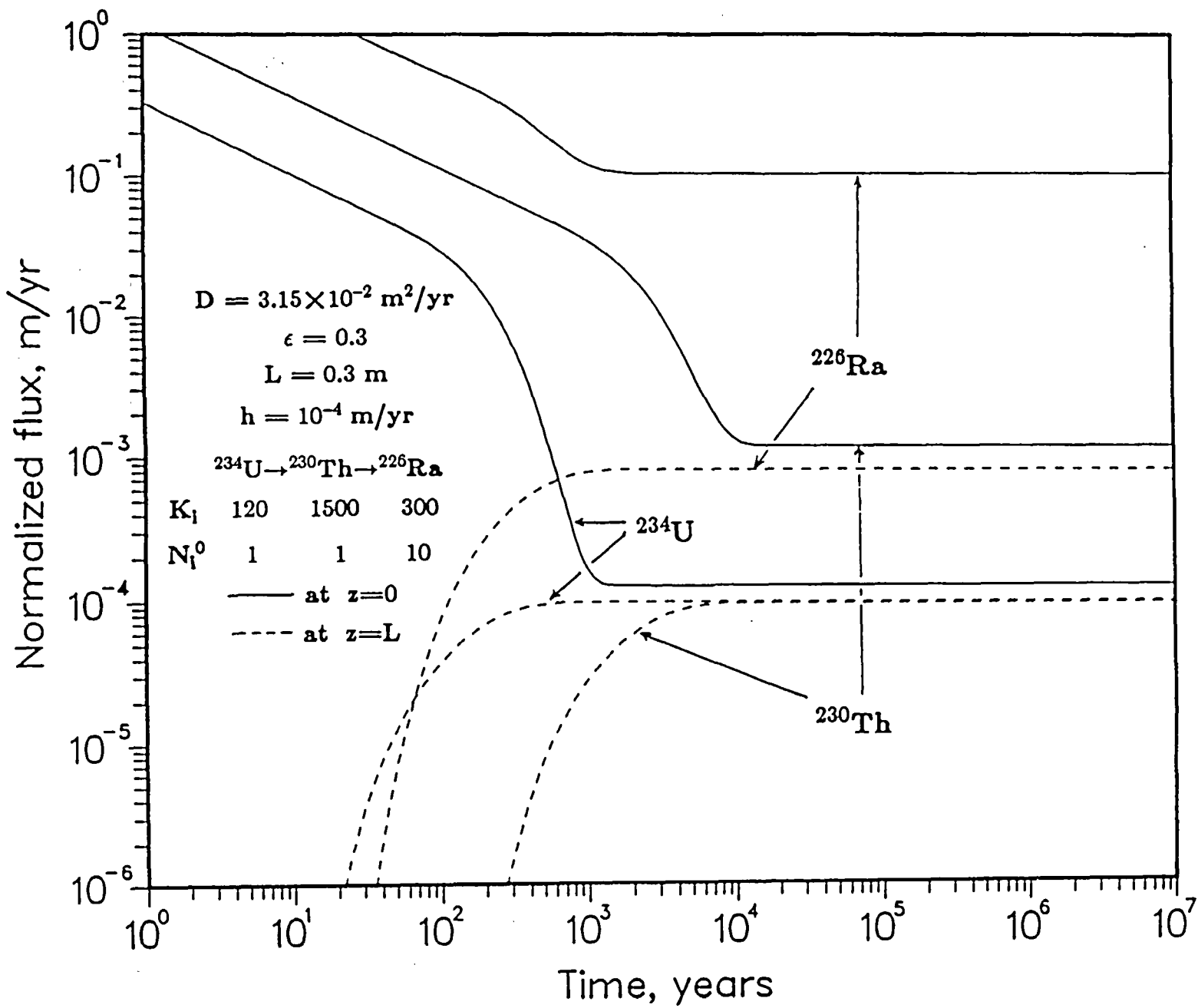


Fig. 3. Normalized concentration profiles for ^{234}U — ^{230}Th — ^{226}Ra at backfill/rock interface as functions of time; concentration-limited boundary condition.

Fig. 4. Normalized mass fluxes for ^{234}U , ^{230}Th , ^{226}Ra at both ends of the backfill layer as functions of time; concentration-limited boundary condition.



show that ^{234}U and ^{226}Ra reach their steady state at about one thousand years while ^{230}Th reaches the steady state at about ten thousand years. Although Fig. 2 shows that ^{226}Ra has decayed about 20% in the backfill (the concentration at $z=L$ is 80% of that at $z=0$) it does not guarantee that the mass flux out of the backfill also decreased. In fact, Fig. 4 shows that the radium flux at $z=L$ is one order of magnitude greater than uranium and thorium, in spite of the shorter half life of ^{226}Ra .

Figure 5 shows the effect of a much higher mass transfer coefficient at $z=L$, with h changed to 10^4 m/yr. At 1000 years, not only ^{234}U and ^{226}Ra have reached their steady states but ^{230}Th is also almost at its equilibrium state, as can be seen in the next two figures. The concentration at outer boundary ($z=L$) drops to such a low level that it can be regarded as zero for all practical purposes. This conclusion has been cross-checked by computations using UCBNE50 based on the solution (2.50). Therefore, we will not show separately the results from UCBNE50, since the results for $h=10^4$ m/yr can be well applied to the case of infinite h (i.e. UCBNE50). Figures 6 and 7 show the concentration at the outer boundary and mass flux at both interfaces as functions of time, respectively, for $h=10^4$ m/yr. In Fig. 6 we have also included the corresponding concentration profile for $h=10^{-4}$ m/yr (the dashed curves) as a comparison. The concentration difference for different h is about six orders of magnitude, and the radium concentration is closer to that of uranium in the large h case than in the small h case. This implies that the large h condition will accelerate the speed of reaching the steady state and the decay effect has very little significance. In fact, Fig. 7 shows that the mass fluxes at $z=L$ are very close to those at $z=0$ at large times (>1000 years) that one can treat all three members as stable nuclides. Comparing

Fig. 5. Normalized concentration profiles for $^{234}\text{U} \rightarrow ^{230}\text{Th} \rightarrow ^{226}\text{Ra}$ in backfill as functions of distance at 10^3 years; $h = 10^4$ m/yr; concentration-limited boundary condition.

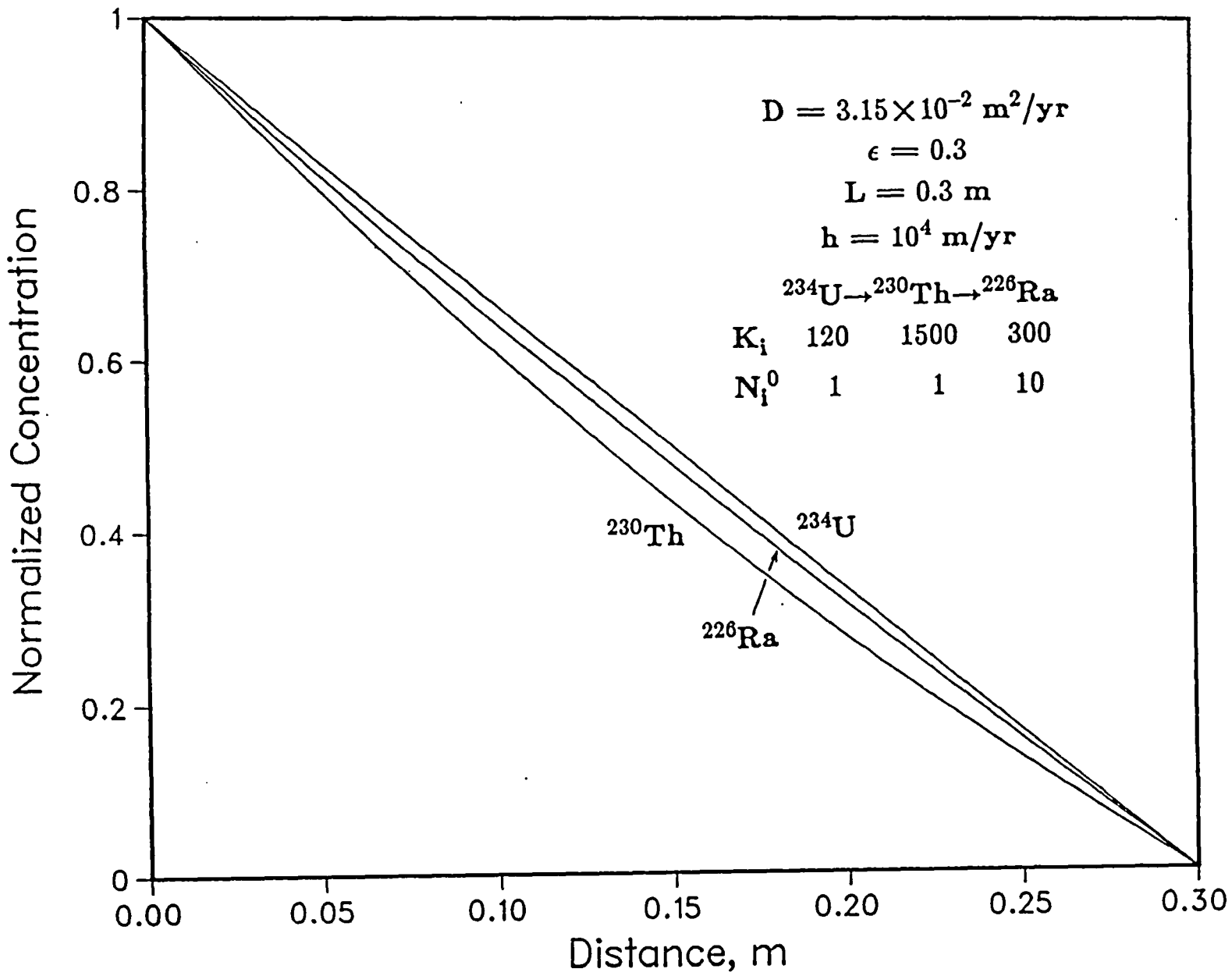


Fig. 6. Normalized concentration profiles for ^{234}U , ^{230}Th , ^{226}Ra at backfill/rock interface as functions of time; concentration-limited boundary condition.

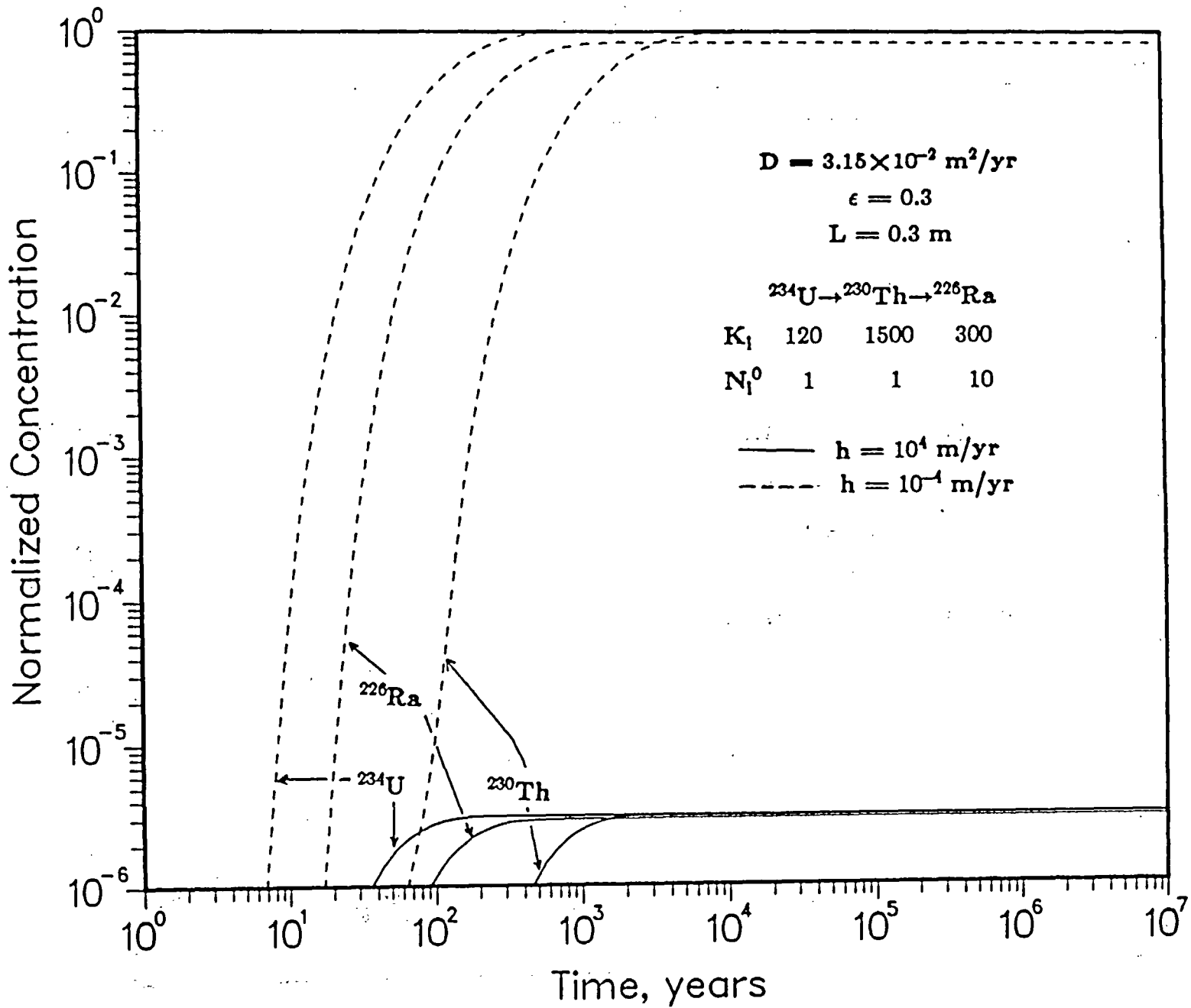


Fig. 7. Normalized mass fluxes for ^{234}U , ^{230}Th , ^{226}Ra at both ends of the backfill layer as functions of time; $h = 10^4$ m/yr; concentration-limited boundary condition.

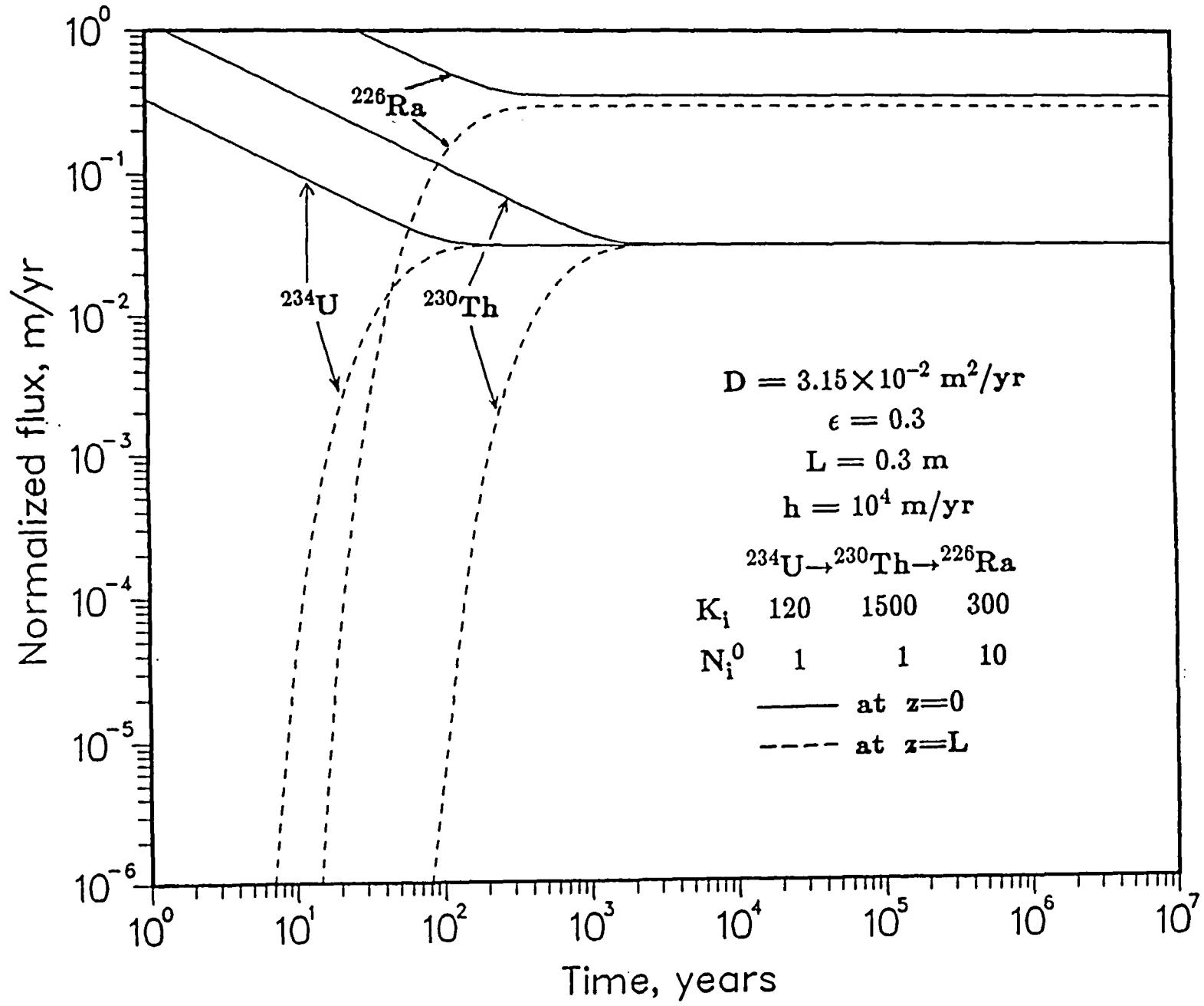
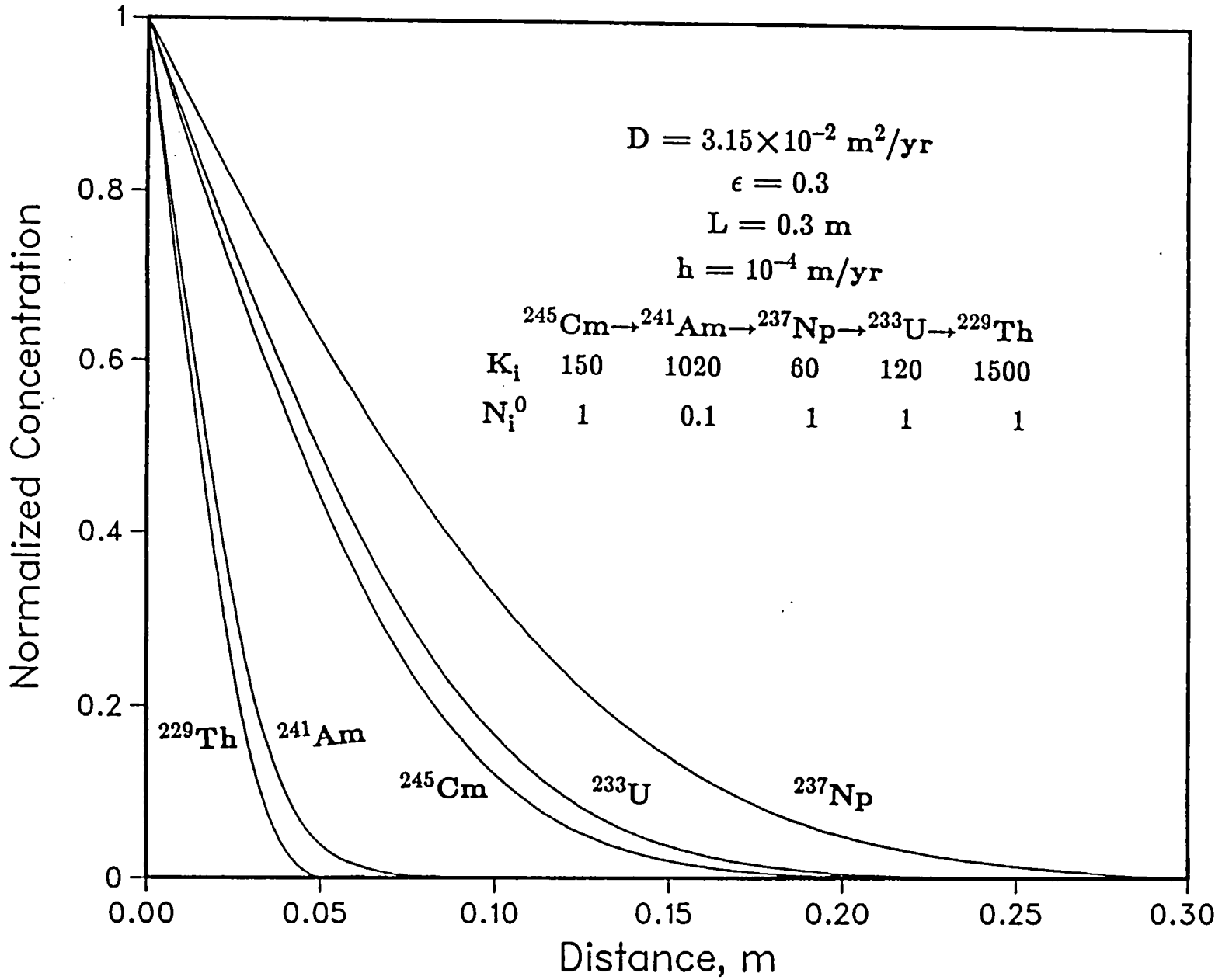


Fig. 7 with Fig. 4 one sees that the mass fluxes increase about two orders of magnitude in the large h case. Though not shown here, we have also made calculations for $h=1$ m/yr and the resultant mass fluxes are identical to those for $h=10^4$ m/yr case. In other words, a mass transfer coefficient of 1 m/yr is large enough to simulate the strong water flow outside the backfill.

To show the capacity of the solution to compute a chain of more than three members, we also present the results for the $^{245}\text{Cm} \rightarrow ^{241}\text{Am} \rightarrow ^{237}\text{Np} \rightarrow ^{233}\text{U} \rightarrow ^{229}\text{Th}$ chain. Figure 8 shows the concentration profile as a function of distance at 10 years. As in Fig. 1, at this time the nuclides have not reached the outer surface and the boundary condition at $z=L$ plays no role in the nuclide migrations. Therefore, the semi-infinite medium solution can also be applied to this time period. The profile of each member is solely determined by the individual retardation coefficient, and decay has not affected the results.

Figures 9 and 10 show the concentration profiles as a function of distance at 1000 years. In Fig. 9 the h value used is 10^{-4} m/yr, while in Fig. 10 it is 10^4 m/yr. Since ^{241}Am has a short half life (430 years) at 1000 years more than 75% of the released amount has decayed to ^{237}Np . On the other hand, ^{237}Np has a very long half life (2.14×10^6 years) and it accumulates in the backfill. For the small h value in Fig. 9, with the boundary at $z=L$ acting as an insulated interface, the increase of ^{237}Np is very significant. For a large value of h in Fig. 10, h accelerates the speed of reaching steady state, and the decay effect is not as pronounced as in the small h case, as discussed previously. Hence when the mass transfer coefficient is sufficiently large all the members of this chain except ^{241}Am can be treated as stable nuclides.

Fig. 8. Normalized concentration profiles for $^{245}\text{Cm} \rightarrow ^{241}\text{Am} \rightarrow ^{237}\text{Np} \rightarrow ^{233}\text{U} \rightarrow ^{229}\text{Th}$ in backfill as functions of distance at 10 years; concentration-limited boundary condition.



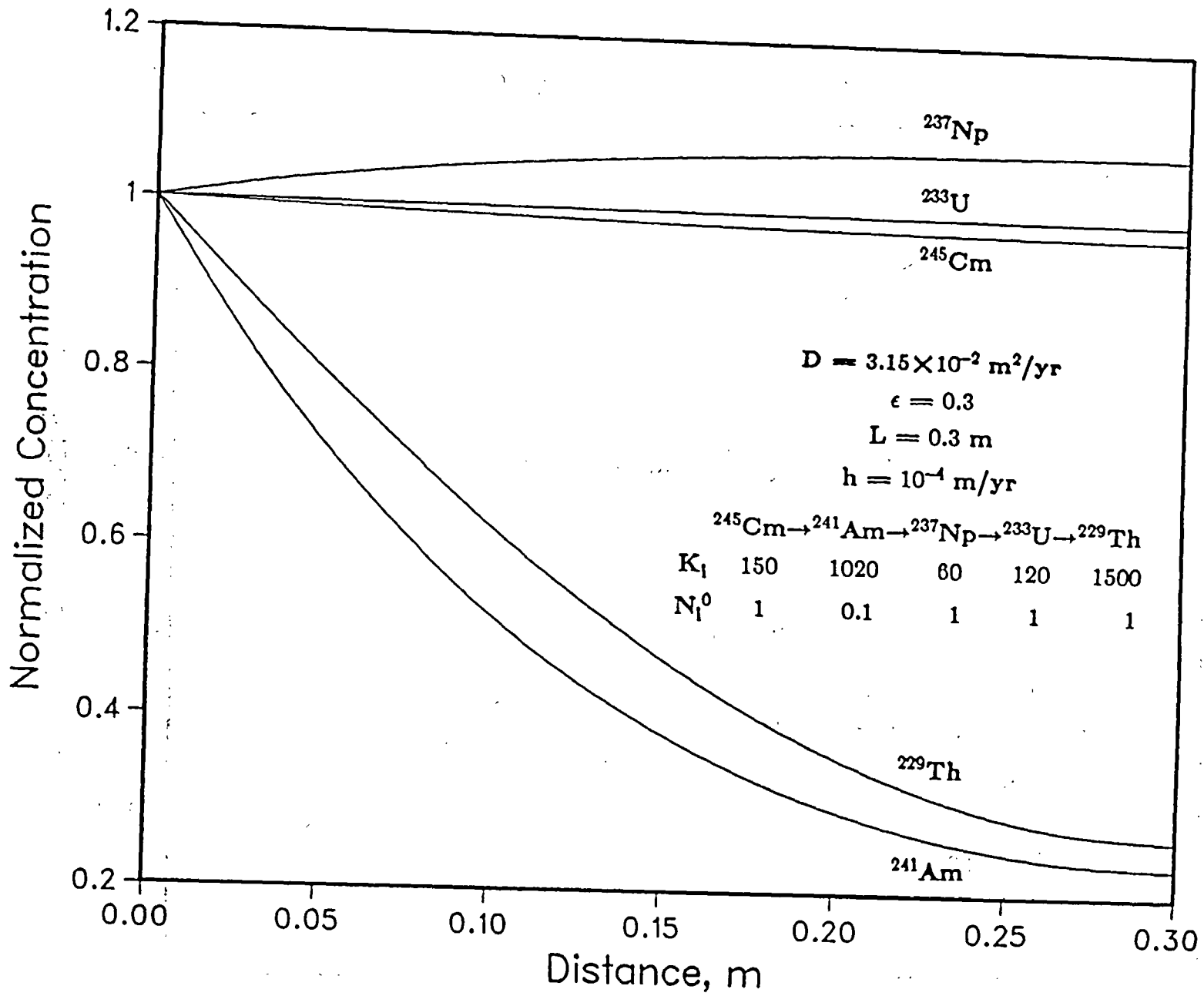


Fig. 9. Normalized concentration profiles for ^{245}Cm — ^{241}Am — ^{237}Np — ^{233}U — ^{229}Th in backfill as functions of distance at 10^3 years; concentration-limited boundary condition.

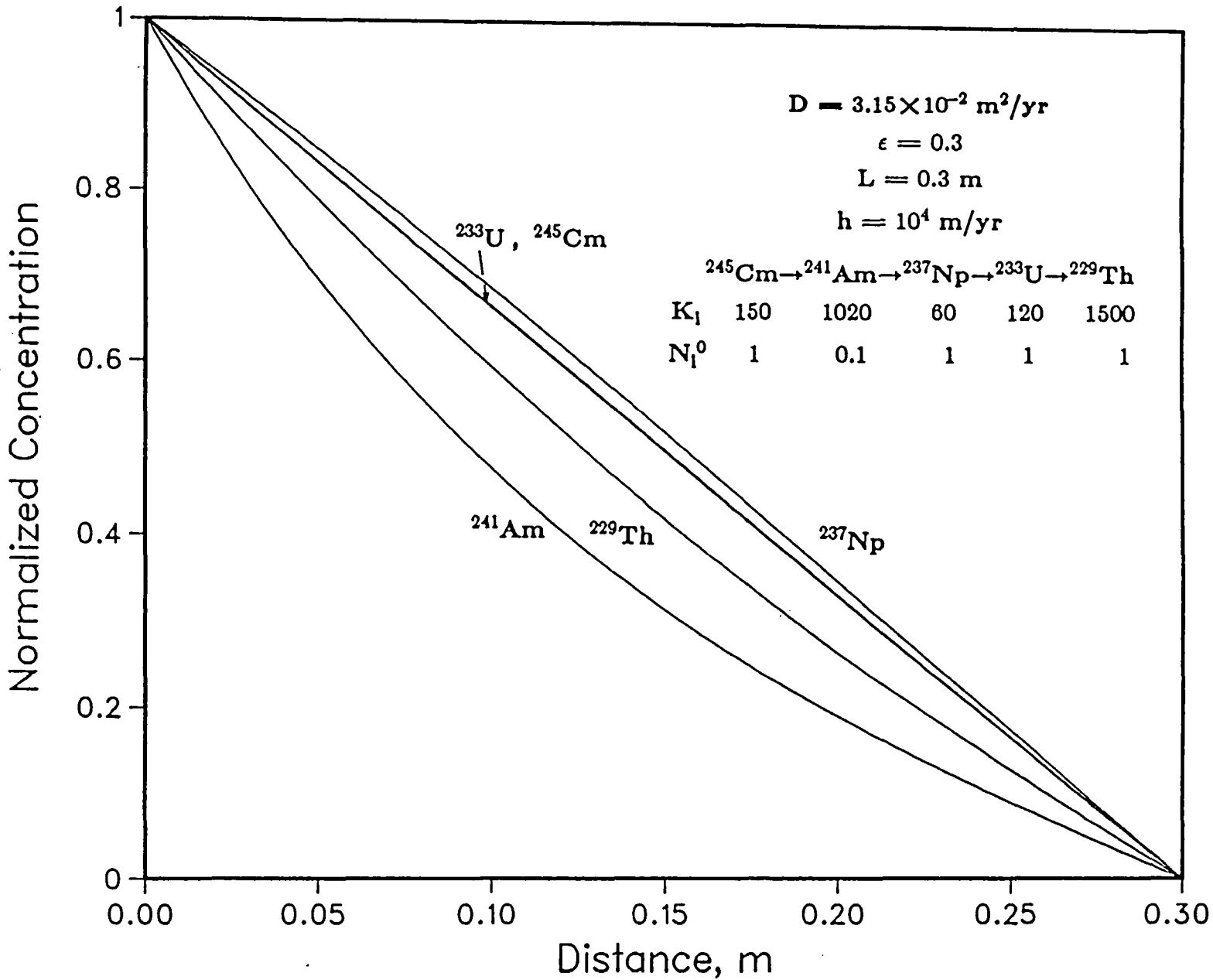


Fig. 10. Normalized concentration profiles for $^{245}\text{Cm} \rightarrow ^{241}\text{Am} \rightarrow ^{237}\text{Np} \rightarrow ^{233}\text{U} \rightarrow ^{229}\text{Th}$ in backfill as functions of distance at 10^3 years; $h = 10^4 \text{ m/yr}$; concentration-limited boundary condition.

The analytic solutions and the computer codes are not limited by the zero pore water velocity assumption. We made additional calculations for the non-zero velocity case and found that for $v=0.01$ m/yr, the difference between the zero velocity results and the non-zero results are less than 5%, while for $v=0.001$ m/yr, the difference is less than 1%, for all times throughout the backfill.

Next we investigate a different boundary condition at the inner surface.

2.2.2. Case 2: Bateman-Type Boundary Condition

In this case, a congruent dissolution, band release mode is assumed. The boundary concentration at $z=0$ obeys the Bateman equation

$$N_i(0,t) = \sum_{j=1}^i B_{ij} e^{-\lambda_j t}, \quad (2.57)$$

while the boundary condition at $z=L$ remains the same form as in (2.51). The Bateman constant B_{ij} in (2.57) is

$$B_{ij} = \sum_{m=1}^j N_m^0 \left(\frac{1}{\lambda_i} \prod_{r=m}^i \lambda_r \right) / \prod_{\substack{\ell=m \\ \ell \neq j}}^i (\lambda_\ell - \lambda_j)$$

where N_m^0 is the initial concentration of the m^{th} nuclide and the product term in the denominator is defined as unity when $m=j=i$. Examining equation (2.28) one sees that the only change should be made is to replace N_i^0 with (2.57). The results are

$$g_i(\beta_m, t) = \sqrt{\frac{2}{L + \ell_m}} \beta_m \sum_{j=1}^i B_{ij} e^{-\lambda_j t}$$

and

$$g_i(\beta_m, t) * e^{-\delta_n t} = \sqrt{\frac{2}{L + \ell_m}} \beta_m \sum_{j=1}^i B_{ij} e^{-\lambda_j t} \frac{1 - e^{-(\delta_n - \lambda_j)t}}{\delta_n - \lambda_j}$$

If we let $\Delta_{nj} = \delta_n - \lambda_j = \frac{D}{K_n}(\beta_m^2 + q_n^2) - \lambda_j = \frac{D}{K_n}(\beta_m^2 + q_n^2)$, where $q_n^2 = q_n^2 - \frac{K_n}{D}\lambda_j =$

$(\frac{v}{2D})^2 + \frac{K_n}{D}(\lambda_n - \lambda_j)$, then (2.56) changes to

$$N_i(z, t) = e^{\frac{vz}{2D}} \frac{D}{K_i} \left\{ \sum_{k=1}^i B_{ik} e^{-\lambda_k t} \sum_{m=1}^{\infty} \left(\frac{2}{L + \ell_m} \right) \frac{\beta_m \sin \beta_m z}{\Delta_{ik}} (1 - e^{-\Delta_{ik} t}) + \right. \\ \left. + \sum_{j=1}^{i-1} C_i^{(j)} \sum_{k=1}^j B_{jk} e^{-\lambda_k t} \sum_{n=j}^i \sum_{m=1}^{\infty} \left(\frac{2}{L + \ell_m} \right) \frac{\beta_m \sin \beta_m z}{\prod_{\substack{r=j \\ r \neq n}}^i (\Gamma_{nr} \beta_m^2 + \gamma_{nr}) \Delta_{nk}} (1 - e^{-\Delta_{nk} t}) \right\}, \\ z > 0, t > 0, i = 1, 2, \dots \quad (2.58)$$

Equation (2.58) has been programmed into a computer code named UCBNE52, and is used to make our numerical calculations in the following examples.

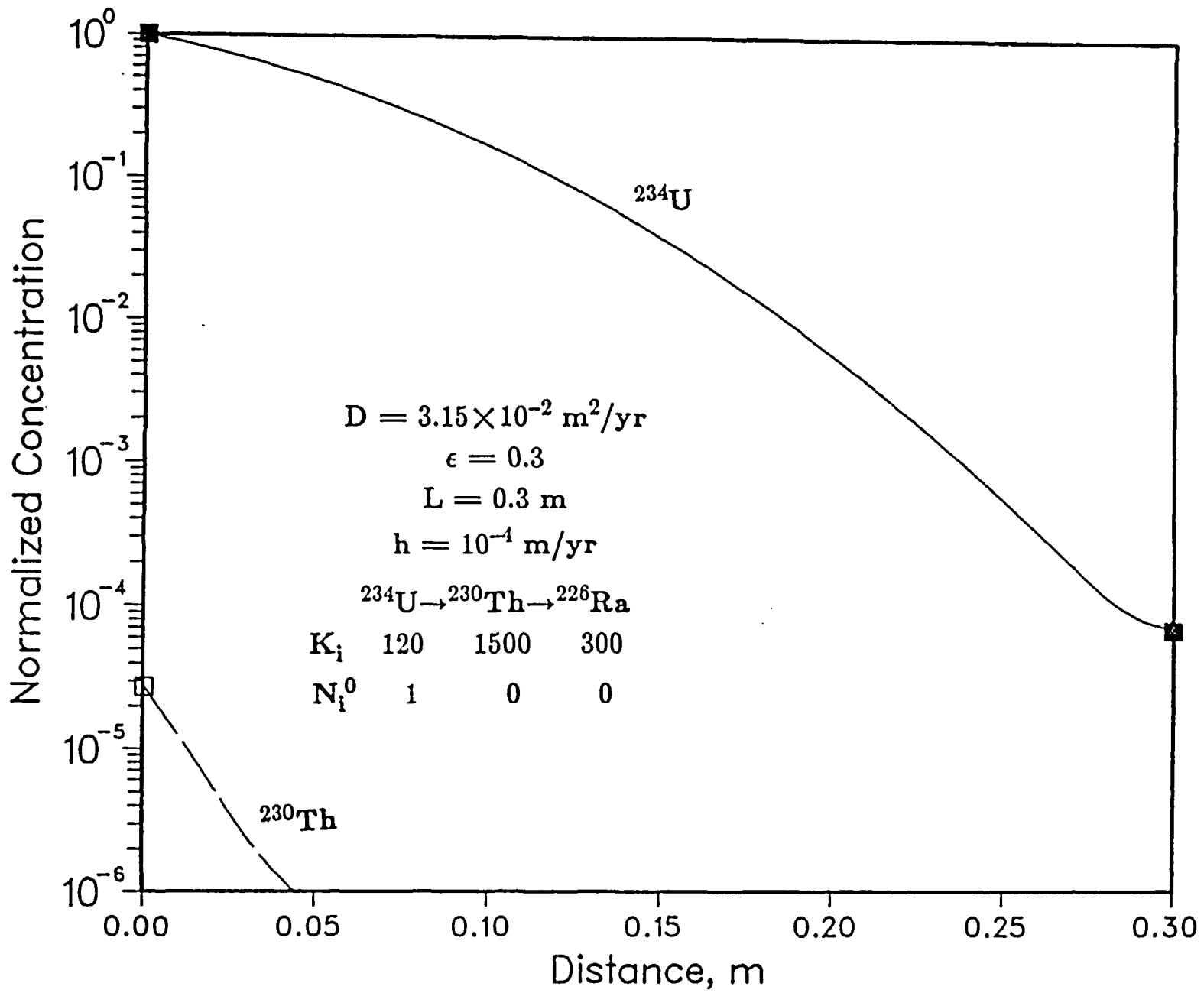
Numerical Examples

For parameters values used in these calculations see the previous section. For a Bateman-type boundary condition, we need to know the initial boundary concentration of each member. To reveal the importance of decay in this case, we make the following assumptions. In both $^{234}\text{U} \rightarrow ^{230}\text{Th} \rightarrow ^{226}\text{Ra}$ and $^{245}\text{Cm} \rightarrow ^{241}\text{Am} \rightarrow ^{237}\text{Np} \rightarrow ^{233}\text{U} \rightarrow ^{229}\text{Th}$ chains, all the daughters have initially no inventory in the waste canister, i.e., $N_i(0,0) = 0$ for $i \geq 2$. The mother members (^{234}U and ^{245}Cm) have a initial concentration of unity, i.e., $N_1(0,0) = 1$. Although we adopt these values as our input data, we want to emphasize that neither the solution (2.58) nor the computer code UCBNE52 is limited by this choice. One can select any reasonable values for the initial boundary concentrations in the chain.

Figures 11 through 15 are for the $^{234}\text{U} \rightarrow ^{230}\text{Th} \rightarrow ^{226}\text{Ra}$ chain. In these figures the h values are 10^{-4} m/yr. The vertical scale now is logarithmic to show the very small amounts of the daughter nuclides. Figure 11 shows the concentration profile, normalized to $N_1(0,0)$, as a function of distance at 10 years for the $^{234}\text{U} \rightarrow ^{230}\text{Th} \rightarrow ^{226}\text{Ra}$ chain. Because initially there is no thorium, all ^{230}Th come from the decay of ^{234}U . This figure shows very little ^{230}Th in the field, since all of it comes from the decay of ^{234}U and ^{234}U has a very long half life. The concentration of ^{226}Ra cannot be shown in this figure because its value is well below the lower limit of the graph (10^{-6}). The solution (2.58) has one more summation term than Eq. (2.56). This implies a longer computation time is required to use this solution than the semi-infinite solutions implemented in UCBNE50 and UCBNE51. Hence the semi-infinite medium solution should be used whenever possible to economize the computing time. At this early time period one observes that the semi-infinite medium solution is a very good replacement for the exact solution (2.58) as mentioned in last section. It means the boundary condition at outer end (2.51) has not entered into the solution, and Fig. 11 can also be applied to other values of h . The semi-infinite medium solution for this kind of boundary condition will also be presented in Section 3.

Figure 12 shows the concentration profile at 1000 years. At this time ^{234}U has reached its steady state while ^{230}Th and ^{226}Ra are still rising. One interesting thing is that the ^{226}Ra shows a maximum inside the backfill. This is because ^{230}Th has a higher retardation coefficient than ^{226}Ra inside the backfill, while in the waste form there is no retardation effect at all. Therefore, the production rate of ^{226}Ra inside the backfill is greater than the rate in the waste form, for they both originate from the decay of

Fig. 11. Normalized concentration profiles for $^{234}\text{U} \rightarrow ^{230}\text{Th} \rightarrow ^{226}\text{Ra}$ in backfill as functions of distance at 10 years; Bateman-type boundary condition.



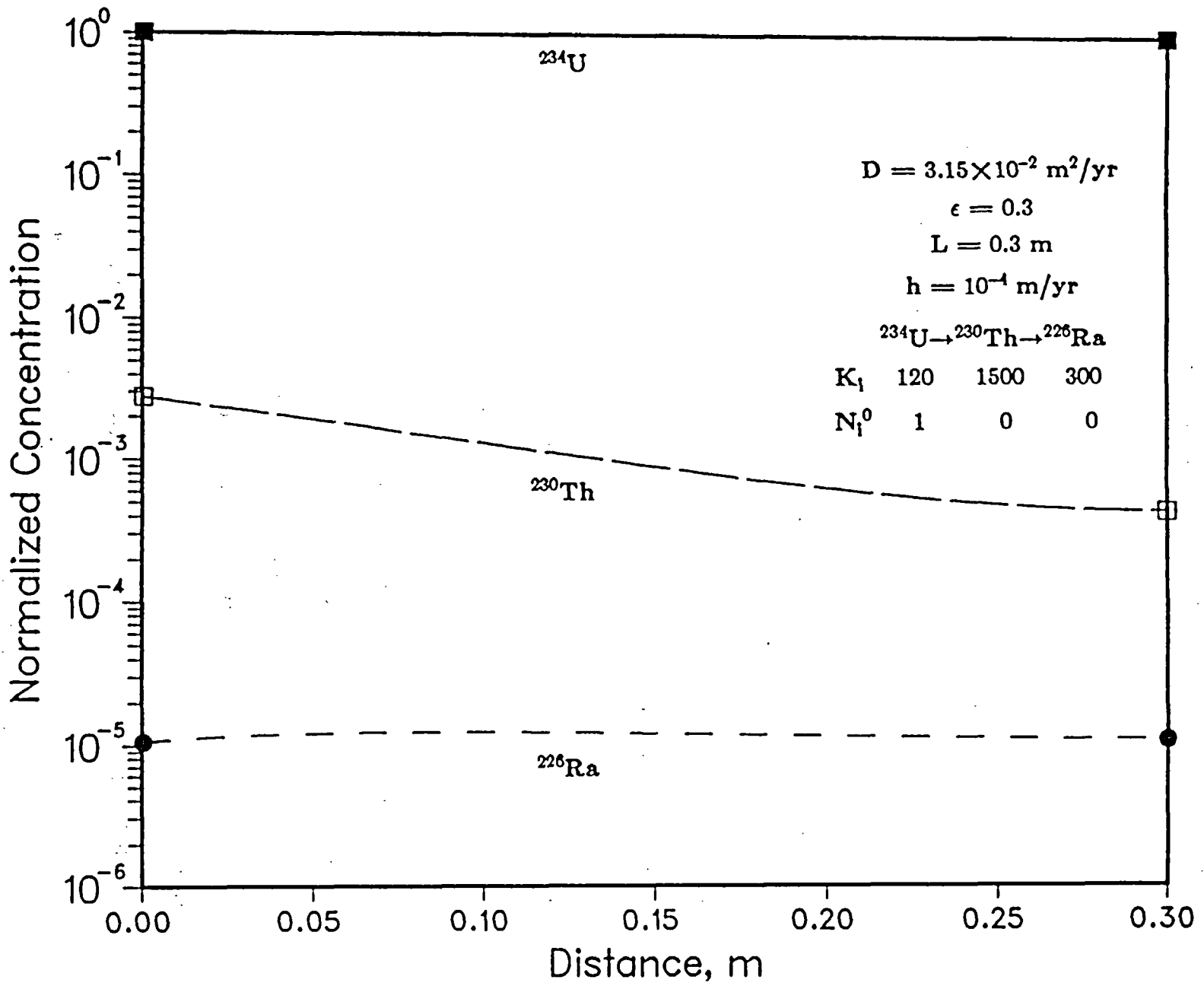


Fig. 12. Normalized concentration profiles for $^{234}\text{U} \rightarrow ^{230}\text{Th} \rightarrow ^{226}\text{Ra}$ in backfill as functions of distance at 10^3 years; Bateman-type boundary condition.

^{230}Th , and ^{230}Th is nearly constant throughout the backfill due to the flat profile of ^{234}U .

Figure 13 shows the concentration profile at $t=10^5$ years. Since ^{234}U has a half life of 2.47×10^5 years, one can see the decay effect starting to take place. The profile of ^{234}U is still flat but at a lower value than at 1000 years. ^{230}Th and ^{226}Ra on the other hand are still rising until one half of ^{234}U has all decayed. Then the concentrations of all three members decrease.

Figures 14 and 15 show the concentration and flux profiles, both normalized to $N_1(0,0)$, respectively, as functions of time at both interfaces of the backfill. In Fig. 14 the solid curves indicate the concentrations at waste surface ($z=0$) while the dashed ones the concentrations at $z=L$. The dotted curve is the ^{234}U concentration at $z=L$ for $h=10^4$ m/yr as a comparison. The ^{230}Th and ^{226}Ra concentrations for a large value of h are less than the lower limit of the plot (10^{-6}) and are not shown here. Due to the interior maximum of ^{226}Ra discussed above, the concentration at $z=L$ is greater than that at $z=0$ after a few hundred years, which is the time to establish the flatness of the ^{234}U profile. After several million years, all three members will have decayed out due to the Bateman-type boundary conditions. As in the case of constant boundary concentrations, the large h represents a strong flow outside the backfill, and the concentration at $z=L$ falls to a very small value (about six orders of magnitude smaller than for the small h case).

In Fig. 15 the solid curves represent the mass fluxes at $z=0$ and the dashed ones the fluxes at $z=L$. We also plotted the mass fluxes of ^{226}Ra for high h at both ends by the dotted curves for comparison. For low h we only show ^{234}U and ^{230}Th fluxes since

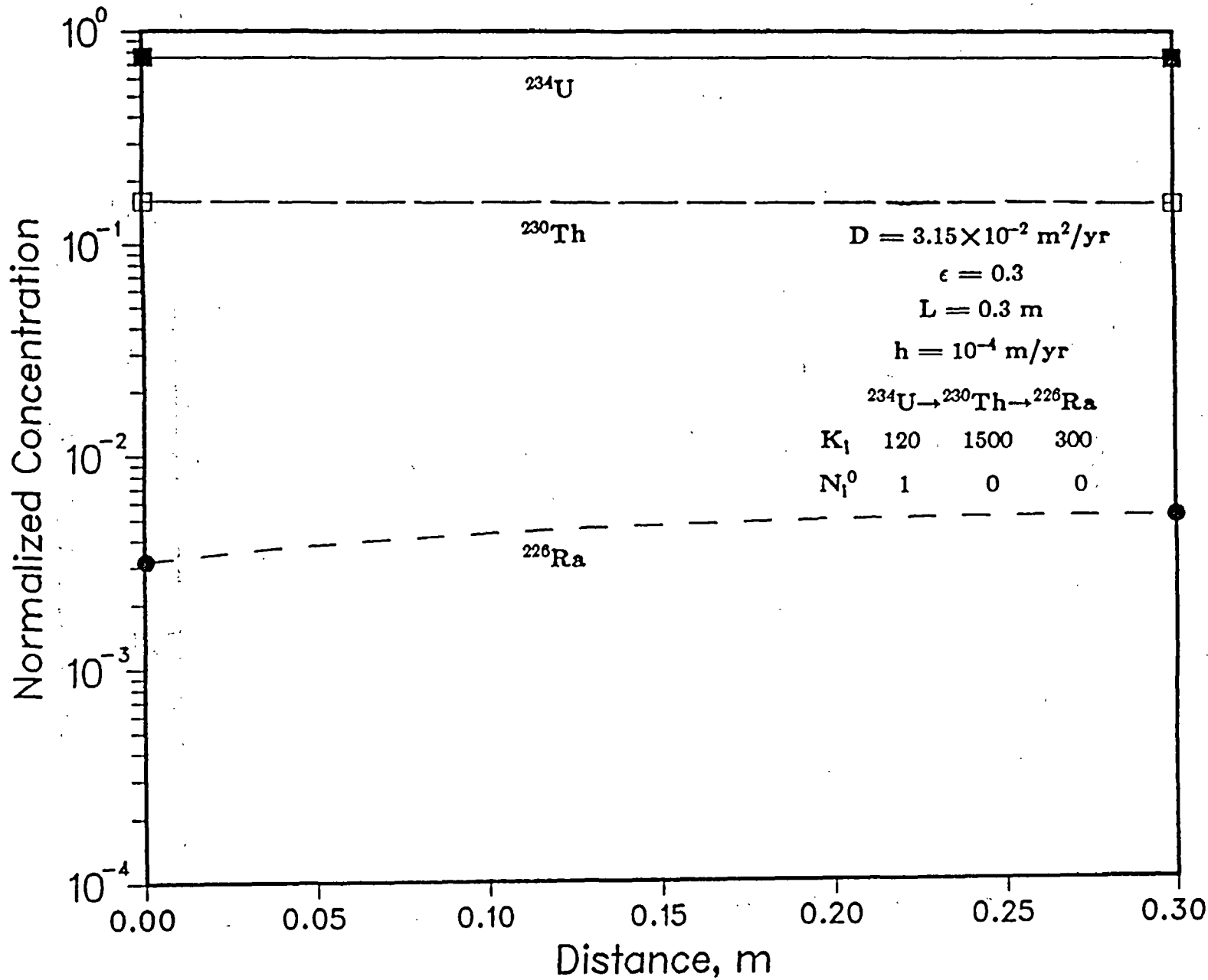


Fig. 13. Normalized concentration profiles for ^{234}U , ^{230}Th , ^{226}Ra in backfill as functions of distance at 10^5 years; Bateman-type boundary condition.

Fig. 14. Normalized concentration profiles for ^{234}U , ^{230}Th , ^{226}Ra at both ends of the backfill layer as functions of time; Bateman-type boundary condition.

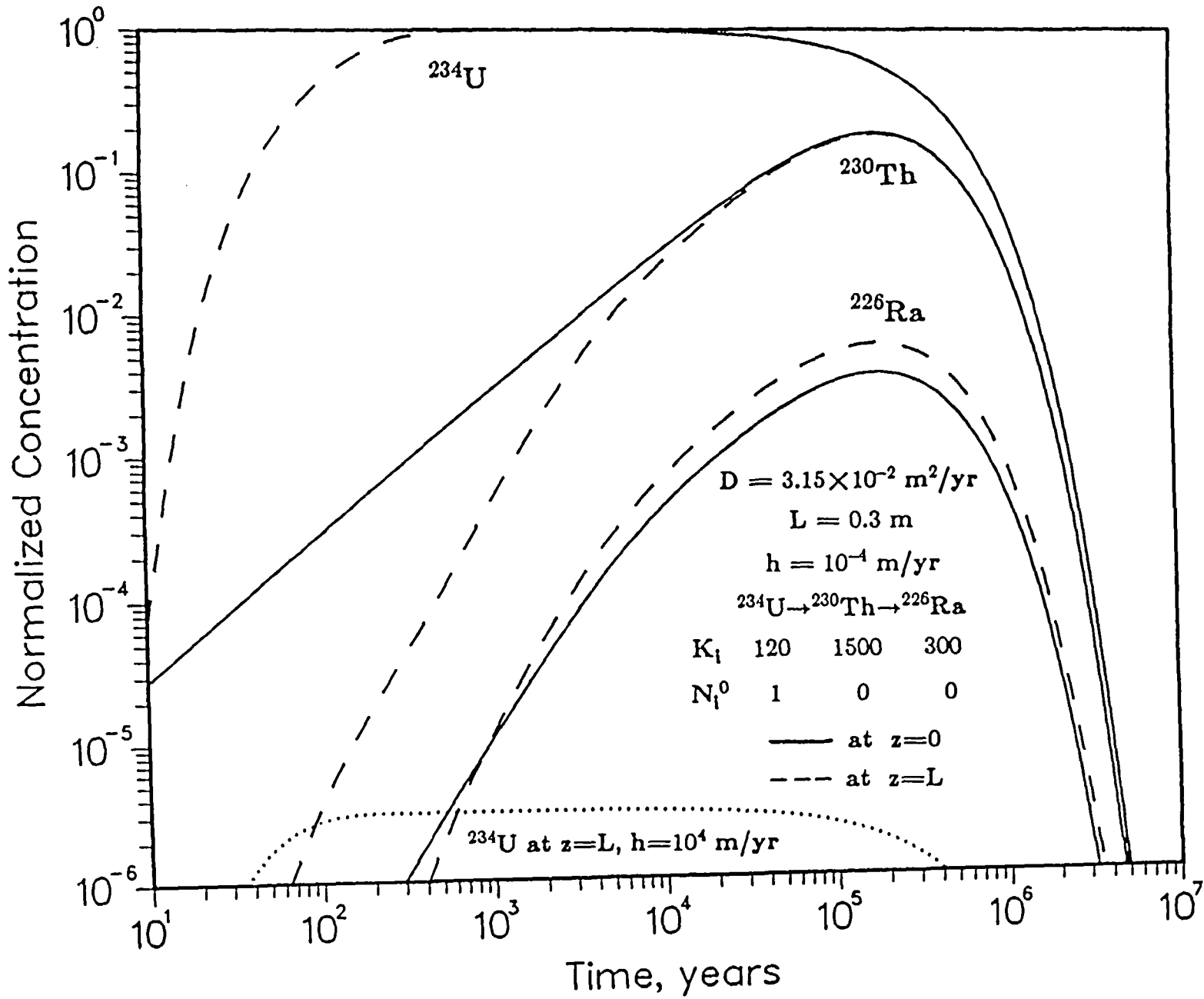
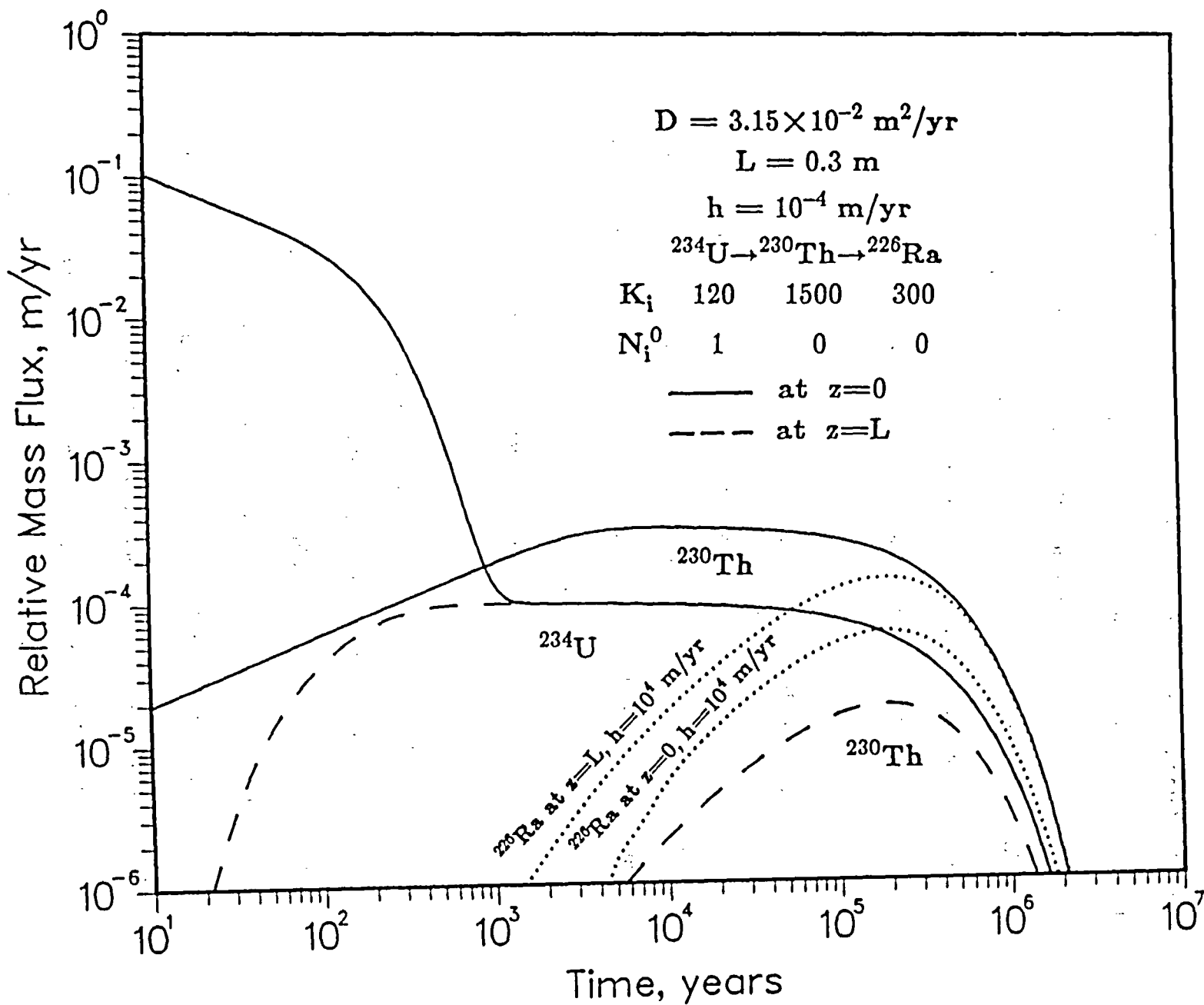


Fig. 15. Normalized mass fluxes for $^{234}\text{U} \rightarrow ^{230}\text{Th} \rightarrow ^{226}\text{Ra}$ at both ends of the backfill layer as functions of time; Bateman-type boundary condition.



^{226}Ra flux is too low to be shown. One can see that after 1000 years ^{234}U has already reached a state that the mass flux at $z=0$ becomes almost equal to that at $z=L$, which means the backfill can no longer retard the migration of uranium. This state is called the saturated state. On the other hand, ^{230}Th does not show the same phenomenon and the backfill still provides some degree of retardation effect for ^{230}Th . This is also true for ^{226}Ra though not shown here. The decay effect is strongly exhibited on thorium flux at $z=0$, since it has even a higher value than its mother, ^{234}U , after one thousand years.

The strong water flow can enhance the mass fluxes at the outer surface of backfill, as can be seen from the dotted curves. Later we will show that for a large value of h , ^{226}Ra has the lowest mass fluxes in the chain at both interfaces. But these lowest mass fluxes are still higher than the mass fluxes of ^{234}U evaluated at the small value of h after 10^5 years. Note that the mass flux of ^{226}Ra at $z=L$ is higher than that at $z=0$ for both values of h due to its faster production inside the backfill than in the waste form.

Figures 16 and 17 show the concentration profiles as a function of distance for $h=10^4$ m/yr at 1000 and 10^5 years, respectively. Strong water flow will decrease the concentrations at the outer interface, which in turn increases the mass fluxes there, the interior maximum of ^{226}Ra is no longer seen. Instead, one finds that the concentration profiles approach the secular equilibrium after 10^5 years, as seen in Fig. 17.

Figure 18 shows the mass fluxes, normalized to $N_1(0,0)$, at both ends of backfill as functions of time for $h=10^4$ m/yr. Again one observes that the large value of h will accelerate the speed of reaching the saturated state and the decay effect inside backfill

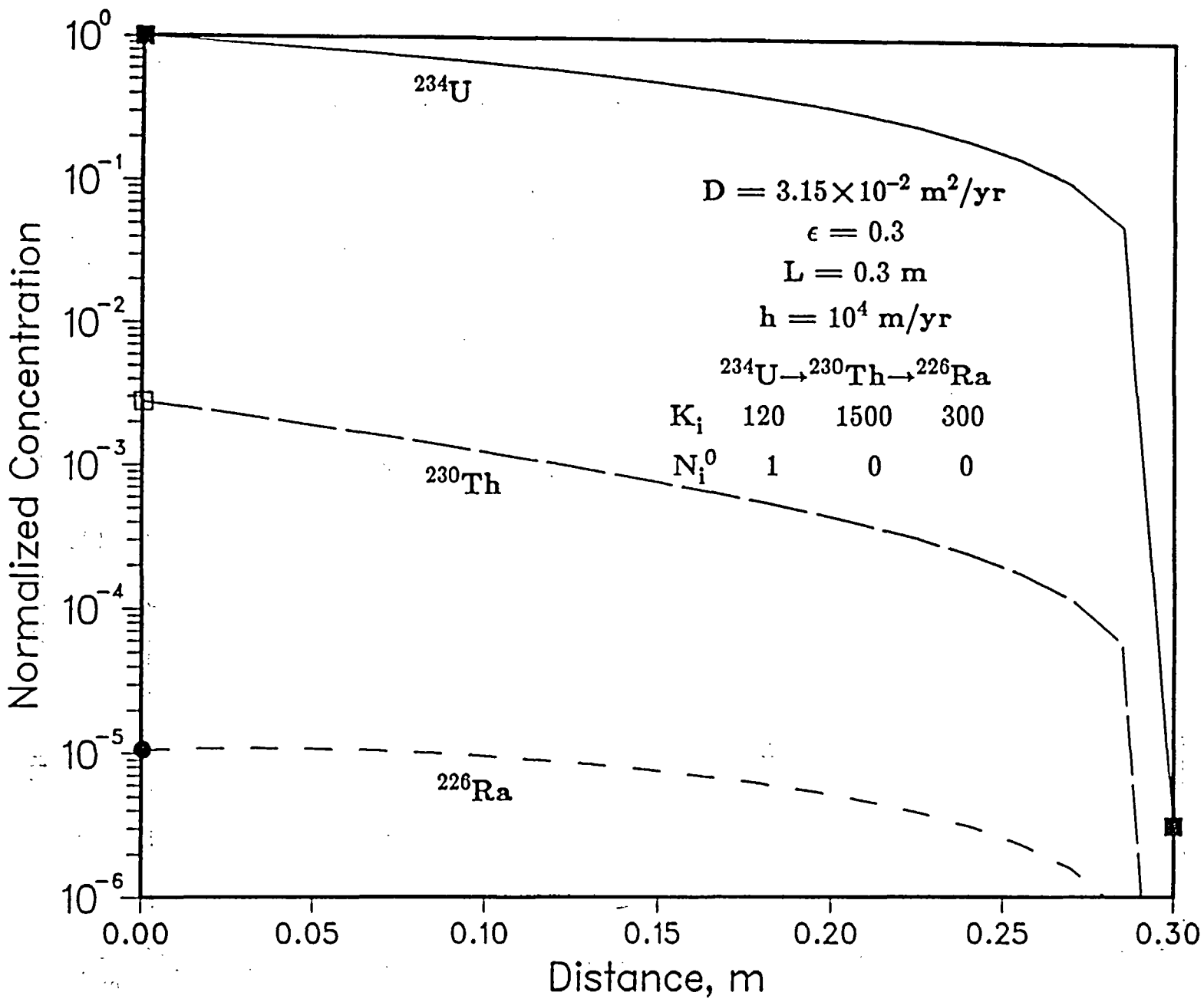


Fig. 16. Normalized concentration profiles for $^{234}\text{U} \rightarrow ^{230}\text{Th} \rightarrow ^{226}\text{Ra}$ in backfill as functions of distance at 10^3 years; Bateman-type boundary condition.

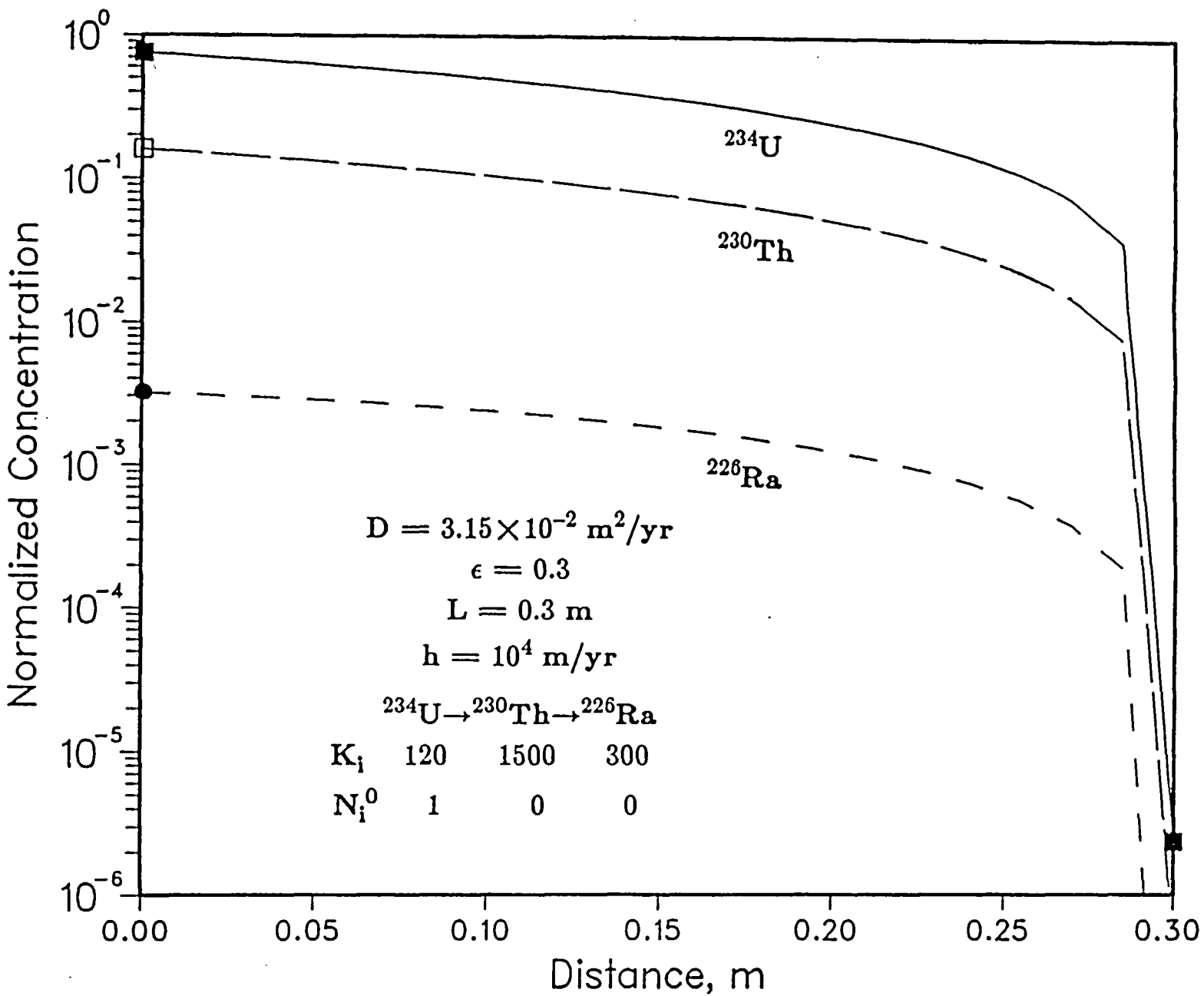
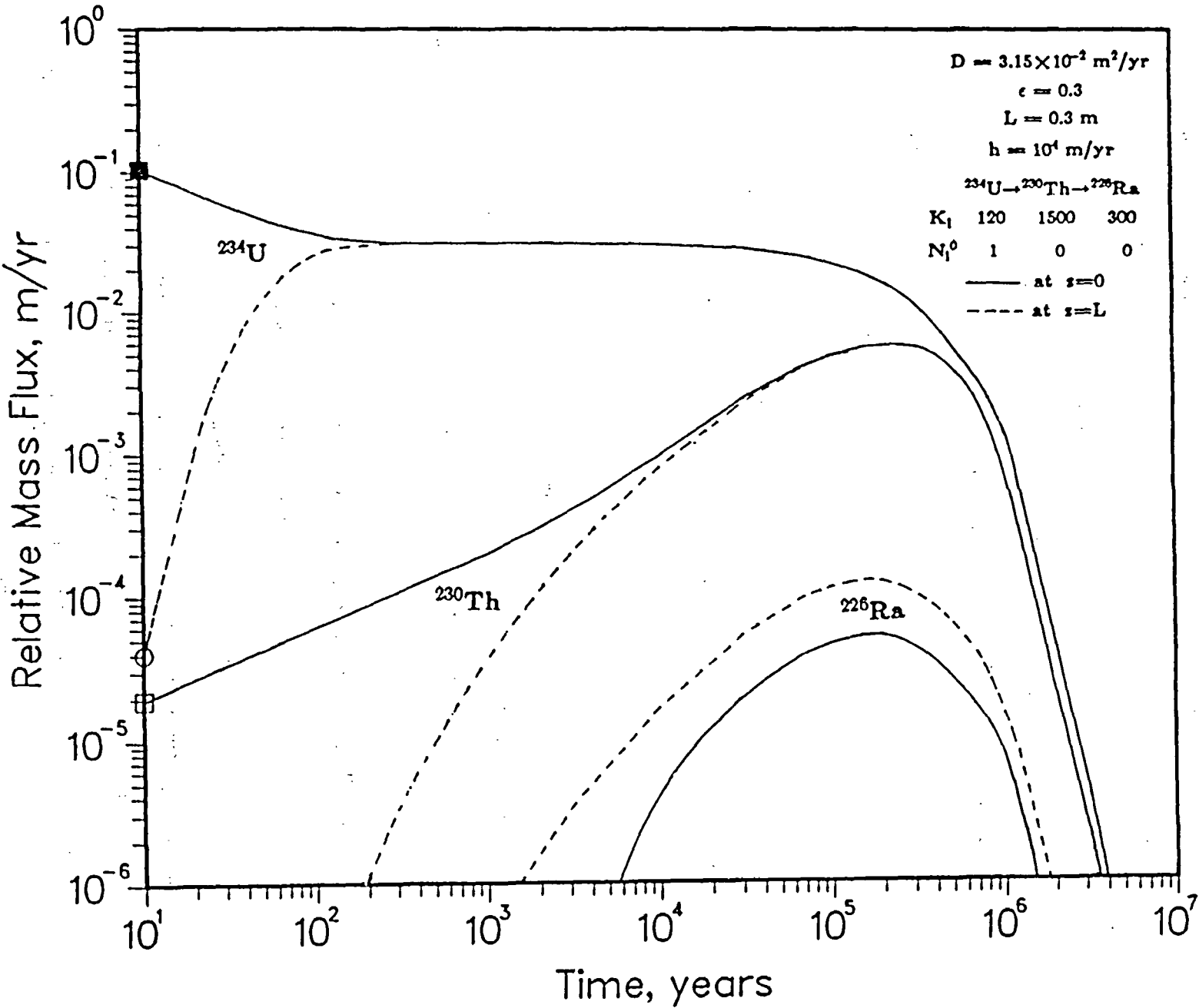


Fig. 17. Normalized concentration profiles for $^{234}\text{U} \rightarrow ^{230}\text{Th} \rightarrow ^{226}\text{Ra}$ in backfill as functions of distance at 10^5 years; Bateman-type boundary condition.

Fig. 18. Normalized concentration profiles for ^{234}U — ^{230}Th — ^{226}Ra at both ends of the backfill layer as functions of time; Bateman-type boundary condition.



has less significance than for the small h case. Compared with Fig. 15 one observes that the time to reach the saturated state for ^{234}U has been reduced from 1000 years to 100 years. Even ^{230}Th now shows some degree of saturation after 30000 years, which is not observed in the small h case. We also see that for a large value of h , ^{230}Th fluxes are always less than those of ^{234}U , in contrast to the situation shown in Fig. 15. As mentioned before, ^{226}Ra fluxes are the lowest among all three members, but the flux at $z=L$ is higher than that at $z=0$ after a few years due to its faster production rate in the backfill.

To show the capacity of handling longer chain, we also made some calculations on the $^{245}\text{Cm} \rightarrow ^{241}\text{Am} \rightarrow ^{237}\text{Np} \rightarrow ^{233}\text{U} \rightarrow ^{229}\text{Th}$ chain. Figure 19 shows the normalized concentration profiles as functions of distance at 10 years. It is seen that at this time period one can use the semi-infinite medium solution to calculate the concentration profile as in ^{234}U chain. Hence this figure can be applied to arbitrary h values. One important thing to note is that ^{237}Np also shows an interior maximum as ^{226}Ra in $^{234}\text{U} \rightarrow ^{230}\text{Th} \rightarrow ^{226}\text{Ra}$ chain. It is due to the higher retardation coefficient of ^{241}Am (1020) than that of ^{237}Np (60). Furthermore, a faster production rate of ^{237}Np appears inside the backfill than in the waste form. The last two members in the chain, ^{233}U and ^{229}Th , have concentrations too low to be shown at this early time.

Figures 20 and 21 show the concentration profiles at 10^5 years for $h=10^{-4}$ and 10^4 m/yr, respectively. In Fig. 20 one notes that all members have reached their saturated states at this time except ^{241}Am due to its short half life (430 years). Since ^{245}Cm has a half life of only 8530 years, one sees that both ^{245}Cm and ^{241}Am concentrations drop to very low values at this time and keep decreasing. On the other hand,

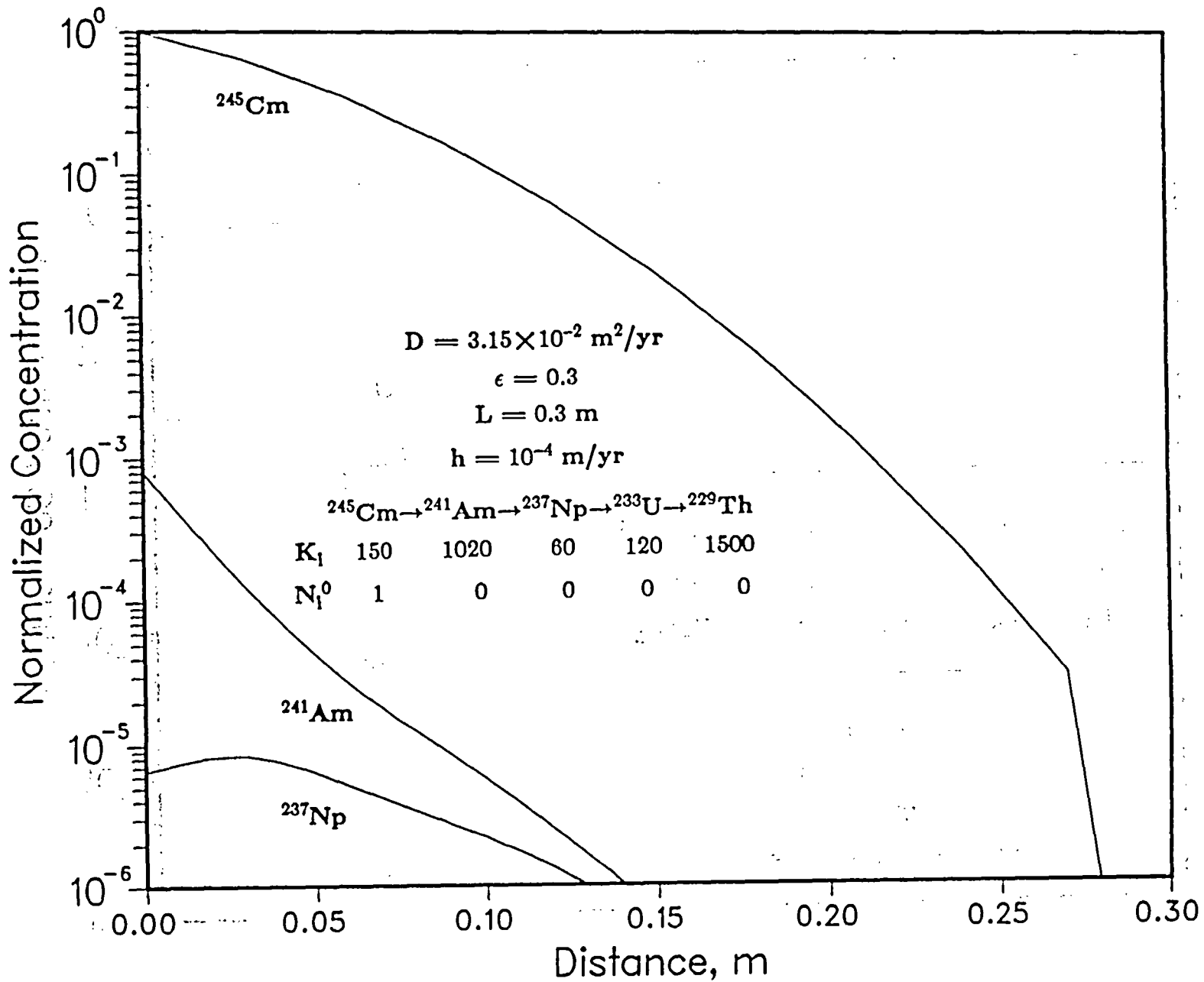
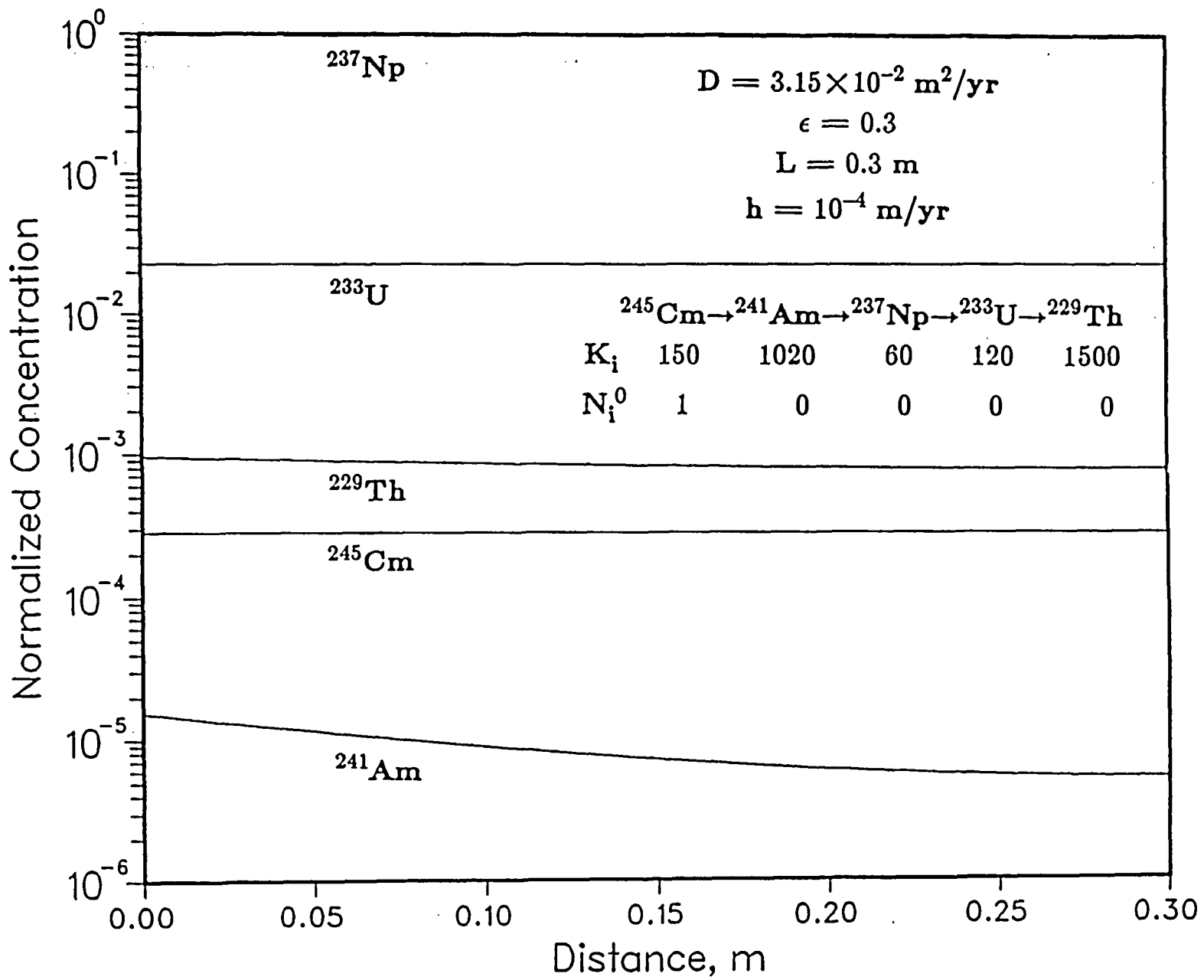


Fig. 19. Normalized concentration profiles for $^{245}\text{Cm} \rightarrow ^{241}\text{Am} \rightarrow ^{237}\text{Np} \rightarrow ^{233}\text{U} \rightarrow ^{229}\text{Th}$ in backfill as functions of distance at 10 years; Bateman-type boundary condition.

Fig. 20. Normalized concentration profiles for $^{245}\text{Cm} \rightarrow ^{241}\text{Am} \rightarrow ^{237}\text{Np} \rightarrow ^{233}\text{U} \rightarrow ^{229}\text{Th}$ in backfill as functions of distance at 10^5 years; Bateman-type boundary condition.



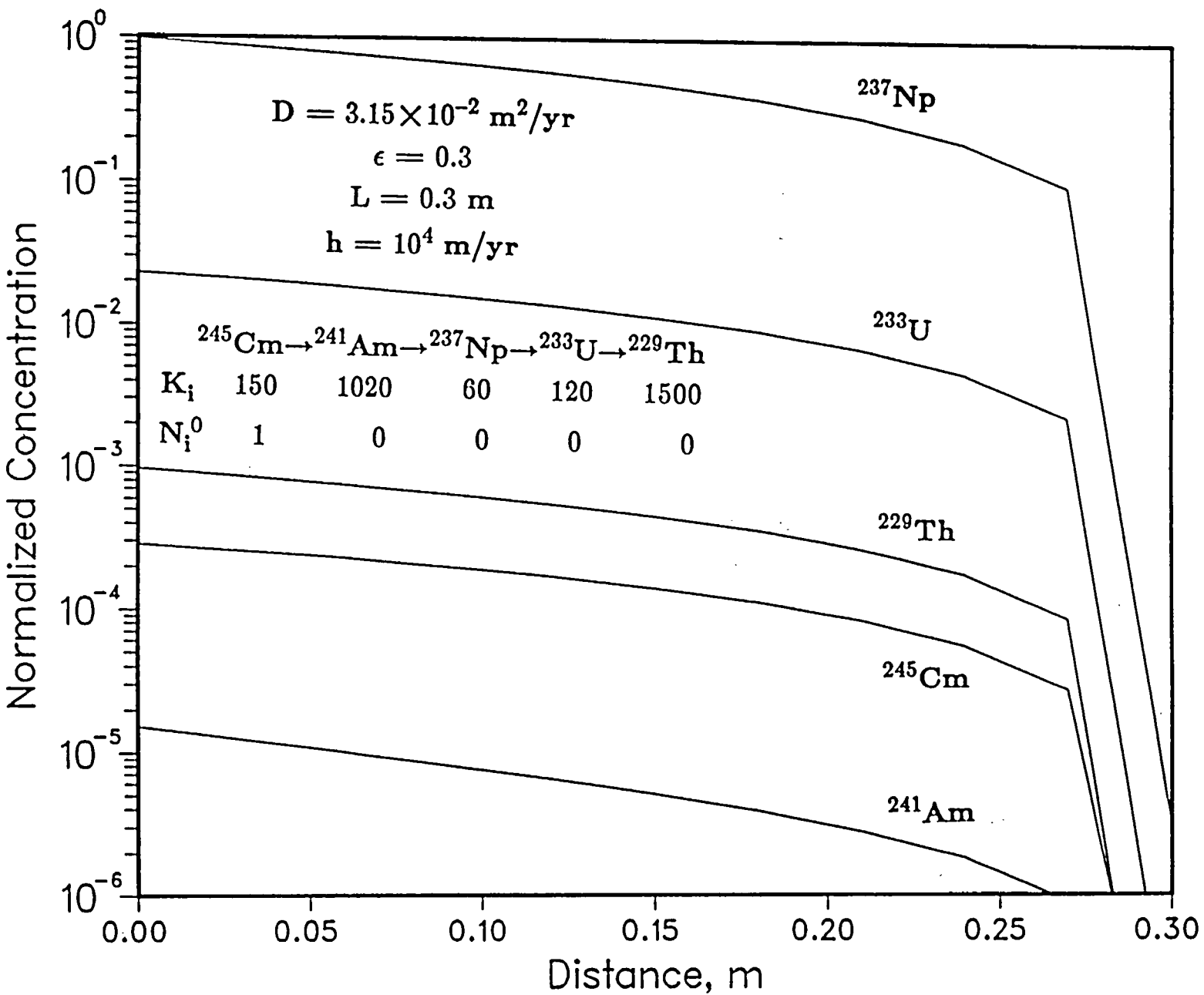


Fig. 21. Normalized concentration profiles for $^{245}\text{Cm} \rightarrow ^{241}\text{Am} \rightarrow ^{237}\text{Np} \rightarrow ^{233}\text{U} \rightarrow ^{229}\text{Th}$ in backfill as functions of distance at 10^5 years; $h = 10^4 \text{ m/yr}$; Bateman-type boundary condition.

^{237}Np has the longest half life in the chain (2.14×10^6 years), it thus remains at a relatively high concentration value and its daughters, ^{233}U and ^{229}Th , are still increasing at this time.

In Fig. 21 one can see that the large value of h accelerates the speed of saturation and the decay effect of each member is not as important. Even ^{241}Am shows some degree of saturation and it is in the secular equilibrium condition with its mother, ^{245}Cm . ^{233}U and ^{229}Th have not yet reached the secular equilibrium, but the tendency is apparent. The equilibrium condition will be established after few hundreds of thousand years. Though not shown here, all previous discussions on the effect of h can be applied to current situation. For example, for a large value of h , all members have lower concentrations and higher mass fluxes at $z=L$ than for the small value of h .

3. Mass Transport through a Semi-infinite Medium

3.1. Theoretical Analysis

All the equations obtained in last section can be applied to present case with only minor changes. That is, we can obtain a set of equations (3.1)-(3.43) identical to (2.1)-(2.43) with some modifications, which will be discussed as follows.

The boundary condition at $z \rightarrow \infty$ (since we are working on a semi-infinite medium) is changed to

$$\frac{\partial^r N_i}{\partial z^r} = O(e^{-kz}), \text{ for } z \rightarrow \infty, k > 0, r=0,1, \dots \quad (3.4)$$

Or in terms of $N_i^{(j)}$ and $n_i^{(j)}$ one has

$$\frac{\partial^r N_i^{(j)}(z,t)}{\partial z^r} = O(e^{-kz}), \text{ for } z \rightarrow \infty, k > 0, r=0,1, \dots \quad (3.9)$$

$$\frac{\partial^r n_i^{(j)}(z,s)}{\partial z^r} = O(e^{-kz}), \text{ for } z \rightarrow \infty, k > 0, r=0,1, \dots \quad (3.17)$$

Now we introduce an infinite Fourier transform with respect to the z variable

$$n_i^{(j)}(p,s) = \int_0^\infty K(p,z) n_i^{(j)}(z,s) dz \quad (3.18)$$

The Fourier kernel $K(p,z)$ satisfies

$$\frac{d^2 K(p,z)}{dz^2} + p^2 K(p,z) = 0, \quad 0 \leq z < \infty \quad (3.19)$$

$$-D\epsilon \frac{dK(p,0)}{dz} + h_1 K(p,0) = 0 \quad (2.20)$$

and instead of (2.20b), $K(p,z)$ satisfies a boundedness condition as $z \rightarrow \infty$. The solution

to this problem is given by*

$$K(p, z) = \sqrt{\frac{2}{\pi}} \frac{p \cos(pz) + \alpha_1 \sin(pz)}{(p^2 + \alpha_1^2)^{1/2}} \quad (3.21)$$

p replaces the eigenvalues β_m in (12.19), and it constitutes a continuous spectrum of range $0 \leq p < \infty$. One now transforms (3.15) with help of (3.18). This leads to a set of steps comparable to (2.22)-(2.27), except that L is replaced by ∞ . On account of the boundedness of $K(p, z)$ and its derivatives and in view of (3.17) the contribution to J at $z = \infty$ vanishes leaving us with

$$n_{\ell}^{(j)}(p, s) = \frac{[\nu_{\ell-1} n_{\ell}^{(j)}(p, s) + \delta_{\ell j} g_{\ell}(p, s)]}{p^2 + \mu_{\ell}}, \quad j \leq \ell \quad (3.27)$$

where

$$g_{\ell}(p, s) = \frac{K(p, 0)}{D\epsilon} N_{\ell}^0 v \epsilon \phi_{\ell}(s) \quad (3.28)$$

and

$$n_{\ell}^{(j)}(p, s) = 0, \quad \ell \leq j$$

The steps of the solution of the difference equation (3.27) are identical to those in Section 2 leading, on inverting with respect to t , to equations (3.29)-(3.38), with β_m replaced by p . However, the Fourier inversion with respect to z transforms to

$$n_i^{(j)}(z, t) = \int_0^{\infty} K(p, z) n_i^{(j)}(p, t) dp, \quad i > j \quad (3.39)$$

$$n_i^{(i)}(z, t) = \int_0^{\infty} K(p, z) n_i^{(i)}(p, t) dp, \quad i = j \quad (3.40)$$

Hence all steps between equations (2.41) to (2.43) remain unchanged and one obtains

*P. L. Chambré, class notes taught in U. C. Berkeley.

the corresponding equations (3.41)-(3.43), except β_m replaced by p and the summation

$\sum_{m=1}^{\infty}$ by $\int_0^{\infty} (\) dp$. The result is the general, non-recursive solution in D_{∞} :

$$N_i(z,t) = e^{\frac{zz}{2D}} \frac{D}{K_i} \left\{ \int_0^{\infty} K(p,z) g_i(p,t) * e^{-\delta_i t} dp + \right. \\ \left. + \sum_{j=1}^{i-1} C_i^{(j)} \sum_{n=j}^i \int_0^{\infty} \frac{K(p,z) g_j(p,t) * e^{-\delta_n t}}{\prod_{\substack{r=j \\ r \neq n}}^i (\Gamma_{nr} p^2 + \gamma_{nr})} dp \right\}, \quad 0 \leq z < \infty, t > 0, i=1,2, \dots \quad (3.43)$$

with $g_i(p,t)$ prescribed by (3.28). One can verify by dimensional arguments of the right hand side of (3.43) that $N_i(z,t) = [gm/cm^3]$.

3.2. Numerical Evaluations

In this section, the general solution (3.43) obtained above will be applied to two special cases so that one can have some insight into this analysis. In either case, a type-I boundary condition will be used at the waste surface and a suitable form of the resulting solution will be derived to make the computational work easier and more practical.

3.2.1. Case 1: Constant Concentration at Boundaries

In this case we assume that the waste package holds intact long enough that all members in the specified decay chain have reached either their solubility limits or the secular equilibrium before they start leaching out. The boundary condition at $z=0$ is then $N_i(0,t) = N_i^0$ and

$$K(p,z) = \sqrt{\frac{2}{\pi}} \sin(pz), \quad g_i(p,t) = \sqrt{\frac{2}{\pi}} p N_i^0.$$

Hence the convolution integral becomes

$$g_i(p,t) * e^{-\delta_n t} = \int_0^t \sqrt{\frac{2}{\pi}} p N_i^0 e^{-\delta_n r} dr = \sqrt{\frac{2}{\pi}} p N_i^0 \left(\frac{1 - e^{-\delta_n t}}{\delta_n} \right)$$

and the solution is reduced to

$$N_i(z,t) = e^{\frac{\nu z}{2D}} \frac{D}{K_i} \frac{2}{\pi} \left\{ N_i^0 \int_0^\infty \frac{p \sin(pz)}{\delta_i} (1 - e^{-\delta_i t}) dp + \sum_{j=1}^{i-1} C_i^{(j)} N_j^0 \sum_{n=j}^i \times \right. \\ \left. \times \int_0^\infty \frac{p \sin(pz)}{\prod_{\substack{r=j \\ r \neq n}}^i (\Gamma_{nr} p^2 + \gamma_{nr})} \frac{(1 - e^{-\delta_n t})}{\delta_n} dp \right\}, \quad z > 0, \quad t > 0, \quad i = 1, 2, \dots \quad (3.44)$$

Although (3.44) is the correct formula, it is not practical for computing. For instance, the first exponential term on the right hand side may be arbitrarily large and exceed the computer limit (e.g., 10^{38} in a VAX-8600 machine) as the distance z increases. On the other hand, as z increases, the frequency of $\sin(pz)$ increases too. This causes the integrand to increase its oscillations, so that the resulting integration is not accurate enough due to the accuracy limit of the computer (e.g., 14 digits in double precision in a VAX machine). To give a numerical illustration, take $\nu=1$ m/yr, $z=500$ m, $D=1$ m²/yr, then the exponential term becomes e^{250} , which cannot be handled by the computer and the calculation would be aborted. To overcome these difficulties, one has to convert (3.44) to some other suitable form. One approach is to use the error functions to replace the integrals and combine the results with the first exponential term. The conversion procedure is given in Appendix A. The coded results are in the computer program UCBNE40, and used in the following examples.

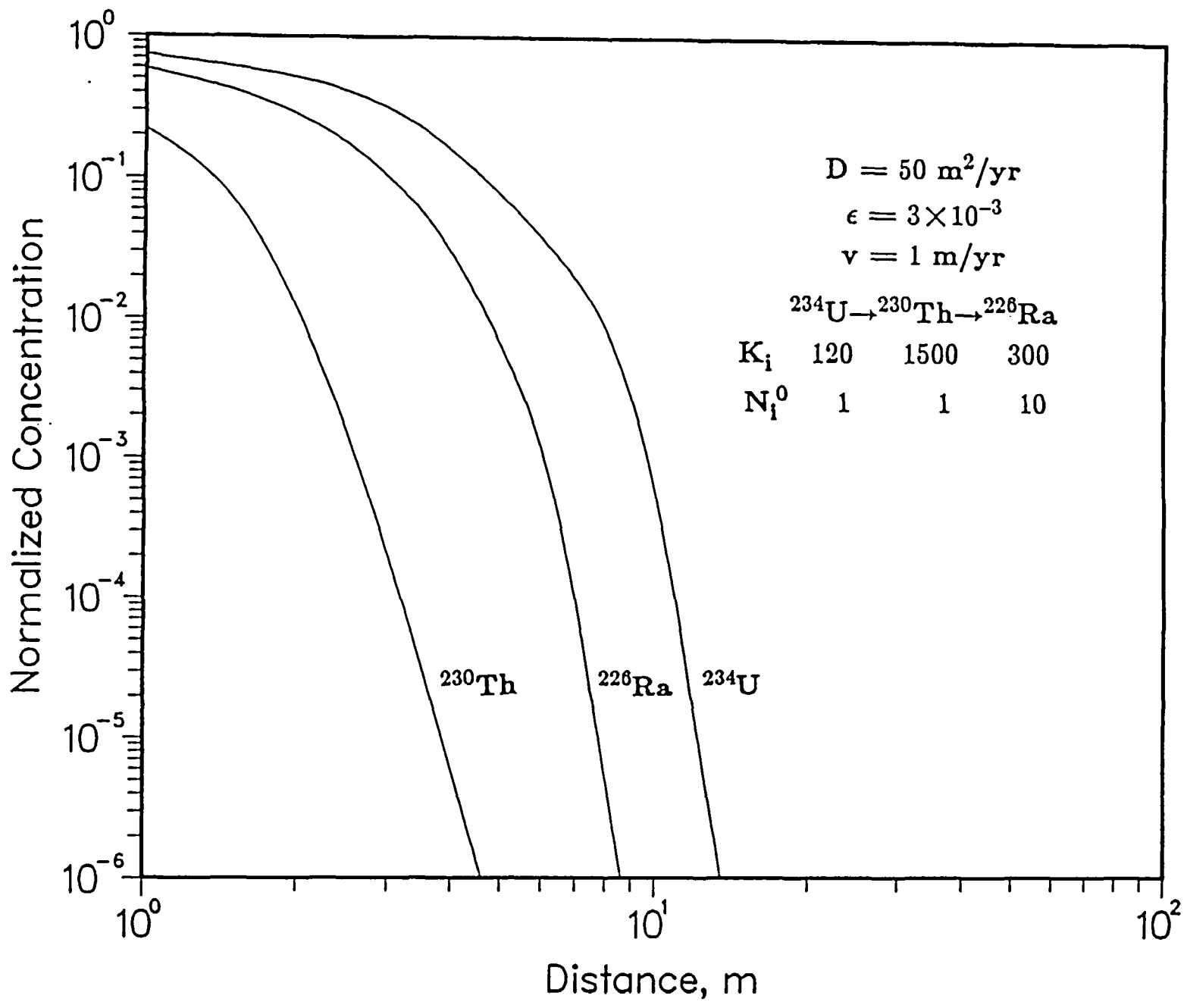
Numerical Examples

As in the finite medium calculations, we investigate two chains, $^{234}\text{U} \rightarrow ^{230}\text{Th} \rightarrow ^{226}\text{Ra}$ and $^{245}\text{Cm} \rightarrow ^{241}\text{Am} \rightarrow ^{237}\text{Np} \rightarrow ^{233}\text{U} \rightarrow ^{229}\text{Th}$. All parameters remain the same as in the previous sections except the following changes. The semi-infinite rock porosity is $\epsilon = 3 \times 10^{-3}$, the pore water velocity is $v = 1$ m/yr, and the dispersion coefficient is $D = 50$ m²/yr. However, the solution and the code are not limited by these choices and can handle any combination of parameters.

Figures 22-24 show the concentration profiles, normalized to N_i^0 , as functions of distance for the $^{234}\text{U} \rightarrow ^{230}\text{Th} \rightarrow ^{226}\text{Ra}$ chain at 10, 1000, and 10^5 years, respectively. At 10 years, the effect of decay is not apparent. ^{234}U travels at the fastest rate because of its smallest retardation coefficient, and covers the largest distance (about 10 meters). ^{230}Th and ^{226}Ra follow the same behavior as ^{234}U .

At 1000 years, one begins to see the decay effect of ^{234}U in the field and the concentration profile for ^{230}Th shows a bend at 30 meters, at which point the derivative of the mass flux with respect to distance becomes negative, i.e., the mass flux of ^{230}Th decreases. This is due to the fact that at this distance, a significant amount of ^{234}U has decayed to ^{230}Th , which causes the concentration gradient to become smaller for thorium. Additional calculations on thorium alone show that if there is no ^{234}U , ^{230}Th itself cannot travel farther than 30 meters at 1000 years due to its retardation. Hence after 30 meters all thorium comes from uranium in the field. From Fig. 23 one can also see that the decay of ^{230}Th occurs mostly within 20 meters. Since during this range ^{226}Ra has a very high concentration one cannot see the increase in its concentration from thorium decay. The traveling speed is still governed by the retardation

Fig. 22. Normalized concentration profiles for $^{245}\text{Cm} \rightarrow ^{241}\text{Am} \rightarrow ^{237}\text{Np} \rightarrow ^{233}\text{U} \rightarrow ^{229}\text{Th}$ in porous rock as functions of distance at 10 years; concentration-limited boundary condition.



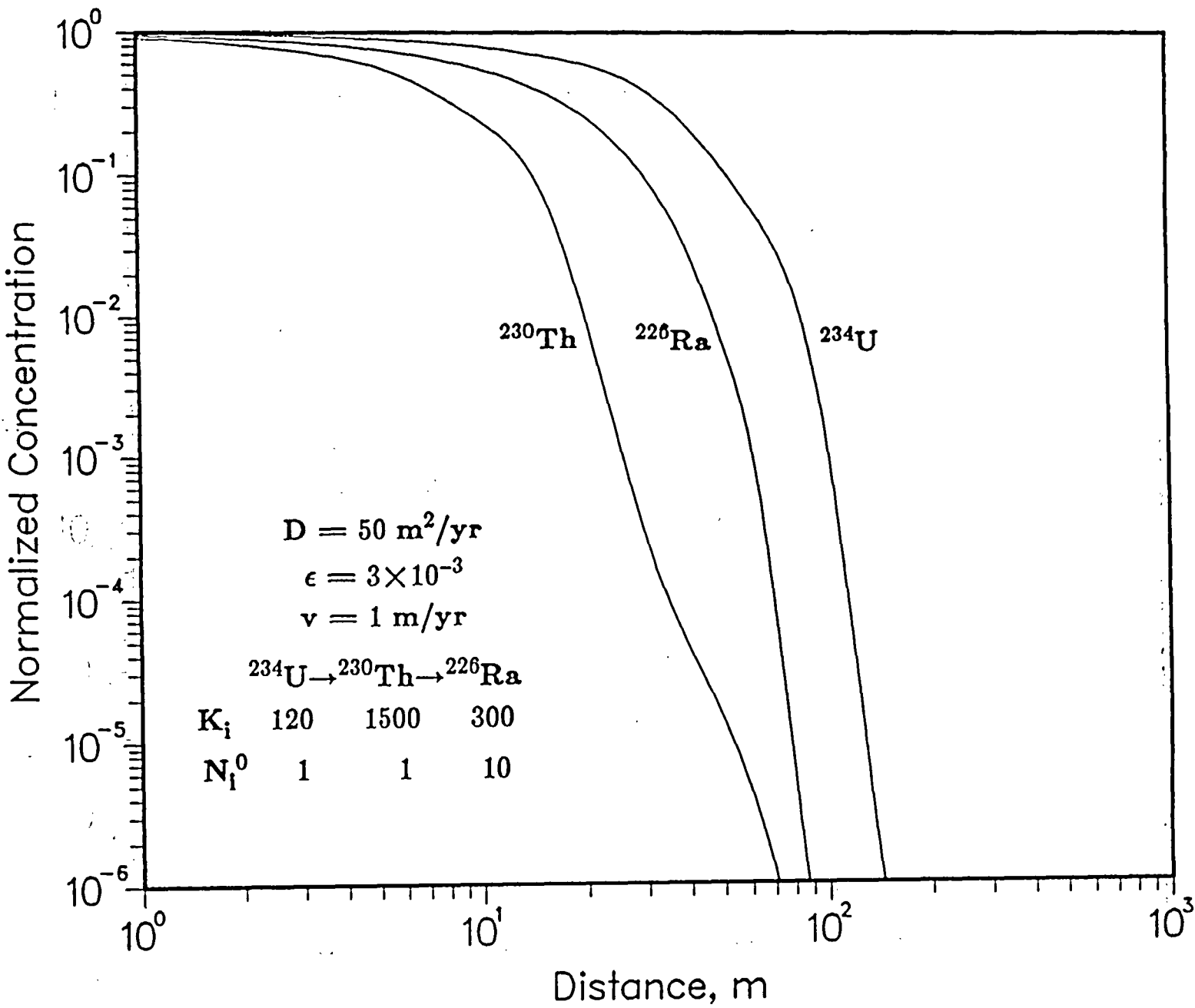


Fig. 23. Normalized concentration profiles for ^{234}U — ^{230}Th — ^{226}Ra in porous rock as functions of distance at 10^3 years; concentration-limited boundary condition.

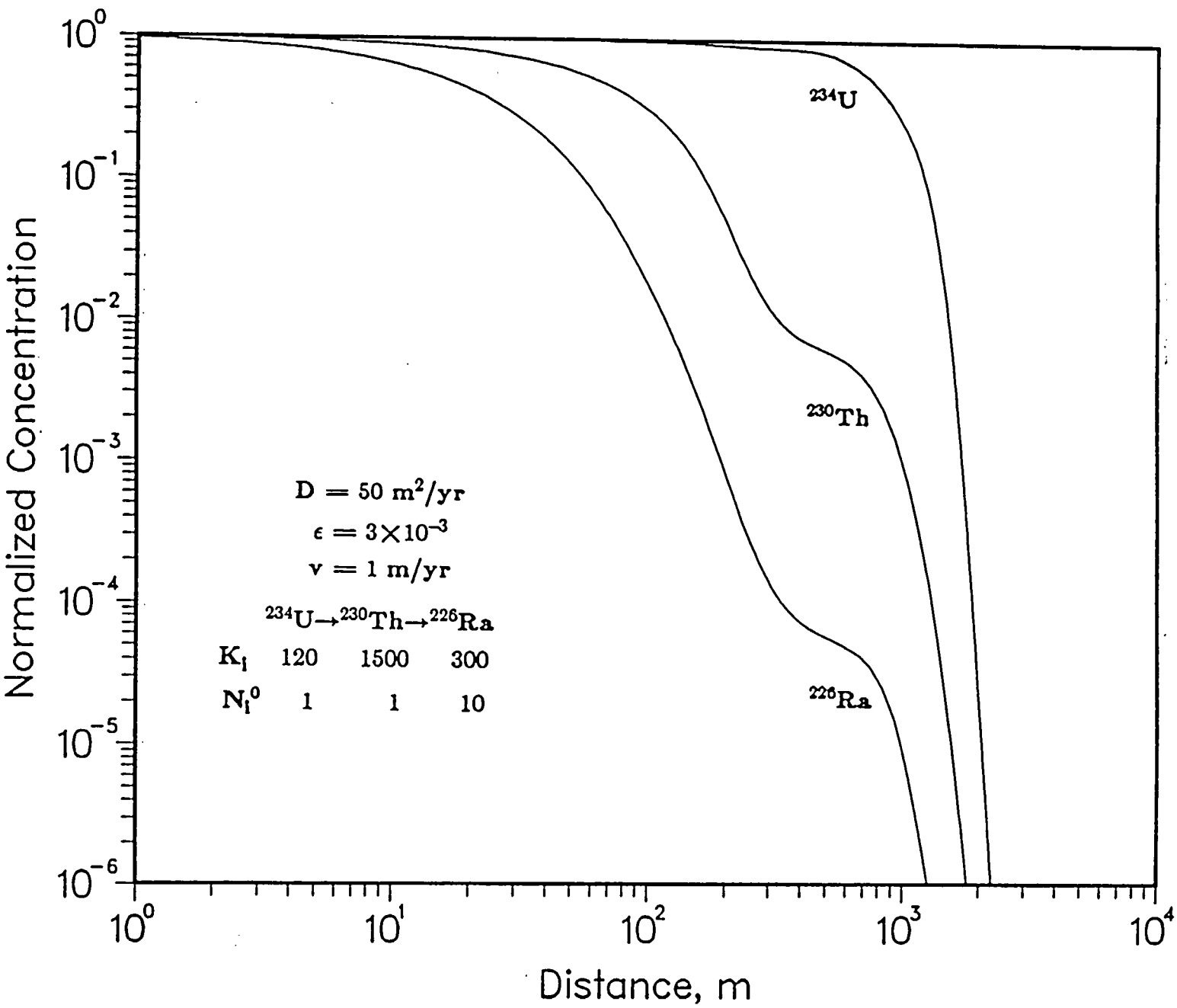


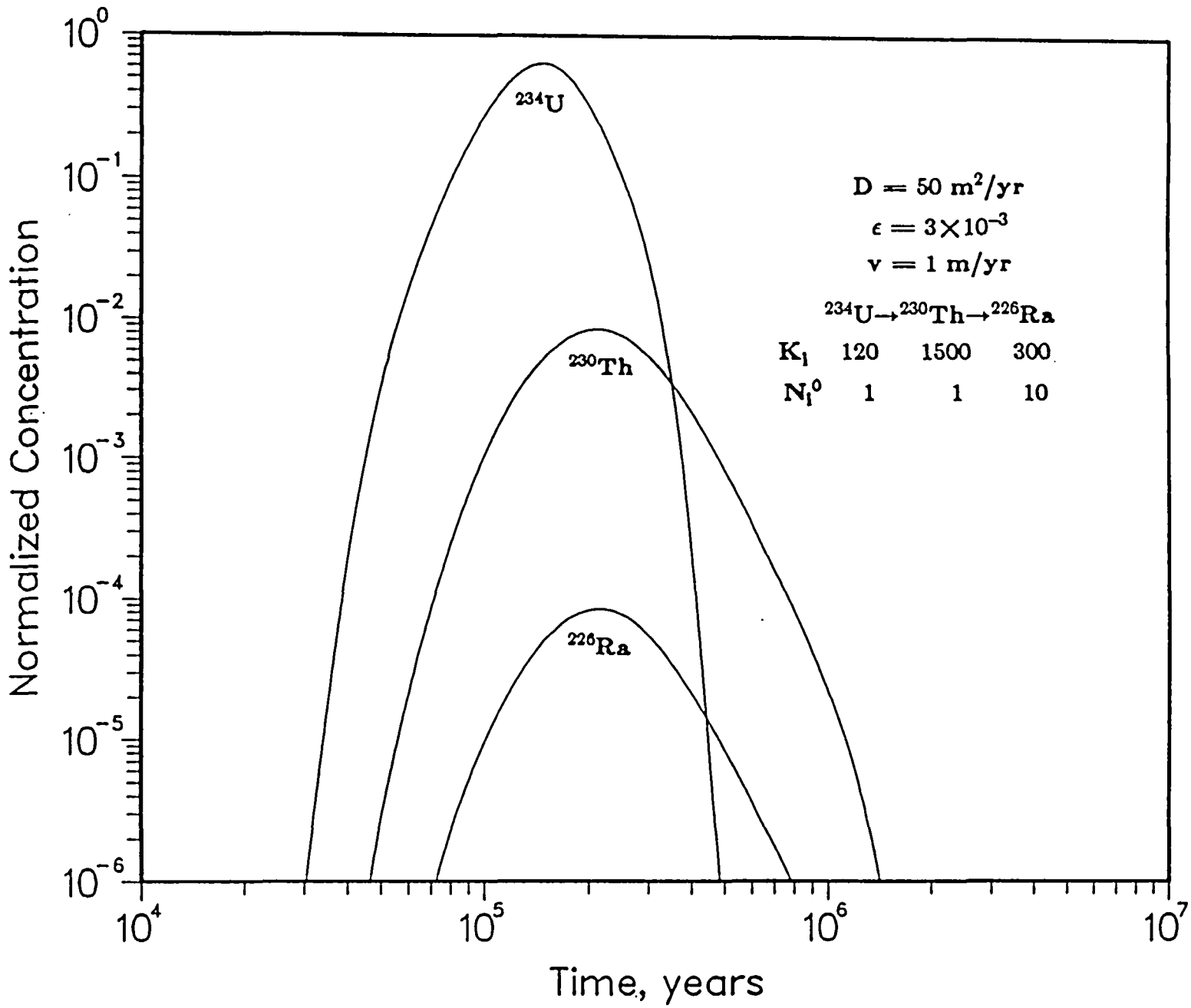
Fig. 24. Normalized concentration profiles for $^{245}\text{Cm} \rightarrow ^{241}\text{Am} \rightarrow ^{237}\text{Np} \rightarrow ^{233}\text{U} \rightarrow ^{229}\text{Th}$ in porous rock as functions of distance at 10^5 years; Bateman-type boundary condition.

coefficient as can be seen in Fig. 23.

Neither ^{230}Th nor ^{226}Ra can travel very far even at 10^5 years, as shown in Fig. 24, since thorium has a high retardation coefficient while radium has a short half life. Separate calculations on thorium and radium show that all ^{230}Th and ^{226}Ra will decay out within one kilometer, had there been no uranium present. The turning points in both thorium and radium profiles are due to uranium decay. Beyond these points the thorium and radium all come from the decay of the mother nuclide, ^{234}U . Another important observation is that at $t=10^5$ years ^{226}Ra falls behind ^{230}Th in the field. This is due to the relatively short half life of ^{226}Ra , i.e., the decay effect of ^{226}Ra is stronger than the retarding effect of ^{230}Th in the field, though both effects limit their migration distance. One can also see that after these turning points thorium and radium tend to reach their equilibrium condition as time goes on. This will be discussed in the next figure.

Figure 25 shows the normalized concentrations as functions of time at a distance of one kilometer. Here we use a leach time of 10^5 years in the calculations. It should be pointed out that the actual radium concentrations are one order of magnitude larger than what is shown here, since the normalization factor for radium (the boundary concentration) is 10 while the normalization factors for the other two members are unity. From the discussion of the last figure we know that were not for the uranium present, neither thorium nor radium would have migrated as far as one kilometer, hence all thorium and radium concentrations in this figure are derived from the decay of ^{234}U . Also, one observes that ^{230}Th and ^{226}Ra are at secular equilibrium at this point. Since ^{234}U has the lowest retardation coefficient, the leading and

Fig. 25. Normalized concentration profiles for $^{245}\text{Cm} \rightarrow ^{241}\text{Am} \rightarrow ^{237}\text{Np} \rightarrow ^{233}\text{U} \rightarrow ^{229}\text{Th}$ in porous rock as functions of time at 10^3 m; concentration-limited boundary condition.



trailing edges all appear earlier than ^{230}Th and ^{226}Ra . This is also true for radium, but it appears at very low concentration range and cannot be shown here.

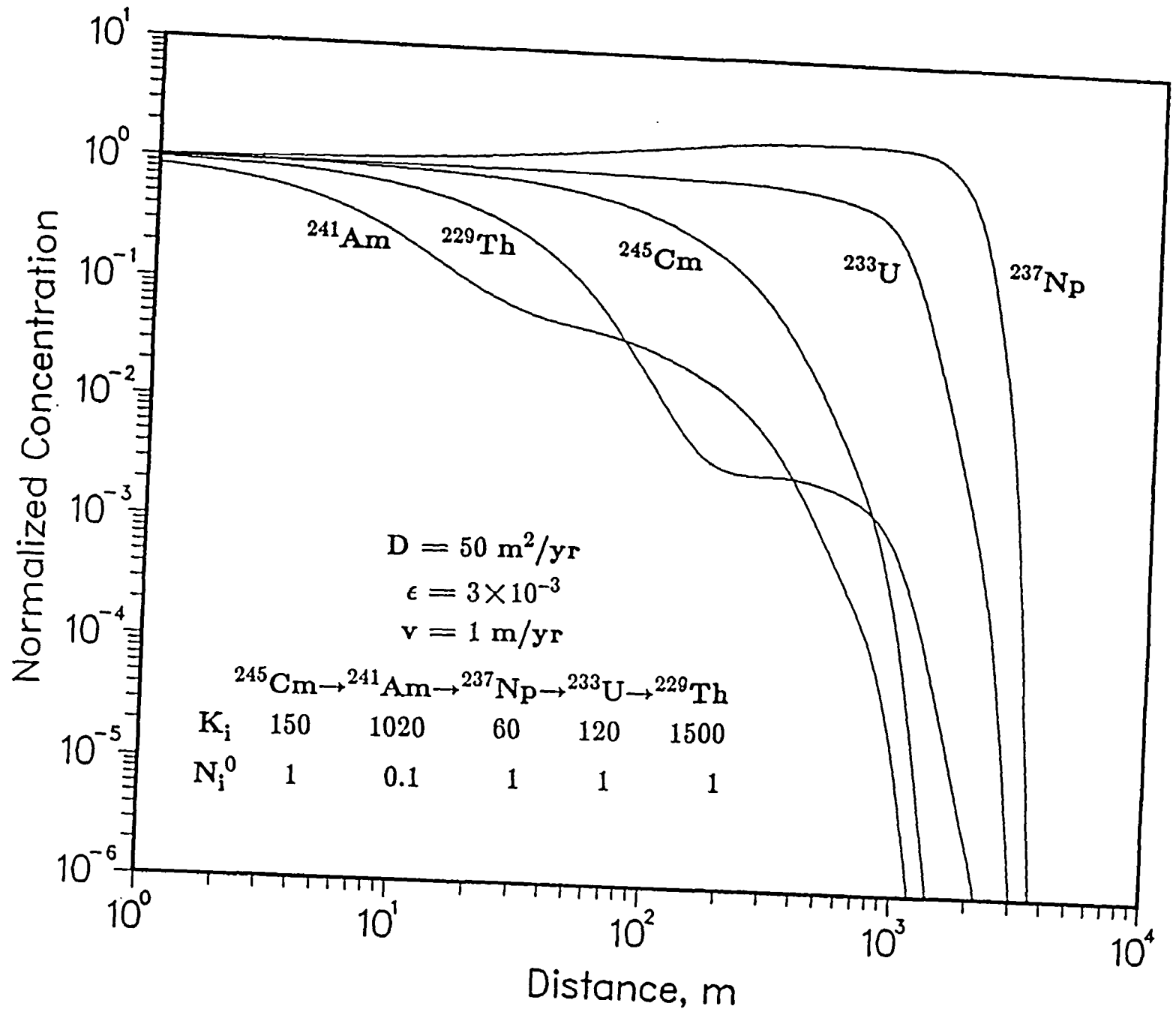
Figure 26 shows the normalized concentrations for the $^{245}\text{Cm} \rightarrow ^{241}\text{Am} \rightarrow ^{237}\text{Np} \rightarrow ^{233}\text{U} \rightarrow ^{229}\text{Th}$ chain as functions of distance at 10^5 years. One can see that the traveling speeds are basically following the same rule, i.e., the higher the retardation coefficient the slower the migration speed, except ^{241}Am due to its very short half life. The decay from ^{241}Am also results in the increase of ^{237}Np concentration in the field for the latter has the longest half life in the chain. From this figure one infers that both ^{241}Am and ^{229}Th would not travel farther than few hundred meters if the parent nuclides were not present in the field. Hence because of the turning points present in ^{241}Am and ^{229}Th profiles, they are produced from the decay of the mother member after these turning points.

Figure 27 shows the normalized concentration profiles as functions of time at 1000 meters with the leach time equal to 10^5 years. Since ^{241}Am and ^{229}Th themselves do not travel this far one can expect that they will be at secular equilibrium conditions with their parent nuclides. This is confirmed in this figure. The leading and trailing edges of each member is determined by its retardation coefficient, hence ^{237}Np appears first, then ^{233}U , and then ^{245}Cm . This rule cannot be applied to ^{241}Am and ^{229}Th since they are produced from their mother members at this time.

3.2.2. Case 2: Bateman-Type Boundary Condition

As in the finite domain case, a congruent dissolution, band release mode is assumed. The boundary concentrations at $z=0$ obey the Bateman equation

Fig. 26. Normalized concentration profiles for $^{245}\text{Cm} \rightarrow ^{241}\text{Am} \rightarrow ^{237}\text{Np} \rightarrow ^{233}\text{U} \rightarrow ^{229}\text{Th}$ in porous rock as functions of distance at 10^5 years; concentration-limited boundary condition.



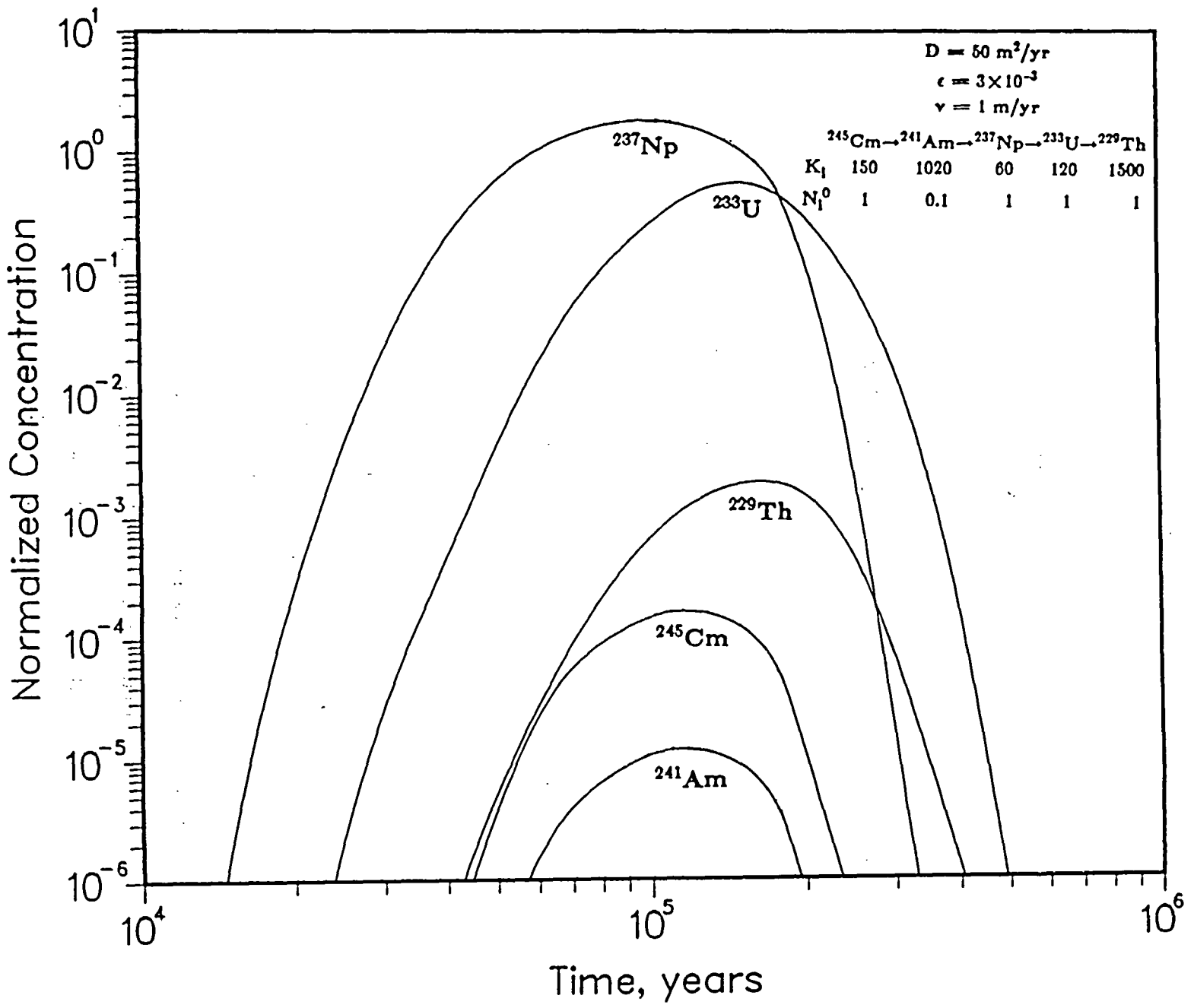


Fig. 27. Normalized concentration profiles for $^{245}\text{Cm} \rightarrow ^{241}\text{Am} \rightarrow ^{237}\text{Np} \rightarrow ^{233}\text{U} \rightarrow ^{229}\text{Th}$ in porous rock as functions of time at 10^3 m; concentration-limited boundary condition.

$$N_i(0,t) = \sum_{j=1}^i B_{ij} e^{-\lambda_j t},$$

and

$$g_i(p,t) = \sqrt{\frac{2}{\pi}} p \sum_{j=1}^i B_{ij} e^{-\lambda_j t}.$$

Hence

$$g_i(p,t) * e^{-\delta_n t} = \int_0^t \sqrt{\frac{2}{\pi}} p \sum_{j=1}^i B_{ij} e^{-\lambda_j(t-\tau)} e^{-\delta_n \tau} d\tau = \sqrt{\frac{2}{\pi}} p \sum_{j=1}^i B_{ij} e^{-\lambda_j t} \frac{1 - e^{-(\delta_n - \lambda_j)t}}{\delta_n - \lambda_j}$$

Let

$$\Delta_{nj} = \delta_n - \lambda_j = \frac{D}{K_n} (p^2 + q_n^2) - \lambda_j = \frac{D}{K_n} (p^2 + q_{nj}^2)$$

where

$$q_{nj}^2 = q_n^2 - \frac{K_n}{D} \lambda_j = \left(\frac{v}{2D}\right)^2 + \frac{K_n}{D} (\lambda_n - \lambda_j) \quad (3.32')$$

then (3.44) changes to

$$N_i(z,t) = e^{\frac{vz}{2D}} \frac{D}{K_i} \frac{2}{\pi} \left\{ \sum_{k=1}^i B_{ik} e^{-\lambda_k t} \int_0^\infty \frac{p \sin(pz)}{\Delta_{ik}} (1 - e^{-\Delta_{ik} t}) dp + \sum_{j=1}^{i-1} C_i^{(j)} \sum_{k=1}^j B_{jk} e^{-\lambda_k t} \times \right. \\ \left. \times \sum_{n=j}^i \int_0^\infty \frac{p \sin(pz)}{\prod_{\substack{r=j \\ r \neq n}}^i (\Gamma_{nr} p^2 + \gamma_{nr})} \frac{(1 - e^{-\Delta_{nk} t})}{\Delta_{nk}} dp \right\}, \quad z > 0, \quad t > 0, \quad i = 1, 2, \dots \quad (3.44')$$

Again some conversions must be made to make the computations workable and practical analogous to those made in the last section. The detailed procedure is shown in Appendix B. The analytic solutions for this case have also been successfully implemented in the computer code UCBNE41 which is used in the following example

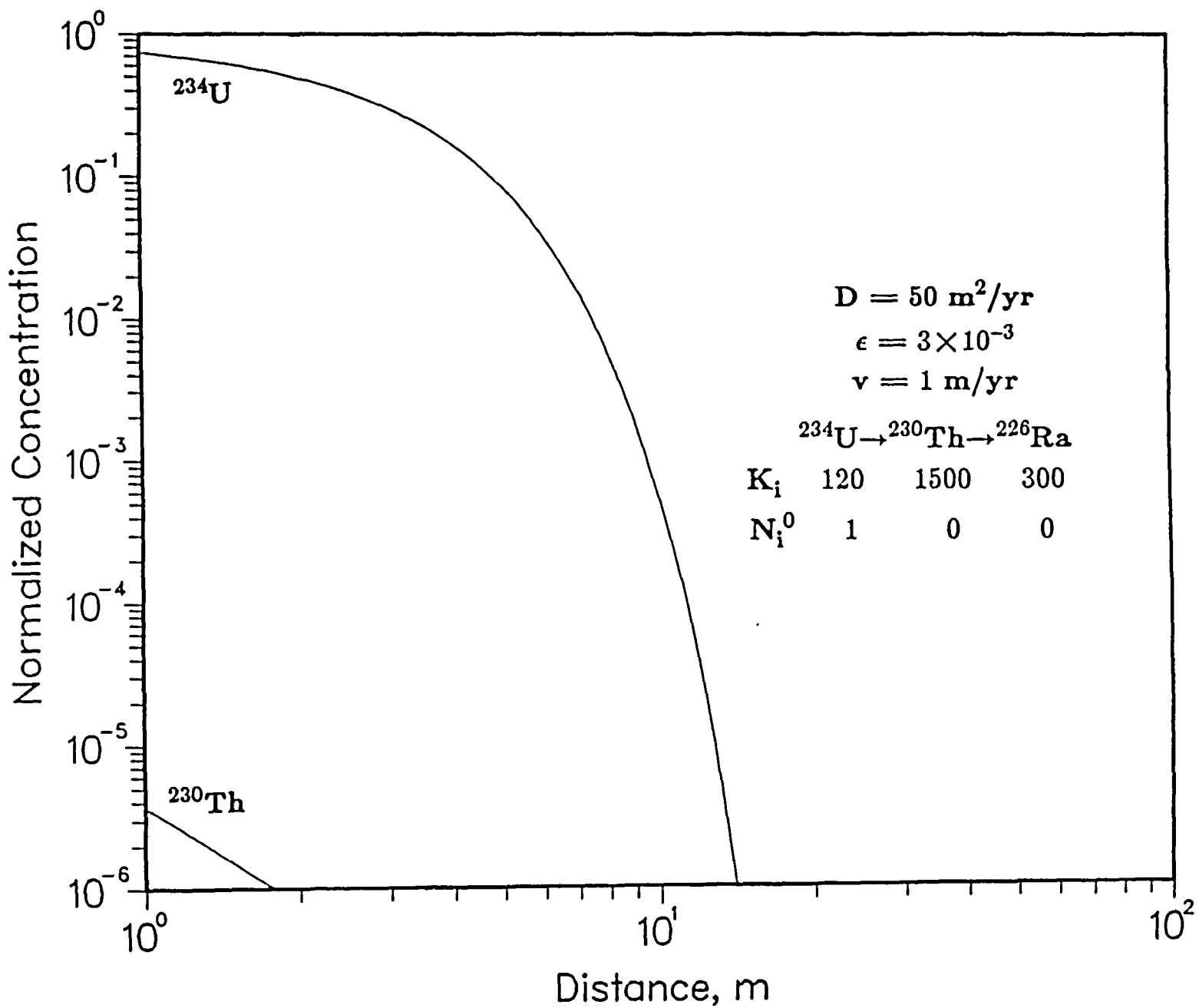
Numerical Examples

All parameters remain the same as in the previous sections except the boundary conditions at $z=0$ is replaced by the Bateman equation (2.57). The initial boundary concentrations are the same as in the corresponding finite medium problem, i.e., unity for mother members and zero for all daughters. As shown in Appendix B, the solution and the program are not limited by this choice, and can be applied to any values of initial concentrations.

Figures 28-30 show the concentration profiles, normalized to $N_1(0,0)$, as functions of distance for $^{234}\text{U} \rightarrow ^{230}\text{Th} \rightarrow ^{226}\text{Ra}$ chain at 10, 1000, and 10^5 years, respectively. In Fig. 28 we see only a small amount of ^{230}Th present near the waste surface originating from the decay of ^{234}U , while the ^{226}Ra concentration is too low to be shown. By comparing this figure with Fig. 22 one sees that the uranium profile is practically identical in these two figures. In fact, even at 1000 and 10^5 years one still sees this same result because of its long half life. Hence we conclude that for ^{234}U the solution for Bateman-type boundary condition will result in the same concentration profile as from the solution for constant boundary concentration case up to 10^5 years.

At 1000 years a significant amount of ^{230}Th and some ^{226}Ra begin to appear as shown in Fig. 29. The decay of ^{234}U in the waste form is the driving force for ^{230}Th migration in the field. Due to the high retardation effect of ^{230}Th it cannot travel beyond a few tens of meters if there is no ^{234}U in the field. Hence the turning in the thorium profile indicates the decay of uranium in the field, i.e., after 20 meters the ^{230}Th concentration totally comes from ^{234}U .

Fig. 28. Normalized concentration profiles for ^{234}U , ^{230}Th , ^{226}Ra in porous rock as functions of distance at 10 years; Bateman-type boundary condition.



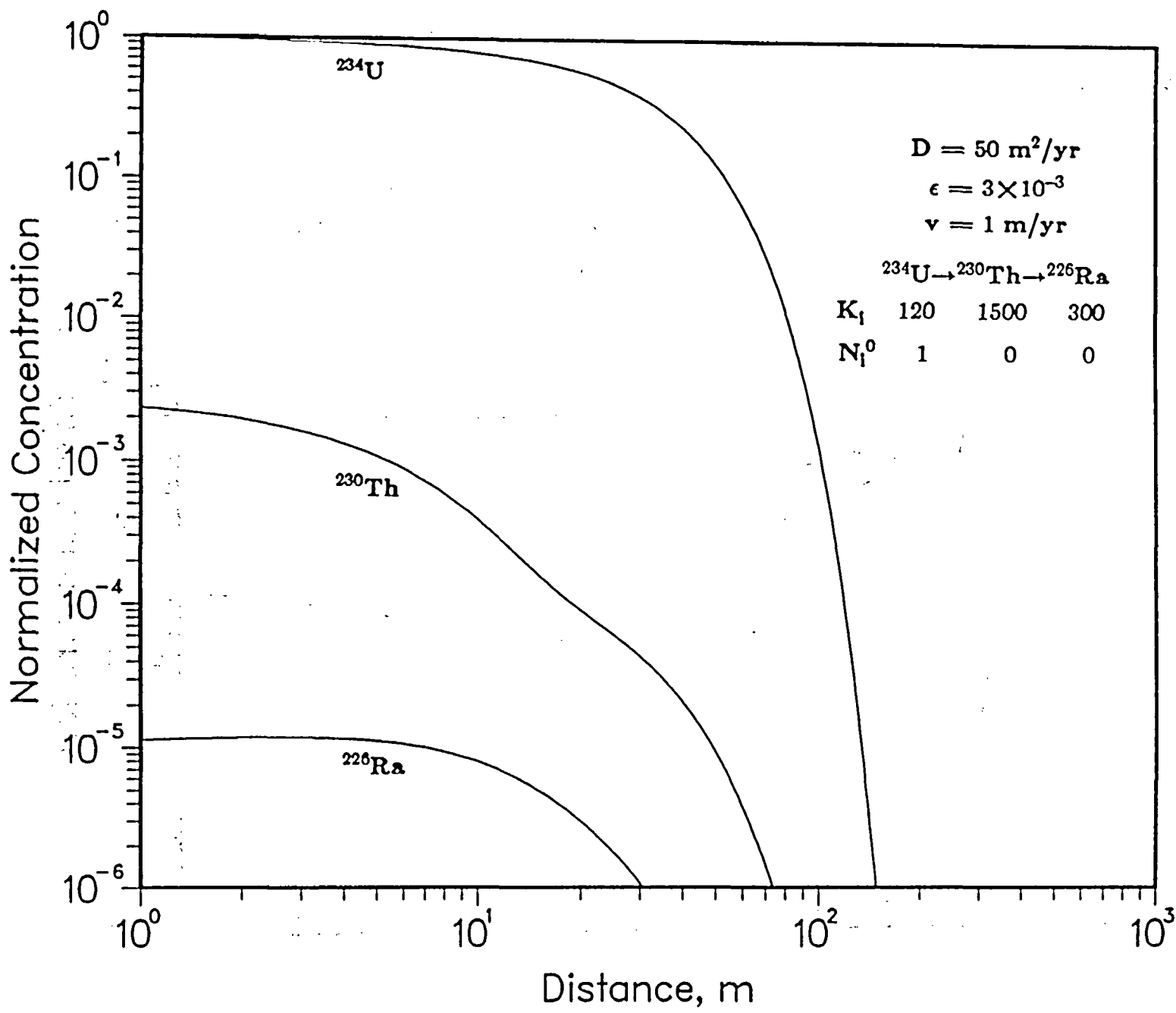


Fig. 29. Normalized concentration profiles for $^{234}\text{U} \rightarrow ^{230}\text{Th} \rightarrow ^{226}\text{Ra}$ in porous rock as functions of distance at 10^3 years; Bateman-type boundary condition.

Fig. 30. Normalized concentration profiles for ^{234}U , ^{230}Th , ^{226}Ra in porous rock as functions of distance at 10^5 years; Bateman-type boundary condition.

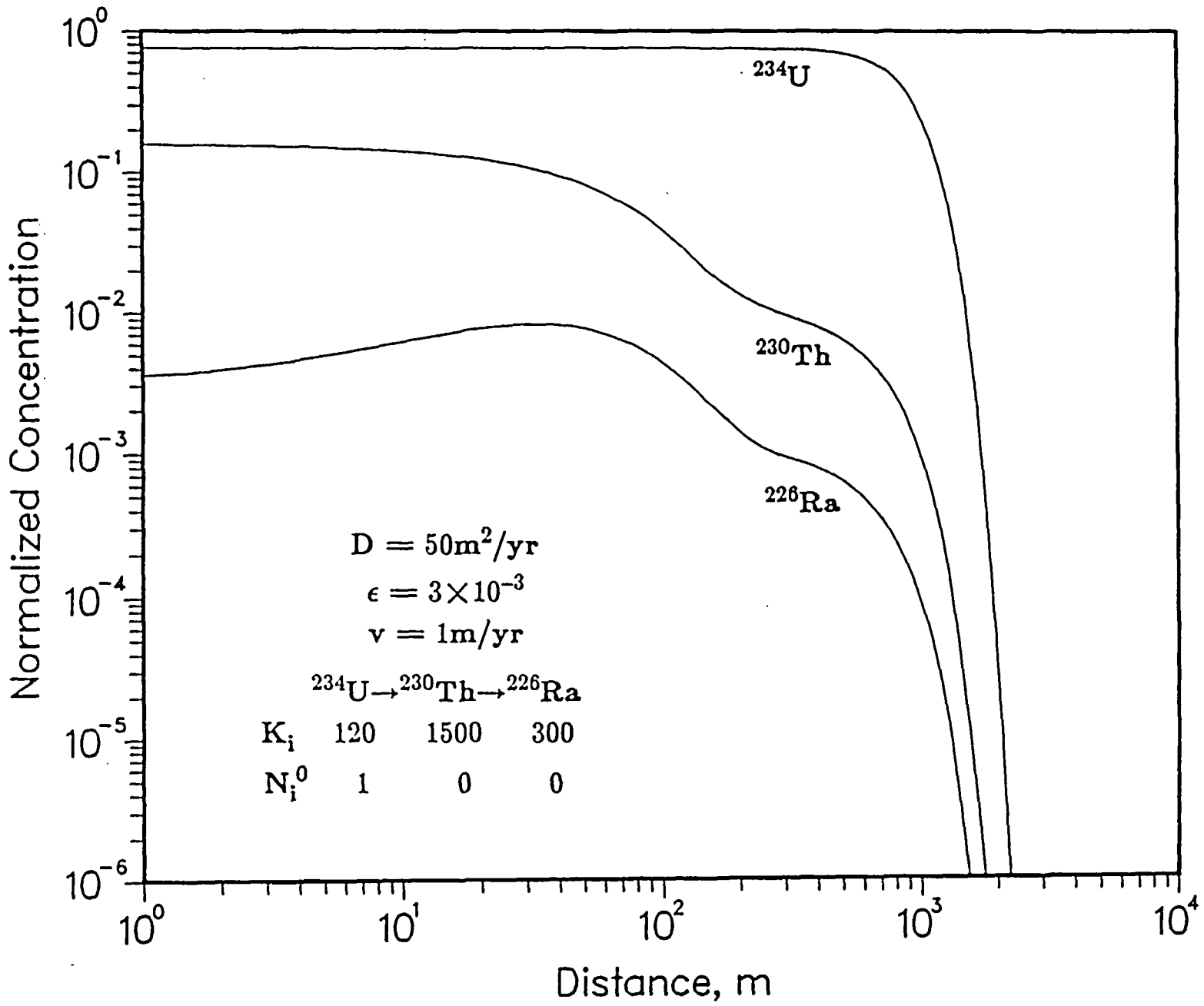


Figure 30 shows that at 10^5 years ^{234}U begins to decay though by a small amount, and ^{230}Th and ^{226}Ra have risen to a significant amount. Like the corresponding results for finite medium in Fig. 13, ^{226}Ra shows an interior maximum due to the faster production rate in the field than in the waste form (cf. Fig. 13). This figure also indicates that after 200 meters, the decay of ^{230}Th and ^{226}Ra become important and the profiles are produced from the decay of ^{234}U after this distance. In fact, one can see that both ^{230}Th and ^{226}Ra would not migrate beyond 1000 meters by themselves.

Figure 31 shows the normalized concentration profiles as a function of time at 1000 meters with a leach time of 10^5 years. From the last figure we know that at this distance all ^{230}Th and ^{226}Ra are produced from the decay of ^{234}U in the field. Hence ^{230}Th and ^{226}Ra are already at secular equilibrium. We see that Fig. 31 is actually the same as Fig. 25, because ^{234}U can be regarded as a stable species at this distance.

Figure 32 shows the normalized concentration profiles as a function of distance for the $^{245}\text{Cm} \rightarrow ^{241}\text{Am} \rightarrow ^{237}\text{Np} \rightarrow ^{233}\text{U} \rightarrow ^{229}\text{Th}$ chain at 10^5 years. As in Fig. 26 one finds that ^{237}Np travels fastest due to its low retardation coefficient and its longest half life. At 10^5 years almost all ^{245}Cm and ^{241}Am have decayed away, but the normalized concentration of ^{237}Np rises to nearly unity for it has not yet started decaying. Again in this figure we see that the migration distance is inversely dependent upon its retardation coefficient except for ^{241}Am and ^{229}Th . They cannot travel very far due to short half life or large retardation coefficient. In fact, this figure shows basically the same features as exhibited in Fig. 26, except at the waste surface.

Figure 33 shows the normalized concentration profiles as a function of time at 1000 meters with a leach time of 10^5 years. Only four members are shown in this

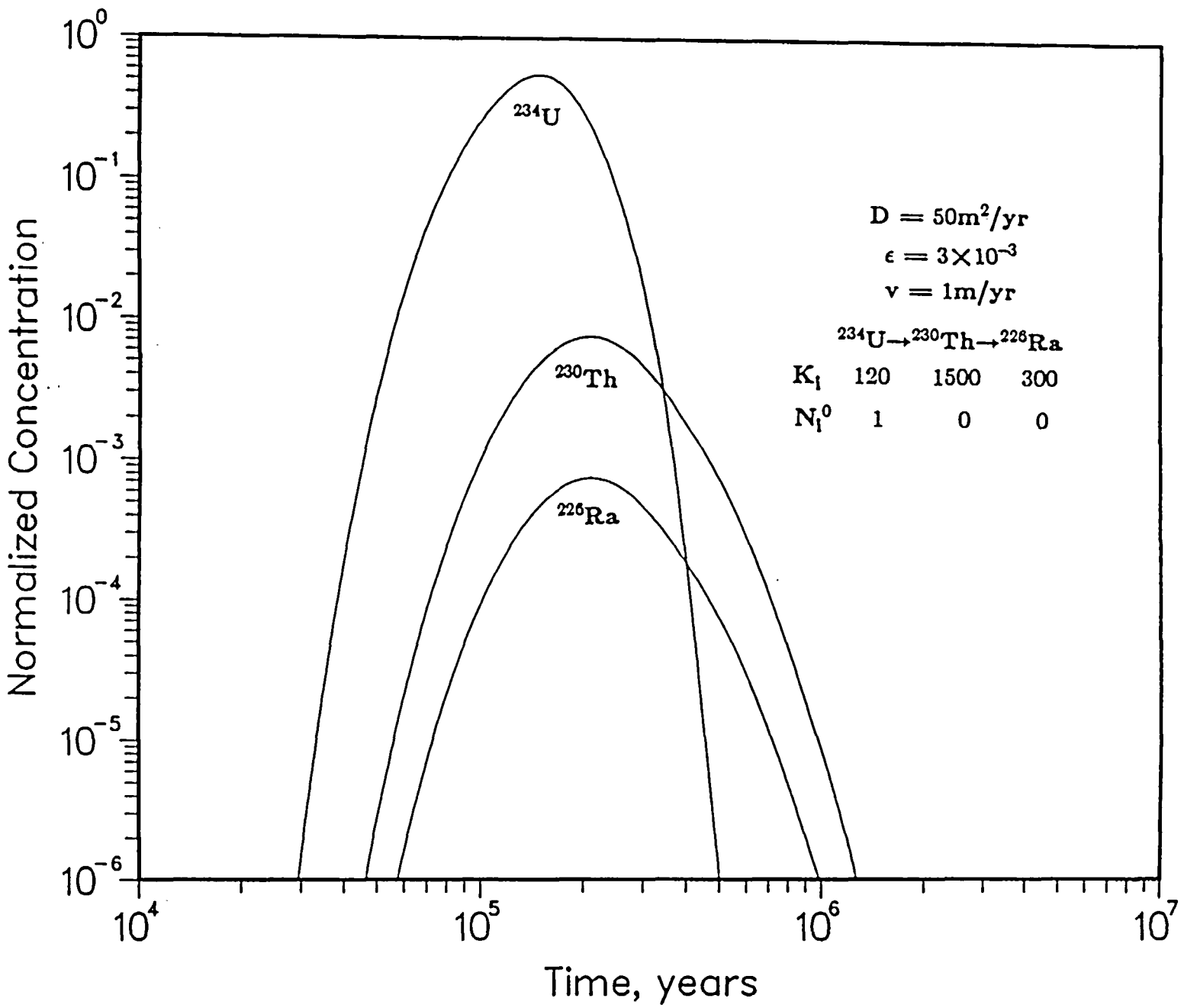
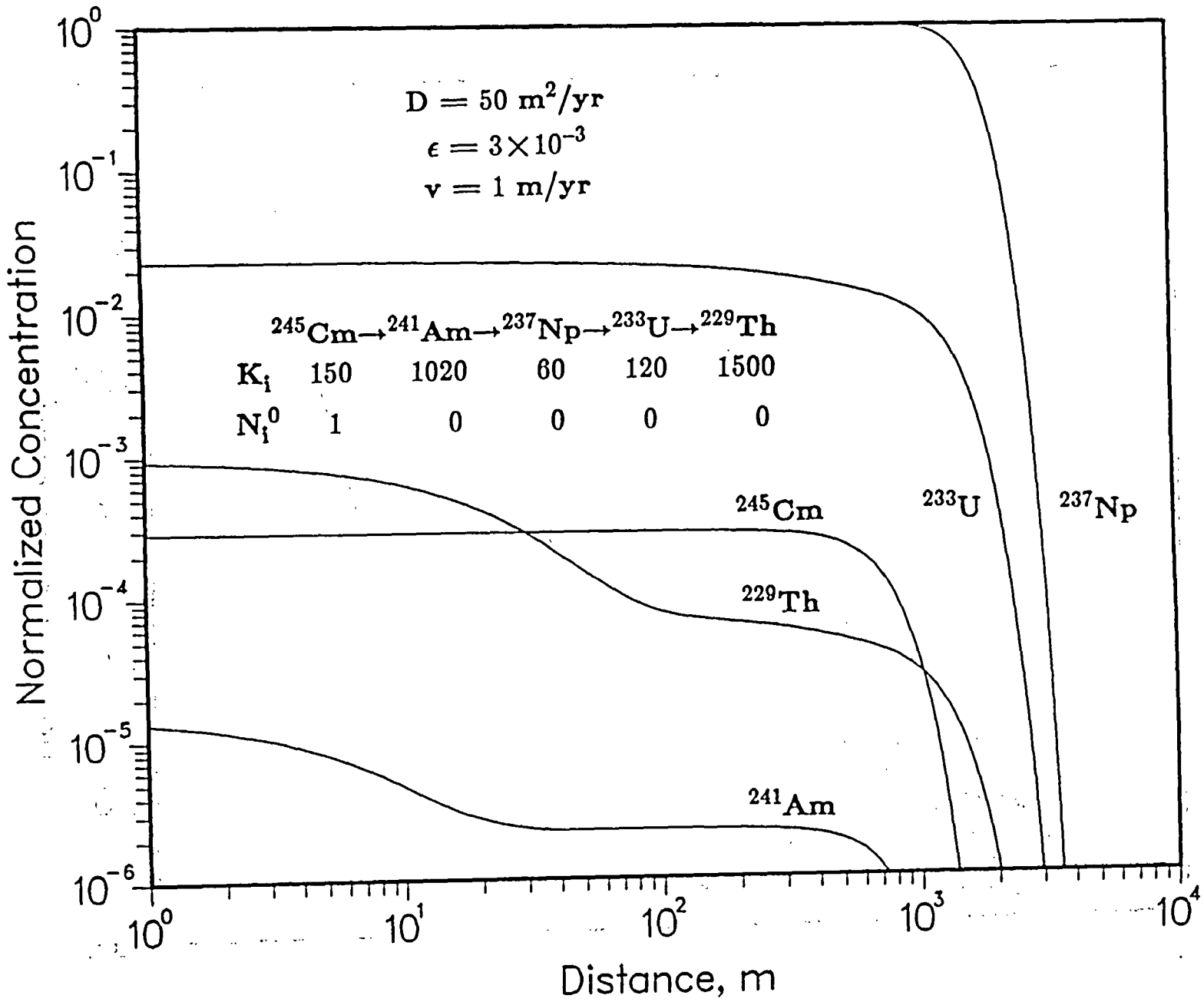


Fig. 31. Normalized concentration profiles for ^{234}U , ^{230}Th , ^{226}Ra in porous rock as functions of time at 10^3 m; Bateman-type boundary condition.

Fig. 32. Normalized concentration profiles for $^{245}\text{Cm} \rightarrow ^{241}\text{Am} \rightarrow ^{237}\text{Np} \rightarrow ^{233}\text{U} \rightarrow ^{229}\text{Th}$ in porous rock as functions of distance at 10^5 years; Bateman-type boundary condition.



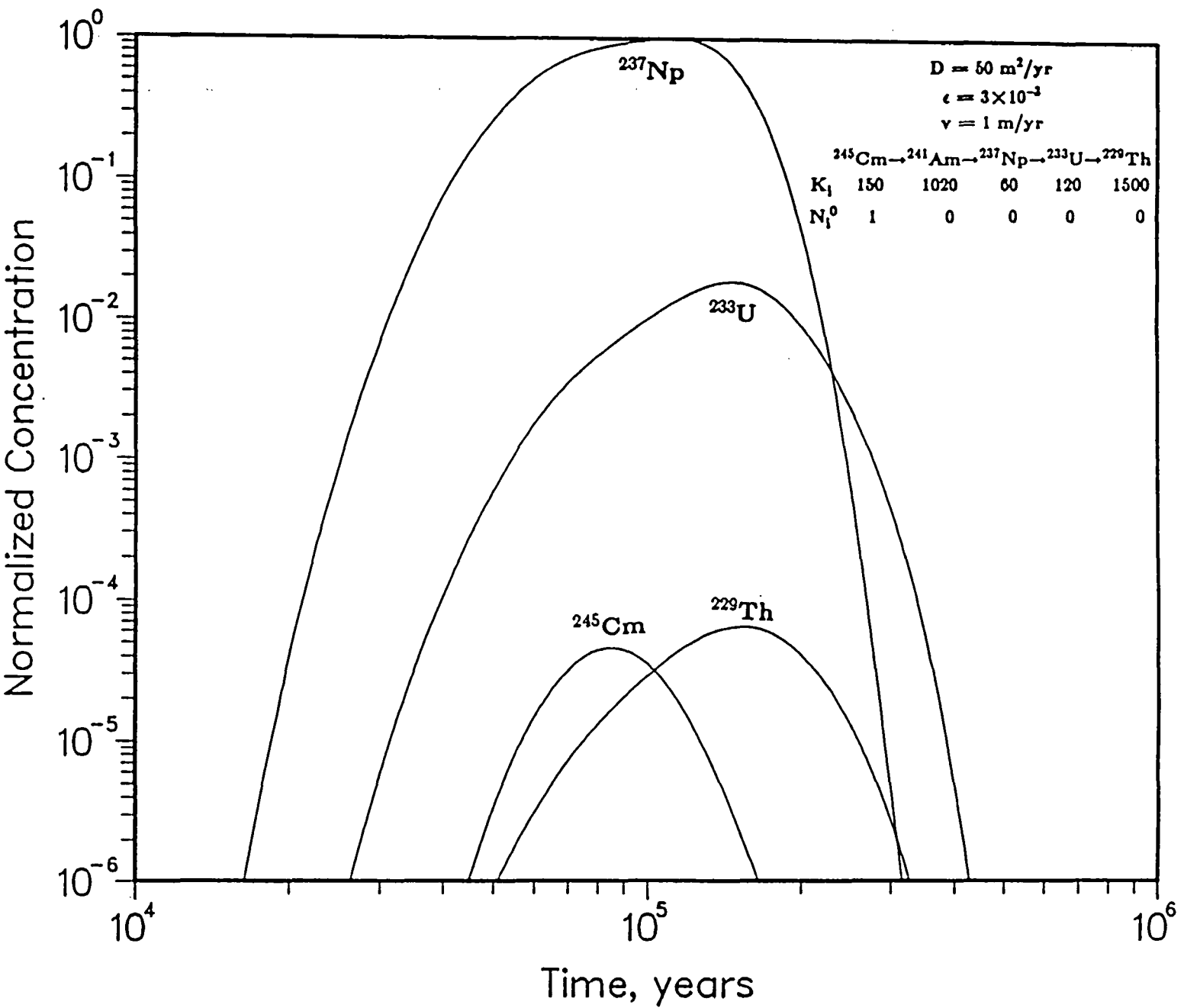


Fig. 33. Normalized concentration profiles for $^{245}\text{Cm} \rightarrow ^{241}\text{Am} \rightarrow ^{237}\text{Np} \rightarrow ^{233}\text{U} \rightarrow ^{229}\text{Th}$ in porous rock as functions of time at 10^3 m ; Bateman-type boundary condition.

graph because ^{241}Am concentration is too low to be plotted. We find that ^{233}U and ^{229}Th are at secular equilibrium after 2×10^5 years since at this distance all thorium comes from the decay of uranium. This is also true for ^{245}Cm and ^{241}Am . The general features of this figure are similar to those in Fig. 27 and all discussions provided there can also be applied here.

One very important point about these calculations is that this code UCBNE41 can be used to replace the popular three-member-chain calculation programs UCBNE10.2 and UCBNE10.3 because it can compute the concentration profile of any member without any numerical difficulties and can also be applied to a chain of arbitrary length. Though not shown in the above figures, it can actually produce the results of the dispersion-free code UCBNE25 by setting the dispersion coefficient to a very small value (e.g., $10^{-4} \text{ m}^2/\text{yr}$). One cannot set D equal to zero in UCBNE41 for a singularity will occur as seen from the solution form developed in Appendix A. But for very small values of D the results indeed have the same graphical trends as those from UCBNE25, with only the small rounding appearing at the leading and trailing edges. These are usually produced by the dispersion-free calculations.

4. Conclusions

In this report, the general non-recursive solutions for the transport of radioactive decay chains are obtained. The first half of the report deals with transport in a finite span such as a backfill layer, while the second half analyzes mass transport in a semi-infinite domain. Two decay chains, $^{234}\text{U} \rightarrow ^{230}\text{Th} \rightarrow ^{226}\text{Ra}$ and $^{245}\text{Cm} \rightarrow ^{241}\text{Am} \rightarrow ^{237}\text{Np} \rightarrow ^{233}\text{U} \rightarrow ^{229}\text{Th}$, are used in the numerical examples.

A mass transfer coefficient $h=10^{-4}$ m/y obtained in two previous studies is used in the finite span calculations. The outer boundary of the backfill acts like an impermeable surface at this value of h , since the flux at this position is nearly zero. Another value of h , 10^4 m/yr, is also used to simulate a strong water flow outside the backfill. The mass transfer rate for this value of h is at least two orders of magnitude greater than that for $h=10^{-4}$ m/yr. Since normally the underground water velocity is low (≤ 1 m/yr, which is equivalent to $h \leq 10^{-4}$ m/yr), the mass flux out of the backfill is quite small.

At early times (< 10 years), the finite medium calculations can be replaced by the semi-infinite medium solution, since the nuclides have not yet reached the backfill/rock interface. We would recommend that future users of these codes do this to reduce computing time and cost, though the finite medium codes UCBNE50, UCBNE51, and UCBNE52 can make the calculations without numerical difficulties.

The zero velocity assumption in backfill used in previous chapters are justified by the finite medium calculations. For pore water velocity $v=0.01$ m/yr, the relative error introduced by the zero velocity assumption is less than 5%; while for $v=0.001$ m/yr it is less than 1%. Since the pore water velocity normally encountered in

repositories is of the order of 10^{-6} to 10^{-9} m/yr, it is believed that the use of the no-flow assumption in backfill calculations is sensible.

In both finite and semi-infinite media calculations, ^{226}Ra always shows an interior maximum within the field. This phenomenon is due to the combined effects of transport, decay, and retardation of radium and its precursors, and can be seen only in the chain calculations. Hence to get more details in the radionuclide migration analysis, this kind of chain calculations becomes necessary.

In several figures, the concentration of a daughter nuclide built up so much in the field that it exceeds the concentration at the source. This would mean a back diffusion of the nuclide towards the source, due to an improperly specified boundary condition. Such a phenomenon occurs mostly in backfill with the lower value of the mass transfer coefficient. Calculations not reported here show that stronger flows outside the backfill would tend to weaken this phenomenon.

In semi-infinite medium calculations, the nuclides with high retardation coefficients, such as ^{230}Th , ^{226}Ra , ^{241}Am , and ^{229}Th , would not travel farther than 1000 meters in the field without transport of their precursors. This means that essentially all these nuclides come from their mothers at this distance. In the numerical examples, the mother members, such as ^{234}U and ^{233}U , which need a few hundred thousand years to travel this far, are already in secular equilibrium with the daughters. Hence only the concentrations of the mother nuclides are required to get the entire concentration profiles after 1000 meters.

Before this analysis became available, sometimes a "compression" method was used to transform a long chain to a 3-member chain by neglecting the short-lived

members in order to use the existing code UCBNE10.2. Now a tool is provided to examine whether this approach is valid or necessary. If not, one has to turn to the solutions obtained here to make more precise calculations.

Possible extensions of the current study would be to include different dispersion/diffusion coefficients for each member of the chain. Another might be to utilize non-constant mass transfer coefficients h . The analysis could also be extended to cover different h_i for each member.

References

1. U. S. Environmental Protection Agency, Title 41, Code of Federal Regulations, Part 191, 1985
2. U. S. Nuclear Regulatory Commission, Title 10, Code of Federal Regulations, Part 50, 1983
3. Harada, M., et al., "Migration of Radionuclides Through Sorbing Media, Analytical Solution - I," LBL-10500, 1980.
4. P. L. Chambré, T. H. Pigford, W. W.-L. Lee, J. Ahn, S. Kajiwara, C. L. Kim, H. Kimura, H. Lung, W. J. Williams, S. J. Zavoshy, "Mass Transfer and Transport in a Geologic Environment," LBL-19430, 1985.
5. J. F. Relyea and M. I. Wood, "An Analytical One-Dimensional Model for Predicting Waste Package Performance," SD-BWI-TI-232, 1984.

Appendix A: Numerical Implementation of Equation (3.44)

In this appendix we discuss the conversions needed to implement the analytic solutions obtained in the main text. The solution for $N_i(z, t)$ is given by

$$N_i(z, t) = e^{\frac{vz}{2D}} \frac{D}{K_i} \frac{2}{\pi} \left\{ N_i^0 \int_0^\infty \frac{p \sin(pz)}{\delta_i} (1 - e^{-\delta_i t}) dp + \sum_{j=1}^{i-1} C_i^{(j)} N_j^0 \sum_{n=j}^i \times \right. \\ \left. \times \int_0^\infty \frac{p \sin(pz)}{\prod_{\substack{r=j \\ r \neq n}}^i (\Gamma_{nr} p^2 + \gamma_{nr})} \frac{(1 - e^{-\delta_n t})}{\delta_n} dp \right\}, \quad z > 0, \quad t > 0, \quad i = 1, 2, \dots \quad (3.44)$$

To implement this solution two transformations* are needed

$$\int_0^\infty \frac{p \sin(pz)}{p^2 + q^2} dp = \frac{\pi}{2} e^{-qz} \quad (3.45)$$

$$\int_0^\infty \frac{p \sin(pz)}{p^2 + q^2} e^{-\beta p^2} dp = \frac{\pi}{4} e^{-\beta q^2} \left[2e^{-qz} - e^{-qz} \operatorname{erfc}\left(\frac{z}{2\sqrt{\beta}} - q\sqrt{\beta}\right) - e^{qz} \operatorname{erfc}\left(\frac{z}{2\sqrt{\beta}} + q\sqrt{\beta}\right) \right] \quad (3.46)$$

Now from the definition of δ_i (3.32) and with the help of (3.45) and (3.46) one gets

$$\int_0^\infty \frac{p \sin(pz)}{\delta_i} (1 - e^{-\delta_i t}) dp \\ = \frac{K_i}{D} \int_0^\infty \frac{p \sin(pz)}{p^2 + q^2} \left[1 - e^{-\frac{D}{K_i}(p^2 + q^2)t} \right] dp \\ = \frac{\pi K_i}{4 D} \left[e^{-q_i z} \operatorname{erfc}\left[\frac{z}{2\sqrt{Dt/K_i}} - (\lambda_i t + \frac{v^2 t}{4DK_i})^{1/2}\right] + e^{q_i z} \operatorname{erfc}\left[\frac{z}{2\sqrt{Dt/K_i}} + (\lambda_i t + \frac{v^2 t}{4DK_i})^{1/2}\right] \right] \quad (3.47)$$

Hence the first term on the right hand side of (3.44) is converted to

*Gradshteyn, I. S., and Ryzhik, I. M., "Table of Integrals, Series, and Products," Eqs. (3.723.3) and (3.954.1), pp. 406, 497, Academic Press, 1980.

$$\frac{N_i^0}{2} \left[e^{-(\sigma_i - \frac{v}{2D})z} \operatorname{erfc} \left[\frac{z}{2\sqrt{Dt/K_i}} - (\lambda_i t + \frac{v^2 t}{4DK_i})^{1/2} \right] + e^{(\sigma_i + \frac{v}{2D})z} \operatorname{erfc} \left[\frac{z}{2\sqrt{Dt/K_i}} + (\lambda_i t + \frac{v^2 t}{4DK_i})^{1/2} \right] \right] \quad (3.48)$$

For the second term on the r.h.s. we do the following:

$$\frac{1}{\prod_{\substack{r=j \\ r \neq n}}^i (\Gamma_{nr} p^2 + \gamma_{nr})} \frac{1}{\delta_n} = \left(\frac{1}{\prod_{\substack{r=j \\ r \neq n}}^i \Gamma_{nr}} \frac{1}{K_n} \right) \cdot \frac{1}{\prod_{r=j}^i (p^2 + d_{nr}^2)} = F_n' \frac{1}{\prod_{r=j}^i (p^2 + d_{nr}^2)} \quad (3.49)$$

where

$$d_{nr}^2 \equiv \begin{cases} \frac{\gamma_{nr}}{\Gamma_{nr}} = \left(\frac{v}{2D}\right)^2 - \frac{K_r K_n}{D} \left(\frac{\lambda_n - \lambda_r}{K_n - K_r}\right), & r \neq n, \quad r = j, j+1, \dots, i; \\ q_n^2, & r = n. \end{cases} \quad (3.50)$$

and

$$F_n' \equiv \frac{1}{\left(\prod_{\substack{r=j \\ r \neq n}}^i \Gamma_{nr}\right) \frac{D}{K_n}} = \frac{1}{\prod_{r=j}^i \left(\frac{D}{K_r}\right)} \frac{1}{\prod_{\substack{r=j \\ r \neq n}}^i \left(1 - \frac{K_r}{K_n}\right)} \quad (3.51)$$

Also

$$\frac{1}{\prod_{r=j}^i (p^2 + d_{nr}^2)} = \sum_{r=j}^i \frac{E_{nr}}{(p^2 + d_{nr}^2)}, \quad E_{nr} \equiv \frac{1}{\prod_{\substack{w=j \\ w \neq r}}^i (d_{nw}^2 - d_{nr}^2)} \quad (3.52)$$

Hence

$$\begin{aligned} & \int_0^\infty \frac{p \sin(pz)}{\prod_{\substack{r=j \\ r \neq n}}^i (\Gamma_{nr} p^2 + \gamma_{nr})} \frac{(1 - e^{-\delta_n t})}{\delta_n} dp \\ &= F_n' \sum_{r=j}^i E_{nr} \int_0^\infty \frac{p \sin(pz)}{p^2 + d_{nr}^2} (1 - e^{-(\sigma_n^2 + p^2)Dt/K_n}) dp \end{aligned}$$

$$\begin{aligned}
&= F_n' \sum_{r=j}^i E_{nr} \left[\frac{\pi}{2} e^{-d_{nr} z} - \frac{\pi}{4} e^{-(q_n^2 - d_{nr}^2)Dt/K_n} \left\{ 2e^{-d_{nr} z} - \right. \right. \\
&\quad \left. \left. - e^{-d_{nr} z} \operatorname{erfc}\left(\frac{z}{2\sqrt{Dt/K_n}} - d_{nr} \sqrt{Dt/K_n}\right) - e^{d_{nr} z} \operatorname{erfc}\left(\frac{z}{2\sqrt{Dt/K_n}} + d_{nr} \sqrt{Dt/K_n}\right) \right\} \right] \\
&= F_n' \sum_{r=j}^i E_{nr} \left\{ \frac{\pi}{2} e^{-d_{nr} z} (1 - G_{nr}(t)) + \frac{\pi}{4} G_{nr}(t) \times \right. \\
&\quad \left. \times \left[e^{-d_{nr} z} \operatorname{erfc}\left(\frac{z}{2\sqrt{Dt/K_n}} - d_{nr} \sqrt{Dt/K_n}\right) + e^{d_{nr} z} \operatorname{erfc}\left(\frac{z}{2\sqrt{Dt/K_n}} + d_{nr} \sqrt{Dt/K_n}\right) \right] \right\} \quad (3.53)
\end{aligned}$$

where

$$\begin{aligned}
G_{nr}(t) &\equiv e^{-(q_n^2 - d_{nr}^2)Dt/K_n} = e^{-\frac{K_n \lambda_n - K_r \lambda_r}{K_n - K_r} t}, \quad r \neq n \\
&= 1, \quad r = n
\end{aligned} \quad (3.54)$$

Therefore, the second term on the r.h.s. of (3.44) becomes

$$\begin{aligned}
&\frac{D}{K_i} \sum_{j=1}^{i-1} C_i^{(j)} N_j^0 \sum_{n=j}^i F_n' \sum_{r=j}^i E_{nr} \left\{ e^{(\frac{\nu}{2D} - d_{nr})z} (1 - G_{nr}(t)) + \frac{G_{nr}(t)}{2} \times \right. \\
&\quad \left. \times \left[e^{(\frac{\nu}{2D} - d_{nr})z} \operatorname{erfc}\left(\frac{z}{2\sqrt{Dt/K_n}} - d_{nr} \sqrt{Dt/K_n}\right) + e^{(\frac{\nu}{2D} + d_{nr})z} \operatorname{erfc}\left(\frac{z}{2\sqrt{Dt/K_n}} + d_{nr} \sqrt{Dt/K_n}\right) \right] \right\} \\
&\quad (3.55)
\end{aligned}$$

Let $S_i(z, t)$ and $P_i(z, t)$ represent the first and the second terms on the right hand side of (3.44), respectively, $N_i(z, t)$ becomes

$$N_i(z, t) = S_i(z, t) + P_i(z, t), \quad z > 0, \quad t > 0, \quad i = 1, 2, \dots \quad (3.56)$$

with $S_i(z, t)$ given in (3.48) and $P_i(z, t)$ given in (3.55).

If we use $A_i^{(j)}$ defined in (3.30) to replace $C_i^{(j)}$ in (3.44), P_i can be rewritten as

$$\begin{aligned}
P_i(z, t) = & \sum_{j=1}^{i-1} A_i(j) N_j^0 \sum_{n=j}^i F_n \sum_{r=j}^i E_{nr} \left\{ e^{\left(\frac{\nu}{2D} - d_{nr}\right)z} (1 - G_{nr}(t)) + \frac{G_{nr}(t)}{2} \times \right. \\
& \times \left. \left[e^{\left(\frac{\nu}{2D} - d_{nr}\right)z} \operatorname{erfc}\left(\frac{z}{2\sqrt{Dt/K_n}} - d_{nr} \sqrt{Dt/K_n}\right) + e^{\left(\frac{\nu}{2D} + d_{nr}\right)z} \operatorname{erfc}\left(\frac{z}{2\sqrt{Dt/K_n}} + d_{nr} \sqrt{Dt/K_n}\right) \right] \right\}
\end{aligned} \tag{3.57}$$

with

$$F_n \equiv \frac{1}{\prod_{\substack{w=j \\ w \neq n}}^i \left(1 - \frac{K_w}{K_n}\right)} = \frac{K_n^{i-j}}{\prod_{\substack{w=j \\ w \neq n}}^i (K_n - K_w)} \tag{3.58}$$

It will be shown later that $S_i(z, t)$ is always bounded, and after some reordering the final form can be evaluated by computer without any difficulty. $P_i(z, t)$, however, still has some problem when put in computer though the integrals are gone. This is due to the numerical values of d_{nr} and $G_{nr}(t)$. From the definition of d_{nr} (3.50) one can see that it may have any value, even imaginary (for $d_{nr}^2 < 0$). On the other hand, (3.54) shows that $G_{nr}(t)$ may be either positively or negatively very large value and (3.57) cannot be handled by the computer. Therefore, a further reduction is needed.

From (3.54) one observes that when $n=r$ the first term in the braces in (3.57) vanishes since $G_{nr}(t)=1$. For $n \neq r$ and with the definition of E_{nr} (3.52) one gets

$$\begin{aligned}
F_n E_{nr} &= \frac{K_n^{i-j}}{\prod_{\substack{w=j \\ w \neq n}}^i (K_n - K_w)} \frac{1}{\prod_{\substack{u=j \\ u \neq r}}^i (d_{nu}^2 - d_{nr}^2)} \\
&= \frac{K_n^{i-j}}{\prod_{\substack{w=j \\ w \neq n}}^i (K_n - K_w)} \frac{1}{\prod_{\substack{u=j \\ u \neq n \\ u \neq r}}^i (d_{nu}^2 - d_{nr}^2)} \frac{1}{(d_{nn}^2 - d_{nr}^2)}, \quad n \neq r, \quad i > j+1
\end{aligned}$$

$$= \frac{K_n}{K_n - K_r} \frac{1}{(d_{nn}^2 - d_{nr}^2)}, \quad n \neq r, \quad i = j + 1 \quad (3.59)$$

Now let's expand $d_{nw}^2 - d_{nr}^2$ and $d_{nn}^2 - d_{nr}^2$ as follows:

$$\begin{aligned} d_{nw}^2 - d_{nr}^2 &= -\frac{K_n K_w}{D} \left(\frac{\lambda_n - \lambda_w}{K_n - K_w} \right) + \frac{K_n K_r}{D} \left(\frac{\lambda_n - \lambda_r}{K_n - K_r} \right) \\ &= \frac{K_n}{D} \left[\frac{-K_w (\lambda_n - \lambda_w)(K_n - K_r) + K_r (\lambda_n - \lambda_r)(K_n - K_w)}{(K_n - K_w)(K_n - K_r)} \right] \\ &= \frac{K_n}{D} \left[\frac{K_n \lambda_n (K_r - K_w) + K_r \lambda_r (K_w - K_n) + K_w \lambda_w (K_n - K_r)}{(K_n - K_w)(K_n - K_r)} \right], \quad r \neq w \neq n \end{aligned} \quad (3.60)$$

$$\begin{aligned} d_{nn}^2 - d_{nr}^2 &= \frac{K_n \lambda_n}{D} + \frac{K_n K_r}{D} \left(\frac{\lambda_n - \lambda_r}{K_n - K_r} \right) \\ &= \frac{K_n}{D} \left(\frac{K_n \lambda_n - K_r \lambda_r}{K_n - K_r} \right), \quad n \neq r \end{aligned} \quad (3.61)$$

Substituting (3.60) and (3.61) back into (3.59) one obtains for $n \neq r$

$$\begin{aligned} F_n E_{nr} &= \frac{K_n^{i-j} \left(\frac{D}{K_n} \right)^{i-j-1} (K_n - K_r)^{i-j-1} \prod_{\substack{w=j \\ w \neq n \\ w \neq r}}^i (K_n - K_w)}{\prod_{\substack{w=j \\ w \neq n}}^i (K_n - K_w) \prod_{\substack{w=j \\ w \neq n \\ w \neq r}}^i [K_n \lambda_n (K_r - K_w) + K_r \lambda_r (K_w - K_n) + K_w \lambda_w (K_n - K_r)]} \frac{\left(\frac{D}{K_n} \right) (K_n - K_r)}{(K_n \lambda_n - K_r \lambda_r)} \\ &= \frac{D^{i-j} (K_n - K_r)^{i-j-1} / (K_n \lambda_n - K_r \lambda_r)}{\prod_{\substack{w=j \\ w \neq n \\ w \neq r}}^i [K_n \lambda_n (K_r - K_w) + K_r \lambda_r (K_w - K_n) + K_w \lambda_w (K_n - K_r)]}, \quad i > j + 1 \end{aligned}$$

$$= \frac{D}{K_n \lambda_n - K_r \lambda_r}, \quad i = j+1 \quad (3.62)$$

For $n=r$, following similarly derivations one gets

$$F_n E_{nn} = \frac{D^{i-j}}{\prod_{\substack{v=j \\ v \neq n}}^i (K_v \lambda_v - K_n \lambda_n)} \quad (3.63)$$

Hence from (3.62) by interchanging n and r one sees that for $n \neq r$

$$F_n E_{nr} = -F_r E_{rn} \quad (3.64)$$

Equation (3.64) is our key formula to make (3.57) computable for any combination of the parameters: D , v , K_i , ϵ , λ_i , z , and t .

Since n and r both range from j to i as seen in (3.57), for every $F_n E_{nr}$, $n \neq r$, there exists exactly one corresponding $F_r E_{rn}$. In addition, $d_{nr} = d_{rn}$ from (3.50), and $G_{nr}(t) = G_{rn}(t)$ from (3.54). Therefore, for $n = j, j+1, \dots, i$; $r = j, j+1, \dots, i$

$$F_n E_{nr} e^{\left(\frac{v}{2D} - d_{nr}\right)z} (1 - G_{nr}(t)) + F_r E_{rn} e^{\left(\frac{v}{2D} - d_{rn}\right)z} (1 - G_{rn}(t)) = 0 \quad (3.65)$$

That is, the summation of the first term in braces in (3.57) from j to i is zero. Thus

$$P_i(z, t) = \frac{1}{2} \sum_{j=1}^{i-1} A_i^{(j)} N_j^0 \sum_{n=j}^i F_n \sum_{r=j}^i E_{nr} G_{nr}(t) \times \\ \times \left[e^{\left(\frac{v}{2D} - d_{nr}\right)z} \operatorname{erfc}\left(\frac{z}{2\sqrt{Dt/K_n}} - d_{nr} \sqrt{Dt/K_n}\right) + e^{\left(\frac{v}{2D} + d_{nr}\right)z} \operatorname{erfc}\left(\frac{z}{2\sqrt{Dt/K_n}} + d_{nr} \sqrt{Dt/K_n}\right) \right] \quad (3.66)$$

To remove the difficulty caused by $G_{nr}(t)$ we make following rearrangement.

Since $G_{nr}(t) = e^{-\frac{Dt}{K_n}(v_n^2 - d_{nr}^2)} = e^{-\lambda_n t} e^{-\frac{v^2 t}{4DK_n} + \frac{Dt}{K_n} d_{nr}^2}$ from (3.32), we have

$$G_{nr}(t) e^{\left(\frac{v}{2D} \pm d_{nr}\right)z} = e^{-\lambda_n t - \left(\sqrt{\frac{t}{4DK_n} + \frac{z}{2\sqrt{Dt/K_n}}}\right)^2} e^{\left(\frac{z}{2\sqrt{Dt/K_n}} \pm d_{nr} \sqrt{Dt/K_n}\right)^2} \quad (3.67)$$

Also, when $n=r$, $G_{nr}(t)=1$, $d_{nr}=q_n$, and

$$e^{\left(\frac{v}{2D} \pm q_n\right)z} = e^{-\lambda_n t - \left(\sqrt{\frac{t}{4DK_n} + \frac{z}{2\sqrt{Dt/K_n}}}\right)^2} e^{\left(\frac{z}{2\sqrt{Dt/K_n}} \pm q_n \sqrt{Dt/K_n}\right)^2} \quad (3.68)$$

Consequently, with $\lambda_i + \frac{v^2}{4DK_i} = q_i^2 \frac{D}{K_i}$, (3.48) and (3.66) are reduced to

$$S_i(z, t) = \frac{1}{2} N_i^0 e^{-\lambda_i t - \left(\sqrt{\frac{t}{4DK_i} + \frac{z}{2\sqrt{Dt/K_i}}}\right)^2} \times \\ \times \left[H\left(\frac{z}{2\sqrt{Dt/K_i}} + q_i \sqrt{Dt/K_i}\right) + H\left(\frac{z}{2\sqrt{Dt/K_i}} - q_i \sqrt{Dt/K_i}\right) \right] \quad (3.69)$$

$$P_i(z, t) = \frac{1}{2} \sum_{j=1}^{i-1} A_i(j) N_j^0 \sum_{n=j}^i F_n \sum_{r=j}^i E_{nr} e^{-\lambda_n t - \left(\sqrt{\frac{t}{4DK_n} + \frac{z}{2\sqrt{Dt/K_n}}}\right)^2} \times \\ \times \left[H\left(\frac{z}{2\sqrt{Dt/K_n}} + d_{nr} \sqrt{Dt/K_n}\right) + H\left(\frac{z}{2\sqrt{Dt/K_n}} - d_{nr} \sqrt{Dt/K_n}\right) \right] \quad (3.70)$$

where

$$H(x) = e^{x^2} \operatorname{erfc}(x) \quad (3.71)$$

For $x \geq 0$, $H(x)$ is always bounded.

Consider the case $\frac{z}{2\sqrt{Dt/K_n}} < d_{nr} \sqrt{Dt/K_n}$, which makes the argument in H function negative, for some $r \neq n$. Since $\operatorname{erfc}(-x) = 2 - \operatorname{erfc}(x)$, one has

$$e^{\left(\frac{v}{2D} - d_{nr}\right)z} \operatorname{erfc}\left(\frac{z}{2\sqrt{Dt/K_n}} - d_{nr} \sqrt{Dt/K_n}\right) = 2e^{\left(\frac{v}{2D} - d_{nr}\right)z} - \operatorname{erfc}\left(d_{nr} \sqrt{Dt/K_n} - \frac{z}{2\sqrt{Dt/K_n}}\right) \quad (3.72)$$

Now $G_{nr}(t) = e^{-(q_n^2 - d_{nr}^2)Dt/K_n} = e^{-\frac{K_n \lambda_n - K_r \lambda_r}{K_n - K_r} t}$ so one more term $2e^{-\frac{K_n \lambda_n - K_r \lambda_r}{K_n - K_r} t + \left(\frac{v}{2D} - d_{nr}\right)z}$

appears in (3.70). If $\frac{z}{2\sqrt{Dt/K_r}}$ is also less than $d_{nr} \sqrt{Dt/K_r}$, then from our key formula (3.64), this extra term will be canceled out. For $\frac{z}{2\sqrt{Dt/K_r}} \geq d_{nr} \sqrt{Dt/K_r}$, one can show with little effort that

$$-\frac{K_n \lambda_n - K_r \lambda_r}{K_n - K_r} t + \left(\frac{v}{2D} - d_{nr}\right) z < 0, \text{ for } d_{nr} > 0 \text{ and } \frac{z}{2\sqrt{Dt/K_n}} < d_{nr} \sqrt{Dt/K_n}. \quad (3.73)$$

Hence when (3.72) is combined with $G_{nr}(t)$, one has

$$G_{nr}(t) e^{\left(\frac{v}{2D} - d_{nr}\right)z} \operatorname{erfc}\left(\frac{z}{2\sqrt{Dt/K_n}} - d_{nr} \sqrt{Dt/K_n}\right) = 2e^{-\frac{K_n \lambda_n - K_r \lambda_r}{K_n - K_r} t + \left(\frac{v}{2D} - d_{nr}\right)z} - H\left(d_{nr} \sqrt{Dt/K_n} - \frac{z}{2\sqrt{Dt/K_n}}\right) \quad (3.74)$$

For $n=r$,

$$d_{nr} = d_{nn} = q_n = \left[\left(\frac{v}{2D}\right)^2 + \frac{K_n \lambda_n}{D} \right]^{1/2} > \frac{v}{2D} \quad (3.75)$$

So (3.72) is still bounded. With the help of (3.74) and (3.75) one obtains the computable form for $N_i(z, t)$ in terms of $S_i(z, t)$ and $P_i(z, t)$ (3.56) for all real d_{nr} :

$$S_i(z, t) = \frac{1}{2} N_i^0 e^{-\lambda_i t - \left(\sqrt{\frac{t}{4DK_i} + \frac{z}{2\sqrt{Dt/K_i}}}\right)^2} \times \\ \times \left[H\left(\frac{z}{2\sqrt{Dt/K_i}} + q_i \sqrt{Dt/K_i}\right) + H\left(\frac{z}{2\sqrt{Dt/K_i}} - q_i \sqrt{Dt/K_i}\right) \right], \text{ for } \frac{z}{2\sqrt{Dt/K_i}} \geq q_i \sqrt{Dt/K_i}; \\ = \frac{1}{2} N_i^0 \left\{ 2e^{\left(\frac{v}{2D} - q_i\right)z} + e^{-\lambda_i t - \left(\sqrt{\frac{t}{4DK_i} + \frac{z}{2\sqrt{Dt/K_i}}}\right)^2} \times \right. \\ \left. \times \left[H\left(\frac{z}{2\sqrt{Dt/K_i}} + q_i \sqrt{Dt/K_i}\right) - H\left(q_i \sqrt{Dt/K_i} - \frac{z}{2\sqrt{Dt/K_i}}\right) \right] \right\}, \text{ for } \frac{z}{2\sqrt{Dt/K_i}} < q_i \sqrt{Dt/K_i}$$

(3.76)

$$P_i(z, t) = \frac{1}{2} \sum_{j=1}^{i-1} A_i(j) N_j^0 \sum_{n=j}^i F_n \sum_{r=j}^i E_{nr} W(z, d_{nr}, \sqrt{Dt/K_n}) \quad (3.77)$$

where

$$\begin{aligned} & W(z, d_{nr}, \sqrt{Dt/K_n}) \\ &= e^{-\lambda_n t - \left(\sqrt{\frac{t}{4DK_n}} - \frac{z}{2\sqrt{Dt/K_n}} \right)^2} \times \\ & \times \left[H\left(\frac{z}{2\sqrt{Dt/K_n}} + d_{nr} \sqrt{Dt/K_n} \right) + H\left(\frac{z}{2\sqrt{Dt/K_n}} - d_{nr} \sqrt{Dt/K_n} \right) \right], \text{ for } \frac{z}{2\sqrt{Dt/K_n}} \geq d_{nr} \sqrt{Dt/K_n}; \\ &= 2e^{-\frac{K_n \lambda_n - K_r \lambda_r}{K_n - K_r} t + \left(\frac{v}{2D} - d_{nr} \right) z} + e^{-\lambda_n t - \left(\sqrt{\frac{t}{4DK_n}} - \frac{z}{2\sqrt{Dt/K_n}} \right)^2} \times \\ & \times \left[H\left(\left(\frac{z}{2\sqrt{Dt/K_n}} + d_{nr} \sqrt{Dt/K_n} \right) \right) - H\left(d_{nr} \sqrt{Dt/K_n} - \frac{z}{2\sqrt{Dt/K_n}} \right) \right], \\ & \quad \text{for } \frac{z}{2\sqrt{Dt/K_n}} < d_{nr} \sqrt{Dt/K_n}, n \neq r; \\ &= 2e^{\left(\frac{v}{2D} - q_n \right) z} + e^{-\lambda_n t - \left(\sqrt{\frac{t}{4DK_n}} - \frac{z}{2\sqrt{Dt/K_n}} \right)^2} \times \\ & \times \left[H\left(\left(\frac{z}{2\sqrt{Dt/K_n}} + q_n \sqrt{Dt/K_n} \right) \right) - H\left(\left| \frac{z}{2\sqrt{Dt/K_n}} - q_n \sqrt{Dt/K_n} \right| \right) \right], \\ & \quad \text{for } \frac{z}{2\sqrt{Dt/K_n}} < q_n \sqrt{Dt/K_n}, n = r \end{aligned} \quad (3.78)$$

Error Functions of Complex Arguments

For $d_{nr}^2 < 0$, d_{nr} is a pure imaginary number, and we have error functions of complex arguments from (3.78). Since

$$\begin{aligned}
 H(x+iy) &= e^{(x+iy)^2} \operatorname{erfc}(x+iy) = e^{x^2-y^2} e^{i2xy} \operatorname{erfc}(x+iy), \\
 H(x-iy) &= e^{(x-iy)^2} \operatorname{erfc}(x-iy) = e^{x^2-y^2} e^{-i2xy} \operatorname{erfc}(x-iy) = \overline{H(x+iy)} \quad (3.79)
 \end{aligned}$$

the sum $H(x+iy) + H(x-iy) = 2e^{x^2-y^2} (\hat{R} \cos 2xy - \hat{I} \sin 2xy) = \text{real}$, where \hat{R} and \hat{I} are the real and imaginary parts of $\operatorname{erfc}(x+iy)$, respectively. Now in (3.70),

$$x = \frac{z}{2\sqrt{Dt/K_n}}, \quad y = \left| d_{nr} \sqrt{Dt/K_n} \right|, \quad x^2 - y^2 = \frac{K_n z^2 - Dt/K_n (-d_{nr}^2)}{4Dt}, \quad 2xy = |d_{nr} z|, \quad \text{and}$$

\hat{R} and \hat{I} are given in the approximate forms* with the relative error bound $\leq 10^{-16}$:

$$\begin{aligned}
 \hat{R} &= \operatorname{erfc}(x) - \frac{e^{-x^2}}{\pi} \left(\frac{1 - \cos 2xy}{2x} + 2 \sum_{n=1}^{\infty} \frac{e^{-\frac{n^2}{4}}}{n^2 + 4x^2} f_n \right) \\
 \hat{I} &= -\frac{e^{-x^2}}{\pi} \left(\frac{\sin 2xy}{2x} + 2 \sum_{n=1}^{\infty} \frac{e^{-\frac{n^2}{4}}}{n^2 + 4x^2} g_n \right) \quad (3.80)
 \end{aligned}$$

where

$$\begin{aligned}
 f_n &= 2x [1 - \cosh(ny) \cos(2xy)] + n \sinh(ny) \sin(2xy) \\
 g_n &= 2x \cosh(ny) \sin(2xy) + n \sinh(ny) \cos(2xy) \quad (3.81)
 \end{aligned}$$

Therefore,

$$\begin{aligned}
 &H(x+iy) + H(x-iy) \\
 &= 2[e^{x^2-y^2} \hat{R} \cos 2xy - e^{x^2-y^2} \hat{I} \sin 2xy] \\
 &= 2 \left\{ e^{-y^2} \left[H(x) - \frac{1 - \cos 2xy}{2\pi x} \right] - \frac{2}{\pi} \times \right. \\
 &\quad \left. \times \sum_{n=1}^{\infty} \frac{2xe^{-y^2 - \frac{n^2}{4}} - 2x \cos 2xy M(n, y) + n \sin 2xy N(n, y)}{n^2 + 4x^2} \right\} \cos(2xy) + \frac{1}{\pi} \times
 \end{aligned}$$

*M. Abramowitz and I. A. Stegun, editors, "Handbook of Mathematical Functions," p. 299, Dover Publications, Inc. New York, 1972.

$$\times \left\{ e^{-y^2 \frac{\sin 2xy}{2x}} + 2 \sum_{n=1}^{\infty} \frac{2x \sin 2xy M(n, y) + n \cos 2xy N(n, y)}{n^2 + 4x^2} \right\} \sin(2xy) \quad (3.82)$$

where

$$M(n, y) = e^{-y^2 - \frac{n^2}{4}} \cosh(ny) = \frac{\left[e^{-\left(y - \frac{n}{2}\right)^2} + e^{-\left(y + \frac{n}{2}\right)^2} \right]}{2}$$

$$N(n, y) = e^{-y^2 - \frac{n^2}{4}} \sinh(ny) = \frac{\left[e^{-\left(y - \frac{n}{2}\right)^2} - e^{-\left(y + \frac{n}{2}\right)^2} \right]}{2} \quad (3.83)$$

Hence the complete solution for $N_i(z, t)$ for any combination of the parameters are given in (3.56), (3.76), (3.77), (3.78), (3.82), and (3.83), and is always bounded.

For the case $K_n \rightarrow K_r$ and $n \neq r$, $F_n E_{nr} \rightarrow 0$ from (3.62) and $|d_{nr}| \rightarrow \infty$ from (3.50). Thus $H\left(\left|\frac{z}{2\sqrt{Dt/K_n}} \pm d_{nr} \sqrt{Dt/K_n}\right|\right) \rightarrow 0$ for both d_{nr} real and imaginary, and $G(z, d_{nr}, \sqrt{Dt/K_n}) \rightarrow 0$. Hence the singularity is not present.

Appendix B: Numerical Implementation of Equation (3.44')

To facilitate the numerical implementation of Equation (3.44') we follow the same procedure as in Appendix A, with q_n replaced by q_{nk} defined in Eq. (3.32') and N_i^0 replaced by $\sum_{k=1}^i B_{ik} e^{-\lambda_k t}$. One obtains the comparable equations (3.45') - (3.83')

with the following changes:

$$G_{nr}(t) = e^{-\frac{K_n \lambda_n - K_r \lambda_r}{K_n - K_r} t + \lambda_k t}, \quad r \neq n$$

$$= 1, \quad r = n \quad (3.54')$$

$$d_{na}^2 - d_{nr}^2 = \frac{K_n}{D} \frac{K_n \lambda_n - K_r \lambda_r - \lambda_k K_n - K_r}{K_n - K_r}, \quad n \neq r \quad (3.61')$$

$$F_n E_{nr} = \frac{D^{i-j} (K_n - K_r)^{i-j-1} / [K_n \lambda_n - K_r \lambda_r - \lambda_k (K_n - K_r)]}{\prod_{\substack{w=j \\ w \neq n \\ w \neq r}}^i [K_n \lambda_n (K_r - K_w) + K_r \lambda_r (K_w - K_n) + K_w \lambda_w (K_n - K_r)]}, \quad \text{for } n \neq r, i > j+1;$$

$$= \frac{D}{[K_n \lambda_n - K_r \lambda_r - \lambda_k (K_n - K_r)]}, \quad \text{for } n \neq r, i = j+1 \quad (3.62')$$

$$F_n E_{nn} = \frac{D^{i-j}}{\prod_{\substack{w=j \\ w \neq n}}^i [K_w \lambda_w - K_n \lambda_n - \lambda_k (K_w - K_n)]} \quad (3.63')$$

$$G_{nr}(t) e^{(\frac{v}{2D} \pm d_{nr})z} = e^{-(\lambda_n - \lambda_k)t - (\sqrt{\frac{t}{4DK_n} - \frac{z}{2\sqrt{Dt/K_n}}} - \frac{z}{2\sqrt{Dt/K_n}})^2 (\frac{z}{2\sqrt{Dt/K_n}} \pm d_{nr} \sqrt{Dt/K_n})^2} \quad (3.67')$$

$$e^{(\frac{v}{2D} \pm q_{nk})z} = e^{-(\lambda_n - \lambda_k)t - (\sqrt{\frac{t}{4DK_n} - \frac{z}{2\sqrt{Dt/K_n}}} - \frac{z}{2\sqrt{Dt/K_n}})^2 (\frac{z}{2\sqrt{Dt/K_n}} \pm q_{nk} \sqrt{Dt/K_n})^2} \quad (3.68)$$

The final solutions are given by

$$N_i(z, t) = S_i(z, t) + P_i(z, t), \quad i = 1, 2, \dots, \quad z > 0, \quad t > 0 \quad (3.56')$$

with

$$\begin{aligned} S_i(z, t) &= \frac{1}{2} \sum_{k=1}^i B_{ik} e^{-\lambda_i t - \left(\sqrt{\frac{t}{4DK_i} + \frac{z}{2\sqrt{Dt/K_i}}}\right)^2} \times \\ &\times \left[H\left(\frac{z}{2\sqrt{Dt/K_i}} + q_{ik} \sqrt{Dt/K_i}\right) + H\left(\frac{z}{2\sqrt{Dt/K_i}} - q_{ik} \sqrt{Dt/K_i}\right) \right], \quad \text{for } \frac{z}{2\sqrt{Dt/K_i}} \geq q_{ik} \sqrt{Dt/K_i}; \\ &= \frac{1}{2} \sum_{k=1}^i B_{ik} \left\{ 2e^{\left(\frac{q}{2D} - q_{ik}\right)z - \lambda_i t} + e^{-\lambda_i t - \left(\sqrt{\frac{t}{4DK_i} + \frac{z}{2\sqrt{Dt/K_i}}}\right)^2} \times \right. \\ &\left. \times \left[H\left(\frac{z}{2\sqrt{Dt/K_i}} + q_{ik} \sqrt{Dt/K_i}\right) - H\left(q_{ik} \sqrt{Dt/K_i} - \frac{z}{2\sqrt{Dt/K_i}}\right) \right] \right\}, \quad \text{for } \frac{z}{2\sqrt{Dt/K_i}} < q_{ik} \sqrt{Dt/K_i}; \end{aligned} \quad (3.76')$$

and

$$P_i(z, t) = \frac{1}{2} \sum_{j=1}^{i-1} A_i^{(j)} \sum_{k=1}^j B_{jk} \sum_{n=j}^i F_n \sum_{r=j}^i E_{nr} W(z, d_{nr}, \sqrt{Dt/K_n}) \quad (3.77')$$

where

$$\begin{aligned} &W(z, d_{nr}, \sqrt{Dt/K_n}) \\ &= e^{-\lambda_n t - \left(\sqrt{\frac{t}{4DK_n} + \frac{z}{2\sqrt{Dt/K_n}}}\right)^2} \times \\ &\times \left[H\left(\frac{z}{2\sqrt{Dt/K_n}} + d_{nr} \sqrt{Dt/K_n}\right) + H\left(\frac{z}{2\sqrt{Dt/K_n}} - d_{nr} \sqrt{Dt/K_n}\right) \right], \quad \text{for } \frac{z}{2\sqrt{Dt/K_n}} \geq d_{nr} \sqrt{Dt/K_n}; \\ &= 2e^{-\frac{K_n \lambda_n - K_r \lambda_r}{K_n - K_r} t + \left(\frac{q}{2D} d_{nr}\right)z} + e^{-\lambda_n t - \left(\sqrt{\frac{t}{4DK_n} + \frac{z}{2\sqrt{Dt/K_n}}}\right)^2} \times \end{aligned}$$

$$\begin{aligned}
& \times [H((\frac{z}{2\sqrt{Dt/K_n}} + d_{nr}\sqrt{Dt/K_n})) - H(d_{nr}\sqrt{Dt/K_n} - \frac{z}{2\sqrt{Dt/K_n}})], \\
& \qquad \qquad \qquad \text{for } \frac{z}{2\sqrt{Dt/K_n}} < d_{nr}\sqrt{Dt/K_n}, n \neq r; \\
& = 2e^{(\frac{\nu}{2D} - q_{nk})z - \lambda_k t} + e^{-\lambda_k t - (\sqrt{\frac{t}{4DK_n} + \frac{z}{2\sqrt{Dt/K_n}}})^2} \times \\
& \times [H((\frac{z}{2\sqrt{Dt/K_n}} + q_{nk}\sqrt{Dt/K_n})) - H(\left| \frac{z}{2\sqrt{Dt/K_n}} - q_{nk}\sqrt{Dt/K_n} \right|)], \\
& \qquad \qquad \qquad \text{for } \frac{z}{2\sqrt{Dt/K_n}} < q_{nk}\sqrt{Dt/K_n}, n = r \qquad (3.78')
\end{aligned}$$

For $d_{nr}^2 < 0$ or $q_{nk}^2 < 0$, i.e., for error functions with complex arguments, Eqs. (3.82')

and (3.83') are identical to (3.82) and (3.83) with $x = \frac{z}{2\sqrt{Dt/K_n}}$, $y = \left| d_{nr}\sqrt{Dt/K_n} \right|$

or $y = \left| q_{nk}\sqrt{Dt/K_n} \right|$.

It can also be shown that for $q_{nk}^2 \geq 0$, $e^{(\frac{\nu}{2D} - q_{nk})z - \lambda_k t} \leq 1$. Hence $N_i(z, t)$ is given by (3.56') and (3.76')-(3.83') with any combination of the parameters, and is always bounded.

*LAWRENCE BERKELEY LABORATORY
TECHNICAL INFORMATION DEPARTMENT
UNIVERSITY OF CALIFORNIA
BERKELEY, CALIFORNIA 94720*